Dynamic Analysis Of The WESMO FSAE Car's Suspension

A thesis

submitted in fulfilment

of the requirements for the degree

of

Master of Engineering

in Mechanical Engineering

at

The University of Waikato

by

Larissa Kopf

THE UNIVERSITY OF
WAIKATO
Te Whare Wānanga o Waikato

2020

Abstract

Over the years motorsport has become a large part of society with many millions of dollars spent on the design and development of the cars. However, with many racing series evening out the playing field between low and high budget teams by introducing restrictions, especially around engine size, suspension and vehicle dynamics analysis have become a big factor in reducing lap times. This is true for high end racing such as Formula 1 down to entry level racing such as Formulae SAE, a racing series where tertiary students design and manufacture single seater race cars.

The following research was centred on the vehicle dynamic analysis of the SAE car manufactured by the University of Waikato in Hamilton, New Zealand, in 2018. In particular, the focus was on suspension tuning and understanding the relationship between suspension and tyre parameters.

Theoretical models were developed based on geometric data and tyre data available for the car. Furthermore, the effect of spring rate, camber angle, tyre pressure and damping rates on traction coefficients were investigated. A low tyre pressure (8 PSI), as well as a high pressure (14 PSI), reduced the lateral force capable of being produced during cornering. A softer spring at the rear (225 lbs/in) allowed more grip and a stiffer front (250 lbs/in) allowed for a good response during steering input, whereas a change in camber between 0° and 3° was negligible on the traction coefficient.

The theoretical models were verified using track data gathered by sensors on the car and logged through a CDL3 MoTeC dash data logger. The lap time for a 1.2 km track could be decreased by up to seven seconds by tuning the suspension parameters to increase the grip of the car during cornering. This was achieved by decreasing the low speed rebound damping on the shocks to allow more compliance between the road and the tyre reducing understeer. Different methods of diagnosing understeer were investigated as the car did not have a yaw sensor. A comparison between front and rear tyre slip angles (calculated based on logged data) gave the most accurate results compared to purely investigating the steering wheel angle or calculating the difference between wheel angle and Ackermann angle. Furthermore, the amount of roll was optimised by implementing a soft antiroll bar at the front and the rear of the car, allowing enough roll for driver feedback but limiting it to eliminate jacking of the wheel.

Overall the beneficial effect of correct and in-depth suspension tuning was found to be substantial. Good tuning, however, is not a remedy for badly designed suspension. The 2018 WESMO car had a well-designed suspension, making tuning possible and beneficial. If the 2018 car's suspension had been tuned properly, the team could have potentially placed third instead of eighth in the autocross event at the 2018 Formula SAE competition at Winton Motor Raceway in Australia.

Acknowledgments

Firstly, I would like to thank my supervisors Dr Mark Lay, Dr Rachael Tighe and Dr Yusuke Mochida for their guidance and help throughout the year. Especially during the write up for always having the time to help me with questions and taking the time to read over the thesis.

I would also like to thank Neel Gosh for driving the car so reliably and consistently and not hating me too much for the bad setups that we tested.

To Jonathan van Harselaar for always having an open ear for me to winch about masters and letting me bounce ideas back and forth. As well as giving me a job to break up the weeks of thesis write up.

To Scott Harvey for making me question the littlest things with tyre data and always having a good yarn.

To Steven Wu for all the coffee break procrastination and vocabulary help.

To Nidhita Gosai for all the late night gossip talks to keep me sane and from stressing out.

And of course to all my family that sent much needed chocolate rations half way around the world. An especially big thank you to my mum that spent hours looking over this thesis finding the smallest formatting mistake.

Contents

List of Figures

List of Tables

Nomenclature

Roman alphabet

a	Acceleration	m/s^2
a	COG Distance from front of vehicle	m
b	COG Distance from rear of vehicle	m
c	Damper constant	kg/s
$\mathbf{c_\alpha}$	Tyres cornering stiffness	kg/°
F	Force	N
g	Gravity of Earth	m/s^2
$\mathbf{h_{COG}}$	Height from road to COG	m
$\mathbf{I_\theta}$	Pitch Inertia	kgm^2
k	Spring constant	N/m
$\mathbf{K_{Roll}}$	Roll stiffness	Nm/°
$\mathbf{k_T}$	Tyre spring constant	N/m
$\mathbf{k_{Tot}}$	Total spring constant	N/m
L	Wheelbase	m
m	Mass	kg
q	Roll stiffness ratio	-
R	Corner radius	m
t	Track width	m
v	Magnitude of cars velocity	m/s
x	Measured shock displacement	mm
z	Displacement	m
$\mathbf{z_{Bump}}$	Displacement caused by bump	m
ż	Velocity	m/s
z̈	Acceleration	m/s^2

Greek alphabet

α	Slip angle	°
α_{Pitch}	Pitch angle	°
α_{Roll}	Roll angle	°
Δm_{Geo}	Lateral weight transfer due to suspension geometry	N
Δm_{Sprung}	Lateral weight transfer due to the sprung mass	N
Δm_{Unsp}	Lateral weight transfer due to the unsprung mass	N
δ	Damping ratio	-
δ_{Acker}	Steering angle to negotiate the corner	°
ε	Camber angle	°
$\ddot{\Theta}$	Angular acceleration	rad/ s^2
μ	Traction or friction coefficient	-
ω_n	Natural frequency	Hz

Subscripts

F or Front	Front
R or Rear	Rear
Sprung	Sprung
Unsp	Unsprung
X and Long	Longitudinal
Y and Lat	Lateral
Z	Vertical

Abbreviations

ARB	Antiroll bar
CAD	Computer Animated Design
COG	Centre of gravity
DOF	Degrees of freedom
ECU	Engine Computer Unit
FL	Front Left
FR	Front Right
HSC	High speed compression damping
HSR	High speed rebound damping
LSC	Low speed compression damping
LSR	Low speed rebound damping
MR	Motion Ratio
PG	Pitch Gradient
RG	Roll Gradient
RL	Rear Left
RR	Rear Right
SAE	Society of Automotive Engineers
TIRF	Calspan Tire Research Facility
W-FS18	WESMO's 2018 car
WESMO	Waikato Engineering Students Motorsport Organisation

Chapter 1 - Introduction

Motor racing has been around for many years, the first proper race taking place in 1895 in France from Paris to Bordeaux and back, covering a distance of 1,200 km [1]. While the average speed of the winner was 24 km/h, much has changed since then. Nowadays Formula 1 drivers race at speeds averaging 250 km/h with top speeds up to 370 km/h. Not only did the speeds go up but also budgets, safety aspects and the engineering that goes into designing, tuning and building race cars. With competition being fierce between the big names in racing such as Scuderia Ferrari Mission Winnow, Mercedes-AMG Petronas and Aston Martin Red Bull Racing it is not surprising that teams keep their designs and car setups under wraps as much as they can. Cars are covered in the pit lanes as soon as the body panels come off. This is true for high end racing such as Formula 1 as well as smaller scale racing series such as the "Castrol Toyota Racing Series" in New Zealand. This is especially true with more and more regulations and rules for standardised parts in most series. Much of the aerodynamic and engine design is now heavily regulated due to safety concerns. Making the contact between the road and the car is the best place to gain an advantage over competitors. However, tyres are often provided by the racing series and teams do not get much choice between different rubber compounds, leaving the suspension as one of the most influential parts of the car's behaviour. Furthermore, if designed properly, suspension parameters can be adjusted quickly depending on the weather, driver and type of track.

The most effective way to decrease lap time, apart from more engine power, is increasing the speed through corners by increasing the amount of grip the car can produce. This is only possible if the lateral and longitudinal forces developed by the tyres are utilized to their full potential maximising the four points of contact with the road. A good suspension will also absorb much of the impact from uneven road surface, enabling a lightweight design for the rest of the car. Furthermore, although secondary, spring and dampers allow for a certain degree of comfort for the driver. This is especially important during long races like the 24 Hours of Le Mans race. With this in mind, it is no surprise that racing teams guard their suspension setups particularly well and release little to no information. The little data and research available is often outdated and rendered invalid by new technical developments.

At very much the other end of the racing spectrum to Formula 1 is the Formula Student Competition. This is an engineering challenge for tertiary education students with the aim to design and build a single seater race car within the rules and regulations of Formula SAE. More research and data is published by universities based on these student built race cars. The Waikato Engineering Students Motorsport Organisation (WESMO) is the University of Waikato's entry into the worldwide

competition Formula SAE (FSAE). The team competes in the Australasian leg of the competition against teams from Australia, New Zealand, Japan, India and many other countries.

Figure 1 - 2016 WESMO car

The competition comprises three static events and four dynamic events. Static events include design judging, where experts from industry are brought in to assess the team's knowledge and understanding and engineering principles behind their vehicle design. The next event is a business presentation where the team must present their take on how the manufactured vehicle could be marketed to the public for sale. The final static event is a cost report where teams outline each manufacturing process undertaken and manufacturing costs in a specified format by FSAE.

Teams compete in four dynamic events beginning with skidpad; an event where maximum lateral loading is applied on the car by completing a figure of eight circuit to test cornering ability. The cars then complete a 75 m straight line run from a standing start to assess their acceleration performance. The autocross event tests the car's dynamic agility and driveability while the endurance event tests the car's reliability, overall speed and performance.

The variety of events means that teams often have different setup options for drivetrain and suspension depending on the event. In order to develop optimal settings, data is gathered from sensors installed on the car and it is up to the team to analyse the data and draw meaningful conclusions from it.

The main event in the competition is the endurance race during which the cars complete 22 km of a cone/corner course as fast as possible. 375 points out of 1,000 points are awarded during this event and is therefore the main focus of many teams when adjusting their car. As it is a corner based course, the effects of engine power and drive train gear ratio are reduced and advantage can be gained by optimising grip to increase cornering speed by fine tuning suspension parameters.

The diversity of events the car competes in makes the understanding the suspension setup of great importance and the teams that win are the ones that have taken the time to develop different setups based on the track and the conditions at the track. As mentioned before grip is one of the biggest influences on lap time and should therefore be maximised to its full potential.

In 2018, the team struggled to sustain good contact between the tyre and the road and the car was frequently lifting the wheel on the inside of the corner (Figure 2).

Figure 2 - W-FS18 Lifting inner rear wheel during skidpad testing

It was decided that more analysis into the dynamic behaviour of the car had to be done in order to find the cause as well as be able to optimise the car better in coming years. The research in this thesis is based on the W-FS18 car with its existing parameters as a case study. It will start by looking at the forces created at the tyres and the resulting friction coefficient and using these to find the theoretical maximum traction the car and tyres are capable of producing. It will then look at the different setup possibilities to increase traction including spring and damper rates as well as antiroll bars to control how much the car rolls during a corner. Theoretical calculations done in MathWorks Matlab and Microsoft Excel, as well as a multibody dynamics simulation, done in Altair HyperWorks, will be compared to data gathered on track with the actual car. A combination between these can then be used to diagnose understeer, loss of traction and general grip levels in order to find the problem with the W-FS18 car setup and improve the handling of it.

Chapter 2 - Literature Review

2.1 Suspension Development

Most innovations do not stem from thin air but are concepts developed and adapted over decades. Suspension systems are no exception. Transportation of goods and people with carts using an axle and wheels dates back to the Roman Empire. However, back then, comfort and speed were not important, and carriages did not have any form of suspension, making for a very uncomfortable ride. After the introduction of springs, the ride became more comfortable but introduced other problems. As with most inventions, the effect of the springs on the behaviour of the car was unpredictable and caused problems. Springs allowed for movement of the wheels independently from the body, this is especially noticeable during cornering (Figure 3).

Figure 3 - Body roll [2]

The centrifugal force experienced by the car during cornering acts on the centre of gravity of the car (COG). Since it is impossible for the centre of gravity of the car to be on the road surface, a moment is created, causing a load transfer towards the outer wheels and thereby decreasing the load on the inner wheels [3]. This change in load affects the grip of the car, too little load transfer does not provide the driver with enough feedback from the car, too much load transfer and the car starts behaving erratically and can cause safety concerns for the driver. The only points of contact between the car and the road are four palm sized patches (~ 70 cm^2 per tyre) between the tyre and the road, dictating if the car grips and makes it around the track safely. It is therefore essential to understand the forces acting on these contact patches [4] and ensure the tyres follow the road surface as well as possible. The weight that is supported by the tyre acts vertically on the contact patch (F_Z), whereas the acceleration (or braking) force acts parallel in the longitudinal direction to the contact patch (F_X) and a lateral cornering force acts perpendicularly (F_Y) (Figure 4).

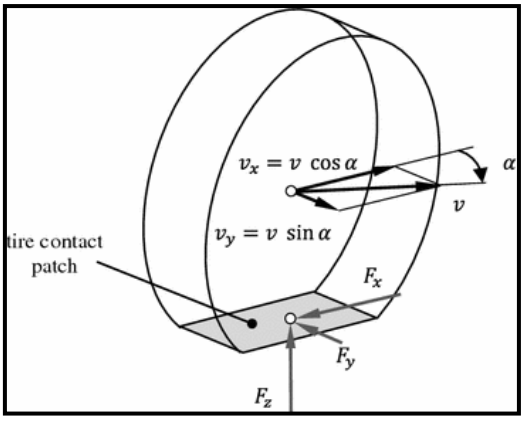

Figure 4 - Forces on the contact patch of the tyre [5]

Lateral and longitudinal forces developed by the tyres are dependent on the down force as well as the traction coefficient which is a tyre property. As the vertical down force increases the traction coefficient decreases. When the tyre loses contact with the road its down force decreases rapidly to zero, causing unexpected behaviour of the car (Figure 5). Once the tyre loses contact with the road, steering input on the tyre becomes useless causing the car to not go in the direction expected.

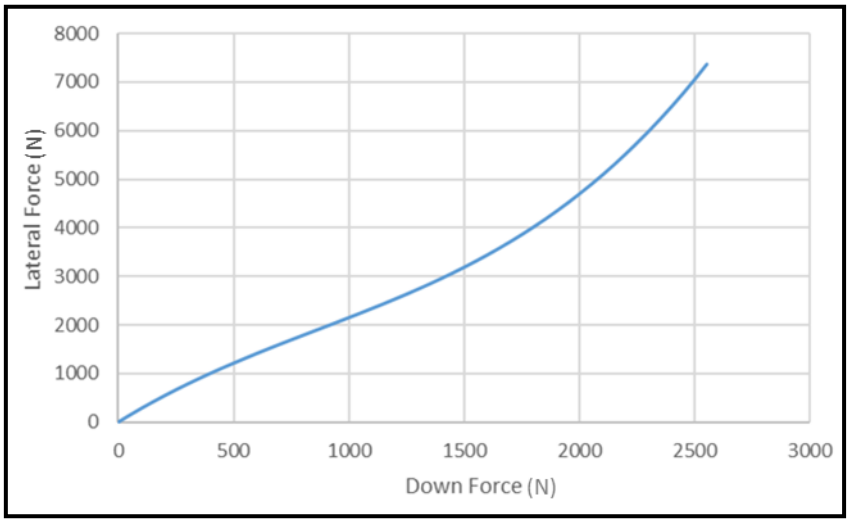

Figure 5 - Arbitrary graph of down force and lateral force

Looking at Figure 3, the left (inner) wheel can be seen to lean towards the right a lot more than the right (outer) wheel. This angle is known as camber and can be defined as the angle of the wheel to the horizontal (Figure 6).

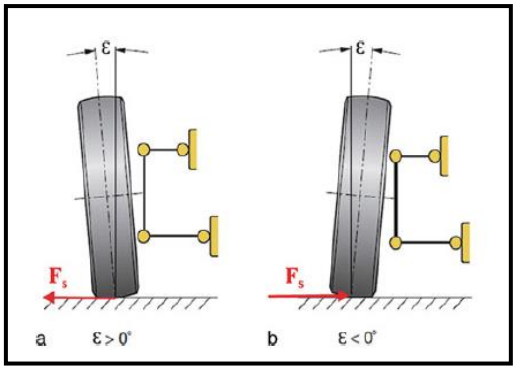

Figure 6 - Positive (a) and negative (b) camber [6]

One could conclude that camber is a negative property as the lean of the tyre reduces the area of contact of the tyre and the road. However, this is not entirely true when considering what happens to the tyre during cornering. Camber thrust is a force caused by the arc of the tyres contact patch trying to straighten when subjected to a lateral force (corner) [7]. The usually elliptical contact patch is forced into a more rectangular shape. If the tyre has negative camber, this force acts towards the inside of the corner, assisting the cornering. However, if the tyre has positive camber, the force will act towards the outside, resisting the cornering forces [8].

The first suspended vehicles built relied on a solid axle connecting the left and right wheels. When one wheel hit a bump, the other side was also affected, creating a dependant system (Figure 7).

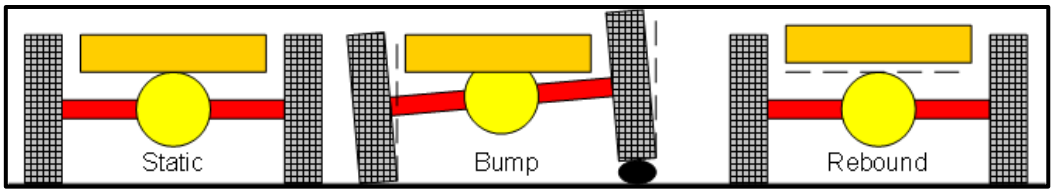

Figure 7 - Solid axle schematic [9]

This dependency results in the change of camber being the same for both sides, no matter where in the travel the suspension was. This has certain advantages when the road is smooth as the tyres wear consistently on both sides, however the main disadvantage is the loss of grip when the inner wheel hits a bump during a corner, rapidly changing camber resulting in a loss of grip. This is a great safety concern and was addressed with the development of independent suspension.

The focus of suspension has shifted over the years but an Formula 1 suspension still relies on the same principles as the first systems (Figure 8).

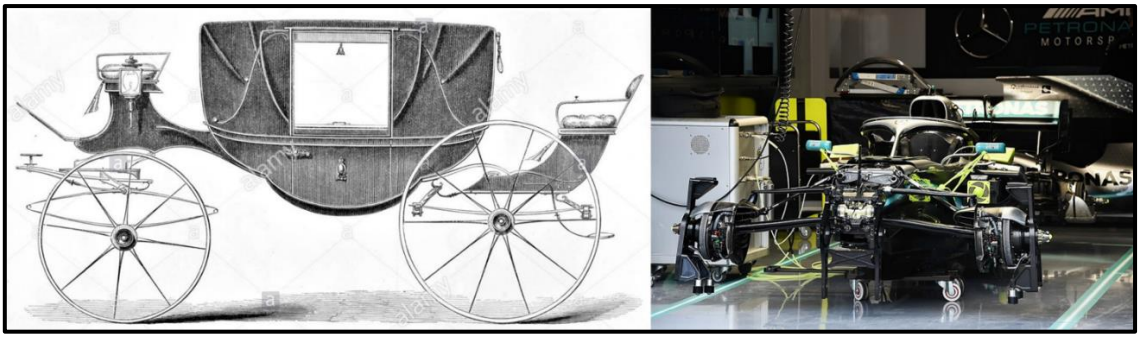

Figure 8 - Suspension systems on a carriage from 1890's and the Mercedes W10 F1 [10], [11]

But for many years after the first engine was introduced, the main focus in automotive development was engine power, while suspension with its many interrelated variables, remained virtually unchanged until the sixties in Britain and even the eighties with Ferrari. The biggest development was the shift away from a dependant solid axle suspension to an independent system, where one wheel can move without affecting the one on the opposite side of the car [12]. After the Second World War, commercial car racing took off and with it, the development of suspension systems. The shift was away from heavy and cumbersome leaf springs in both race and road cars to the MacPherson strut, which became widely used (Figure 9). The focus of the suspension system still was to provide a soft ride and comfort was key.

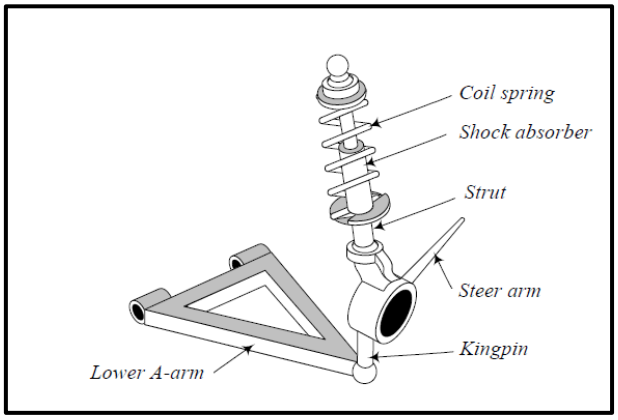

Figure 9 - MacPherson strut suspension [12 p. 466]

The true development of racing suspension came when John Cooper put the engine at the rear of the car and combined leaf springs with a double wishbone geometry as well as an antiroll bar to control the amount of roll. However, this resulted in a questionable geometry and a heavy suspension system. Colin Chapman (founder of Lotus Cars) pioneered the system that is still used in most sports cars to this day: the double wishbone geometry with a simple and lightweight coil spring (Figure 10).

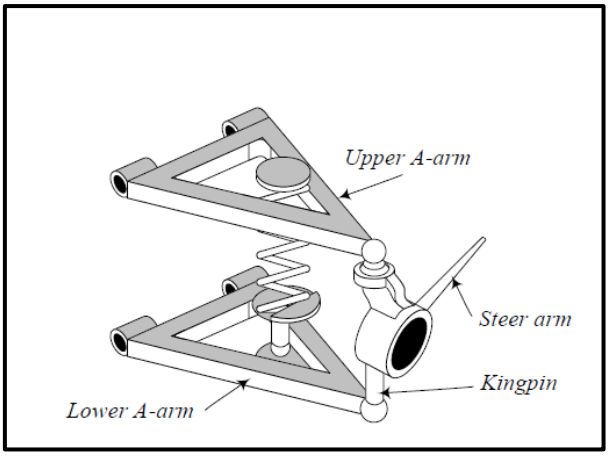

Figure 10 - Double wishbone suspension [12 p. 221]

In the initial design the top and bottom arms were parallel and of equal length as this resulted in no camber gain during a bump (Figure 11 a). However, the change in track (Δb) is large which results in an unfavourable change in driving behaviour. Furthermore, with this geometry, the roll centre location (the point about which the car rolls about in a corner) changes drastically resulting in an unexpected and sudden change in handling. By the end of the eighties, most competitive race cars utilized unequal length wishbones (Figure 11 b), coil springs with some kind of damper, and an antiroll bar as well as consideration for geometry of the arms and all the arcs they move through during travel [13]. With this geometry camber gain (Δε) during a pure bump is present but the change in track is small. Being able to position the arms however the designer wants to, allows for a geometry that minimises the camber gain or purposefully adds camber (usually more negative) to aid handling during corners.

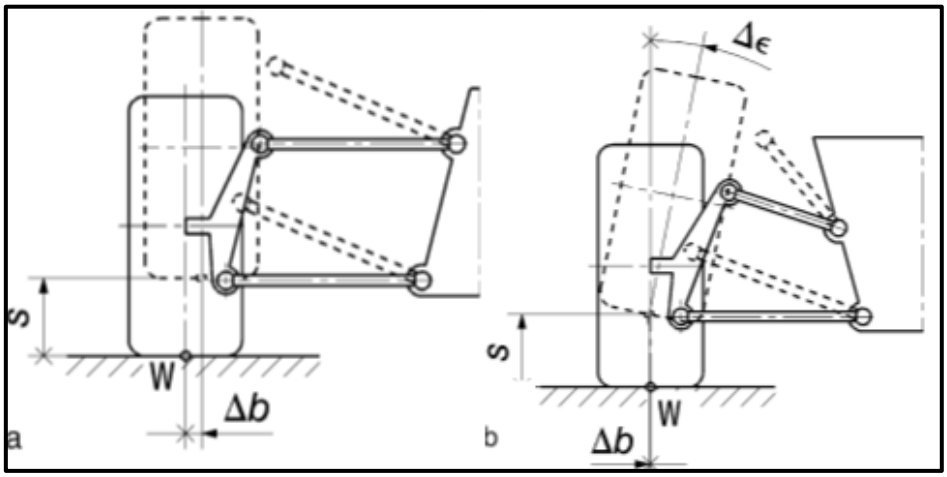

Figure 11 - a) Equal length, parallel wishbones b) Unequal length, non-parallel wishbones [6 p. 221]

These varied in execution (i.e. materials, attachment) but not in principle. The goals of a good suspension system have held valid for more than a quarter of a century and have been copied, adapted and developed over time but still are based on "…keeping the wheel and tyre vertical to the road

surface at all times, eliminating alterations caused by squat or nose-dive, road bumps or roll in corners and keeping the roll centre in one place and track constant." [13 p. 20]. To this day this applies for both road and race cars, although care has to be taken as to not eliminate load transfer completely as it allows feedback for the driver.

Further development and practical implementation of active suspension is currently underway. With a passive suspension, the wheel movement is dictated by the road surface whereas an active suspension controls the movement of the wheels relative to the chassis with the use of an onboard system [14]. The concept of an active suspension, creating the perfect smooth ride, has been around since 1954 when Citroën first put a hydropneumatic suspension on the rear axle of its DS19. With the development of electronic loop controllers, sophisticated sensors, and permanent magnetic materials, active suspension is becoming increasingly popular in supercars. However, development has been slow as many racing series have banned active suspensions and it is therefore limited to high end sport supercars due to its price and complexity [3].

Suspension development has mainly been focused on materials, actuation and tuning in the past years. With many racing series introducing engine displacement limits as well as aerodynamic limitations, suspension tuning is the most effective way to decrease lap times in racing [15].

2.2 Vehicle Dynamics

The suspension system of a car is essential for its performance and is therefore optimised specifically for race cars. There are three main reasons for the importance of the suspension system. The first one relates to the lateral and longitudinal forces developed in the tyres. These forces can only be utilised to their maximum potential if the tyres are always loaded and can follow the road surface. The springs and the damper in the suspension allow for this motion. The suspension system also allows for a certain degree of comfort while driving. While this is secondary to the performance of the race car, it is important especially for long races. Lastly, springs in the suspension system reduce the amount of impact energy transferred directly to the chassis allowing for a lightweight chassis. Furthermore, the suspension is the link between sprung and unsprung mass. Unsprung mass can be defined as the mass that is not supported by the spring, this includes the weight of the wheel, uprights and brake components. The mass that is supported by the spring is termed as sprung weight and includes the driver, chassis, engine and aerodynamic devices. As the unsprung mass cannot be controlled by the suspension, it is essential to minimise it to reduce inertia of the unsprung mass so the tyre can better follow the road to maximise controllability of the car.

2.2.1 Vehicle Movement

A vehicle can move around its three primary axes, the longitudinal (X), the lateral (Y) and the normal (Z) axis. Along each axis, there are two degrees of freedom, resulting in a six DOF system. Compression and rebound motion of the springs are caused by motion along these axes, termed rolling, pitching and yawing (Figure 12).

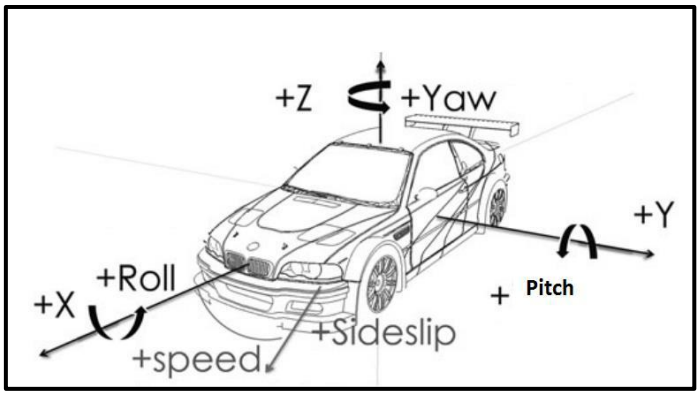

Figure 12 - Conventional automotive coordinate system [16 p. 28, (translated from German)]

Generally, two tyres rebound when the other two compress. An example of this is braking, a motion about the Y-axis, during which a load transfer occurs towards the front, due to an induced moment. This change in load causes the front springs to compress and the rear ones to rebound. A similar phenomenon can occur when driving through a curve. The outer wheels compress while the inner ones rebound, resulting in a rolling motion around the X-axis.

The motion about the Z-axis (yawing) can be used to diagnose under- and oversteer. As the name suggests, oversteer is the car's tendency to turn too much through a corner, often the driver describes this as the rear "kicking out", whereas during understeer the car tries to keep going straight rather than turn the corner (Figure 13). This type of behaviour is often related to the dynamic change in properties, for example camber gain and change in forces at the contact patch and is caused by excessive load transfer through rolling. Too much lateral force on the front axle or too little force on the rear tyres can cause the car to display over- and understeer. It is essential that the suspension minimises the occurrence of over- and understeer as both not only increase lap times but also are unpredictable for the driver creating a safety concern for high speed corners.

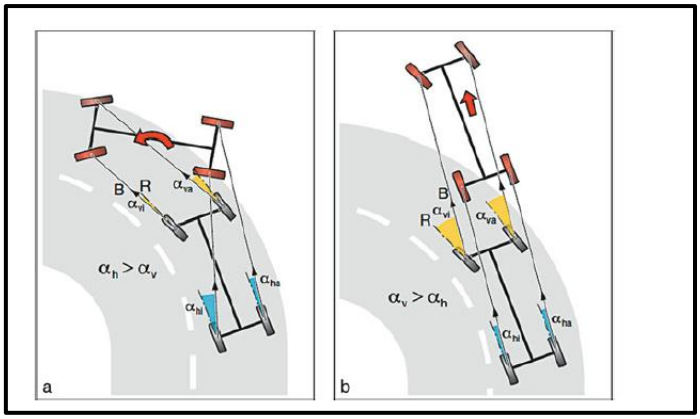

Figure 13 - Oversteer (a) and Understeer (b) [16]

If too much load transfer occurs, the wheels can lose contact with the road, resulting in slower lap times and therefore needs to be eliminated. In general, the suspension dictates how far a wheel compresses or rebounds, whereas the damper determines how fast the wheel undergoes this motion. Both can be tuned to optimise grip levels.

2.2.2 The five phases of a curve

A well-designed suspension is the key to being able to drive as fast as possible through a curve. It is therefore essential to understand the phases of a curve (Figure 14). Recognizing these phases enables design of a suspension capable of fast turning as well as making any necessary adjustments to the system by recognising under- and oversteer.

Phase 1: Initial turning

The driver brakes and starts to turn into the curve. The slip angle at the front wheels increases and the first lateral forces are developed. The Centre of Gravity (COG) and the back wheels are still in a straight motion.

Phase 2: Starting to roll

About one revolution after the initial turning effort, the front wheels are generating enough lateral force to cause the entire car to begin turning. The back wheels now also develop lateral forces. Centrifugal forces cause the sprung mass of the car to begin rolling. This results in the outer wheels compressing and the inner ones rebounding. If an antiroll bar is used, it starts to twist at this stage, restricting roll of the car.

Phase 3: Middle of the curve

Once centrifugal force has reached a maximum for the corner, constant rolling of the sprung mass begins. The car has reached a form of stability during this phase. However small disturbances like

steering or an uneven road surface will jeopardise that stability. The outer wheels are still under compression whereas the inner wheels are rebounded, so that the antiroll bar has twisted as far as will go for that particular corner.

Phase 4: Back rolling

As soon as the driver starts to turn out of the curve, lateral forces decrease and the sprung mass begins to roll back. It is most common that the driver will also start to accelerate again. All springs start to move back to their initial positions and thereby decrease the twist and effectiveness of the antiroll bar.

Phase 5: Finish turning

Depending on the driver, Phase 4 and 5 can become one. However, it can be useful to differentiate between the two phases, especially when looking at sensor data. Due to the acceleration, the load transfer towards the back increases. This longitudinal load transfer combined with the loads on inner wheels still being less than static (rolling motion), can cause a “power understeer” by the front inner tyre loosing contact to the road surface. [16]

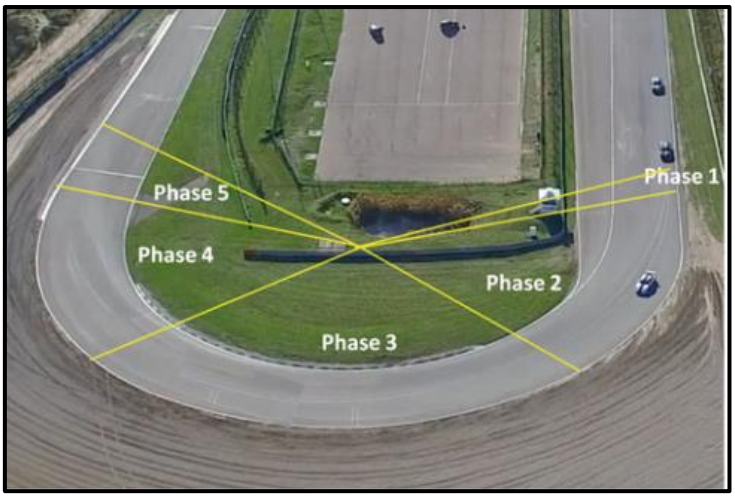

Figure 14 - The five phases of a curve [16 p. 30]

2.2.3 Tyres

The focus of the suspension is to transmit loads developed in the tyres to the chassis. To design a suspension system that can withstand these loads it is essential to start at the point of development of these forces, the tyres. These forces are created by the elasticity of the tyres and are therefore dependant on the compound of rubber used and tyre pressure. The tyre can be thought of as a six degrees of freedom system (Figure 15).

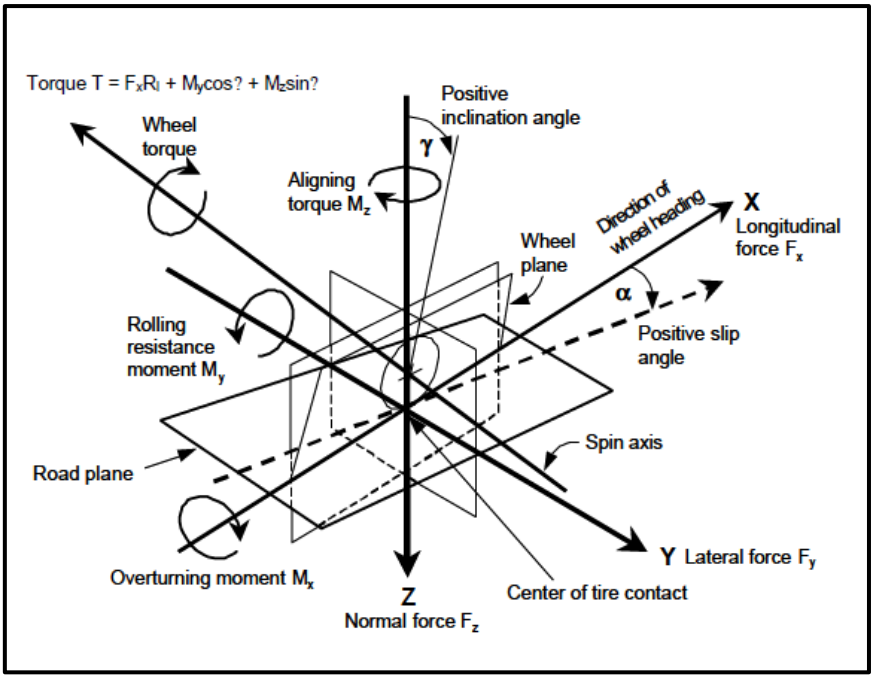

Figure 15 - Forces and moments created at the tyre [17]

The vertical load or normal load (F_Z) is the force acting on the tyre in a direction perpendicular to the road [15]. This force incorporates both static and dynamic parts. Static vertical loads include the mass not dynamically controlled by the suspension, termed the unsprung mass. This mass includes the weight of the tyre, upright and the A-arms. Dynamic loads include the load transfer of the sprung mass (i.e. mass controlled by the suspension) created by rolling and pitching movement [17].

Each tyre has a coefficient of traction (or friction, μ) [18] which can be used to obtain the maximum lateral and longitudinal force the tyre can generate before slipping. Experiments performed by Milliken Research in the Tire Test Consortium can be used to obtain a value for the traction coefficient in the lateral and the longitudinal direction based on vertical load on the tyre (Figure 16).

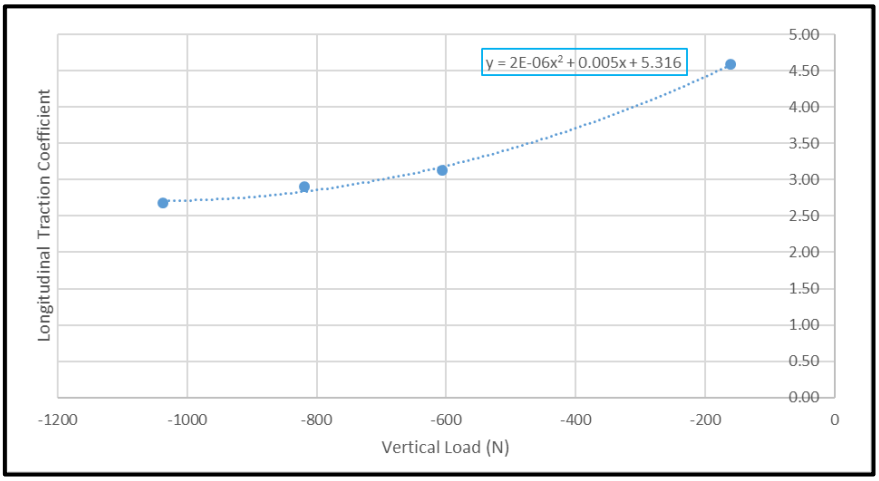

Figure 16 - Arbitrary example of the effect of vertical load on longitudinal traction coefficient

The friction equations (1) and (2) can then be used to calculate the expected lateral and longitudinal loads (F_{Lat} and F_{Long}).

$$F_{Lat} = F_Z * \mu_{Lat} \quad (1)$$

$$F_{Long} = F_Z * \mu_{Long} \quad (2)$$

Knowing the maximum lateral and longitudinal forces the tyre is capable of developing helps the driver to push the car to its maximum potential during cornering.

2.2.4 Slip Angle

Slip angle (α in Figure 15) is defined by Smith as "the angular displacement between the plane of rotation of the wheel and the path that the rolling tyre will follow on the road surface" [15 p. 14]. As the car goes around a corner, lateral forces start developing in the tyres contact patch with the road. This force will cause the surface of the tyre to deform towards the inside of the corner. The slip angle can be defined as the angle between the deformed contact patch and the direction of the rolling wheel (Figure 17).

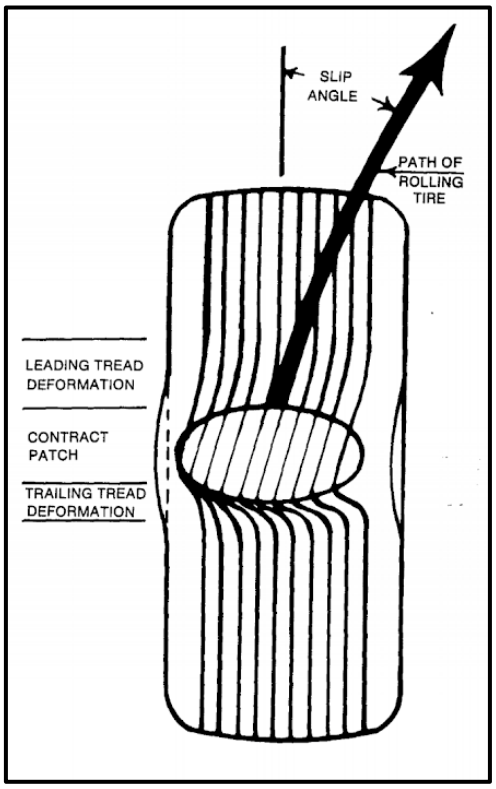

Figure 17 - Tyre Slip Angle [15 p. 14]

The traction coefficient is dependent on slip angle and the cornering forces the tyre is capable of producing therefore also depend on the slip angle [15 p. 15]. Initially the coefficient increases linearly

with slip angle until reaching a maximum at which point too much slip has occurred and the tyre cannot support the load anymore and starts to slide (Figure 18).

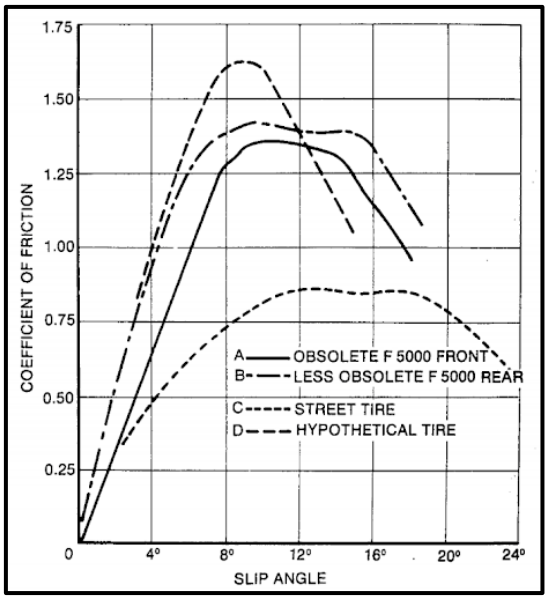

Figure 18 - Relationship between slip angle and traction coefficient [15 p. 15].

2.2.5 Camber

One of the most common ways to affect driving behaviour is setting the static camber. As mentioned before, the tilting of the wheel and tyre along the y-axis creates positive or negative camber (Figure 19).

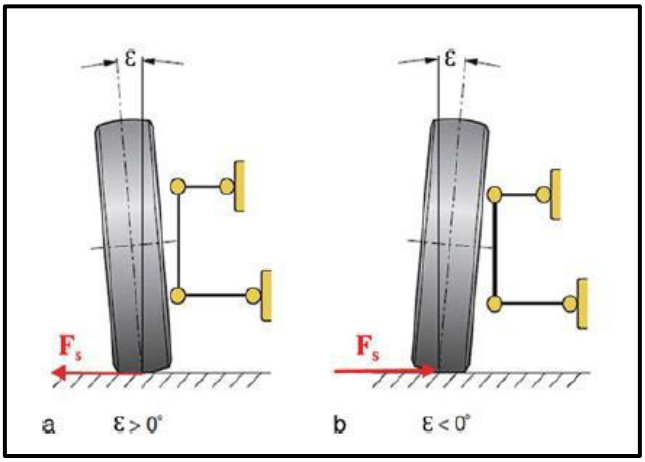

Figure 19 - Positive (a) and negative camber (b) [6 p. 13, 16]

A negative camber reduces the deformation on the sidewall of the tyre thereby increasing the lateral forces transmitted as well as creating a more even temperature and wear across the tyre. The temperature and the wear of a tyre can therefore be used to investigate if the camber setup is ideal (Table 1). However, camber can dynamically change depending on the steering and suspension setup.

Large changes in camber will lead to a change in behaviour of the car that the driver is not able to predict.

In an ideal scenario the tyre is loaded equally through its entire width, creating an even temperature distribution and maximising the size of the contact patch and thereby the grip. A temperature difference indicates that the tyre is loaded unequally due to too much or too little camber and the grip can be improved by simply creating a larger contact between the tyre and the road.

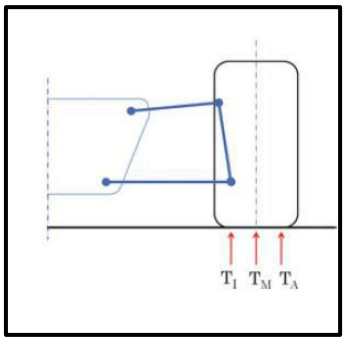

Figure 20 - Measured temperatures [16 p. 110]

Table 1 - Temperature analysis as a means to evaluate camber, tyre pressure and toe [16 p. 110]

Inner	<	Middle	<	Outer	Too little camber or too much toe out
Inner	<	Middle	>	Outer	Tyre pressure too high
Inner	<	Middle	=	Outer	Too little camber or tyre pressure too high, too much toe out
Inner	>	Middle	<	Outer	Tyre pressure too low
Inner	>	Middle	>	Outer	Too much camber or too much toe in
Inner	>	Middle	=	Outer	Too much camber or tyre pressure too low, too much toe in
Inner	=	Middle	<	Outer	Too little camber or tyre pressure too low, too much toe out
Inner	=	Middle	>	Outer	Too much camber or tyre pressure too high, too much toe in
Inner	=	Middle	=	Outer	Ideal settings

2.2.6 Load Transfer

The Society of Automotive Engineers (SAE) defines load transfer as “The vertical load transfer from one tyre to another that is due to accel eration, rotational or inertial effects in either the lateral or longitudinal direction” [19 p. 31]. Since it is not possible to have the centre of gravity (COG) on the road surface, load transfer will occur. The COG of the car is the point (in 3D space) that all reaction forces during acceleration (any direction) are assumed to act about. When a force is induced on the

COG it creates a moment between the wheels on the road surface. This moment is converted to a force on each wheel, termed load transfer.

In the longitudinal direction, load transfer is initiated by a force due to acceleration or braking. Under braking, this force (acting through the COG) creates a moment which increases the load on the front wheels thereby reducing the load at the rear. The increase in load at the front results in better grip and therefore better braking at the front, however has the opposite effect on the rear, making accidental brake locking a greater possibility [3].

The derivation of these formulas can be demonstrated by the use of an example (Table 2).

Table 2 - Arbitrary variable values

Mass	m	200	kg
Wheelbase	l	1.5	m
Acceleration	a_x	1	g
Acceleration	a_x	9.81	m/s^2
CG Height from Road Surface	h_{COG}	0.2	m
COG Distance from front of vehicle	a	0.9	m
COG Distance from rear of vehicle	b	0.6	m
Force due to Gravity	g	9.81	m/s^2
Wheel Track	t	0.8	m
Lateral Acceleration	a_y	0.5	g
Lateral Acceleration	a_y	4.905	m/s^2

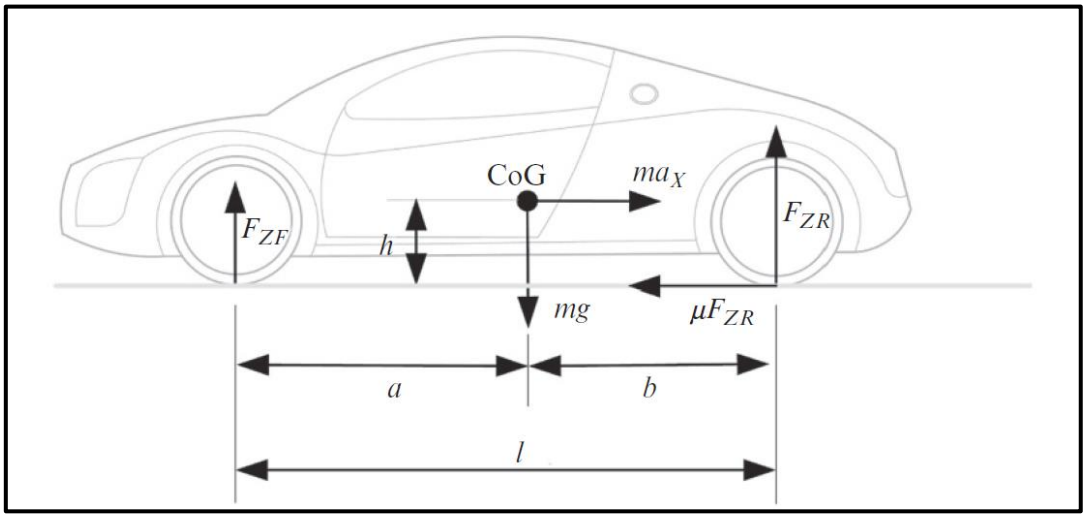

Figure 21 - Free body diagram for longitudinal load transfer [7 p. 54]

From the values given, static forces on each wheel can be calculated based on a force/moment equilibrium.

$$F_{Z,static,Front} = mg\frac{b}{l} \quad (3)$$

$$F_{Z,static,Rear} = mg\frac{a}{l} \quad (4)$$

$$F_{Z,Static,Front} = 200 * 9.81 * \frac{0.6}{1.5} = 784.8N = 80\ kg$$

$$F_{Z,Static,Rear} = 200 * 9.81 * \frac{0.9}{1.5} = 1177.2N = 120\ kg$$

If we assume a constant longitudinal acceleration of 1 g (acceleration) an equation for the increase in force can be found by taking the sum of moment about the front tyre contact.

$$\sum M = 0 => -F_{Z,Dynamic,Rear} * l + mg * a + ma_x * h_{CoG} = 0$$

$$\Rightarrow F_{Z,Dynamic,Rear} = \frac{ma_x * h_{CoG} + mg * a}{l} = F_{Z,Static,Rear} + ma_x * \frac{h_{CoG}}{l} \quad (5)$$

$$F_{Z,Dynamic,Rear} = 1177.2 + \frac{0.2}{1.5} * 200 * 9.81 = 1438.8N = 146.67kg$$

$$F_{Z,Dynamic,Front} = 784.8 - \frac{0.2}{1.5} * 200 * 9.81 = 523.2N = 53.33kg$$

It can be seen that the formula for the load transfer to the front is the same just with the opposite sign (i.e. subtraction). This example shows how drastic the change in load during acceleration can be and it should not be neglected. During braking, the load transfer will be towards the front and the formula should be adapted accordingly.

Lateral load transfer is slightly more complicated to calculate although it relies on the same principal. Lateral load transfer can be split into three components; the effect of the unsprung mass, the sprung mass and the geometric component (Figure 22).

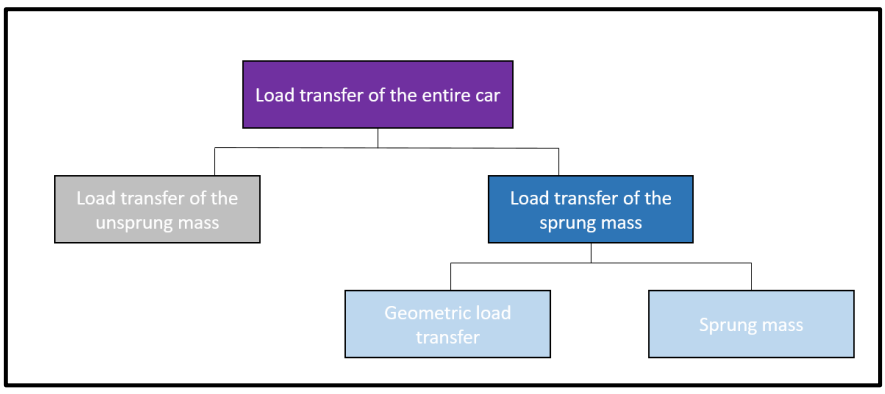

Figure 22 - Components of lateral load transfer

When considering the lateral forces, it is essential to keep in mind that the action force is always developed in the tyres (i.e. lateral force) whereas the reaction force always acts through the COG (i.e. centrifugal force). In most cars the COG is in the middle of the car, from a lateral point of view, as to not create any pull towards the left or the right. Both the sprung mass and geometric components depend on the height of the roll centre, whereas the unsprung component is dependent on the height of the COG. SAE defines the roll centre as "The point in the transverse vertical plane through any pair of wheel centres at which lateral forces may be applied to the sprung mass without producing suspension roll" [20 p. 293]. In simpler terms, it is the point about which the car rolls. This point is dependent on the suspension geometry and therefore can be different for the front and rear. The axis connecting those two points is called roll axis. As the suspension moves through its rebound and compression motions the roll centre location might change vertically as well as laterally [4]. The total load transfer of the car can be calculated by using the sum of moments in the front view of the car (Figure 23).

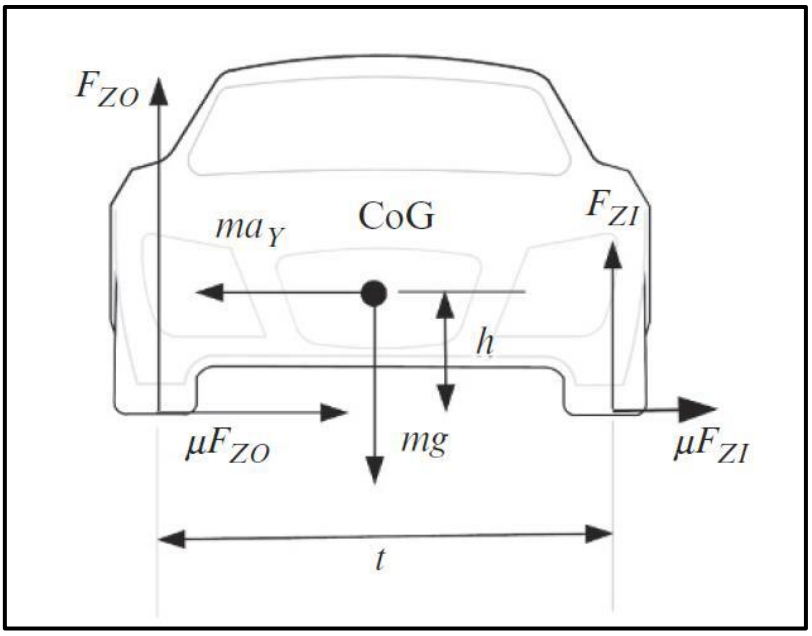

Figure 23 - Free Body diagram of a car accelerated laterally [7 p.56]

$$\sum M = 0 => F_{Z,O} * t - mg * \frac{t}{2} - ma_Y * h = 0$$

$$F_{Z,O} = \frac{mg}{2} + \frac{ma_Y * h}{t} \quad (6)$$

This equation however can only be used to calculate the overall load transfer of the car. It is often interesting to know how much of this load transfer comes from the front and rear. To do this, the overall load transfer has to be split into its components.

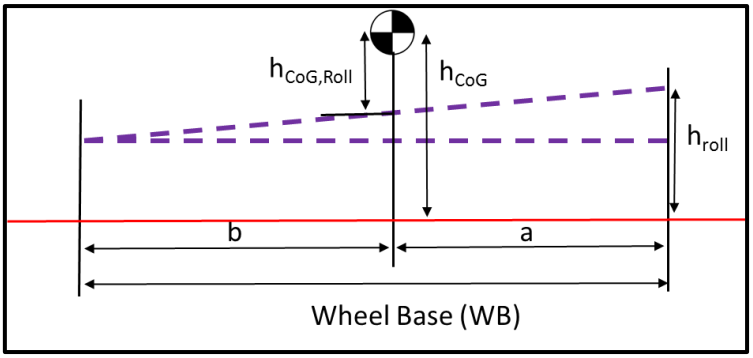

Figure 24 - Roll centre geometry

$$\Delta m_{unsp,F} = \frac{m_{unsp,F} * h_{unsp,CoG,F} * a_{lat}}{track_F} \quad (7)$$

$$\Delta m_{geo,F} = \frac{m_{sprung,F} * h_{roll,F} * (\frac{a}{WB}) * a_{lat}}{track_F} \quad (8)$$

$$\Delta m_{sprung,F} = \frac{m_{sprung,tot} * h_{CoG,Roll,F} * a_{lat}}{track_F} * q \quad (9)$$

The effect the sprung mass has on the load transfer depends on the roll stiffness ratio of the front and rear (q). The roll stiffness ratio is often chosen during suspension design and should therefore be known; alternatively it can be calculated with roll gradients (10).

$$q = \frac{K_{roll,F}}{K_{roll,F} + K_{roll,R}} = \frac{RollGradient_R}{RollGradient_R + RollGradient_F} \quad (10)$$

The load transfer for the rear axle can be calculated in the same way by swapping ‘a’ and ‘b’ as well as replacing ‘q’ with ‘(q-1)’. The total load transfer for each axle can be calculated by the sum of the three components

$$\Delta m_{total,F} = \Delta m_{unsp,F} + \Delta m_{geo,F} + \Delta m_{sprung,F} \quad (11)$$

$$\Delta m_{total,R} = \Delta m_{unsp,R} + \Delta m_{geo,R} + \Delta m_{sprung,R} \quad (12)$$

It is important to note that the unsprung load transfer cannot be measured by potentiometers or load cells applied to the suspension of a car as the mass is not supported by the suspension. However, it still needs to be accounted for when considering tyre forces. Similarly, the geometric transfer can also not be measured directly but rather is applied directly to the tyre contact patch. This means that only the sprung mass affects shock position.

Many vehicle dynamic tutorials online define lateral load transfer simply as in Equation (6) and stop there ([21] and [22]), leaving a misconception that load transfer does not depend on spring rates or antiroll bar stiffness. In reality the three components mentioned above (geometric, sprung and unsprung) all affect the load transfer distribution on one axle and should not be overlooked [3]. Figure

25 shows a comparison between the lateral load transfers calculated using equation (6) and using the components from equations (7) to (9). For both calculations change in COG and roll centre height based on setup changes was neglected. It can be seen that when the antiroll bar is not connected the difference between components and overall calculations makes almost no difference (7 N between total lateral load transfers). The small difference is due to the components method looking at front and rear separately, i.e. difference in track and COG height. Whereas the overall method uses averages of track and COG heights. However, the difference becomes noticeably larger once the ARBs are connected at the middle for both front and rear (24 N). It is interesting to note that for both cases the overall method showed more load transfer than the components calculation. Mixing the ARB settings for front and rear (front soft, rear stiff) shows a large increase in discrepancy between the load transfers (77 N). However, using the components now yields a larger load transfer.

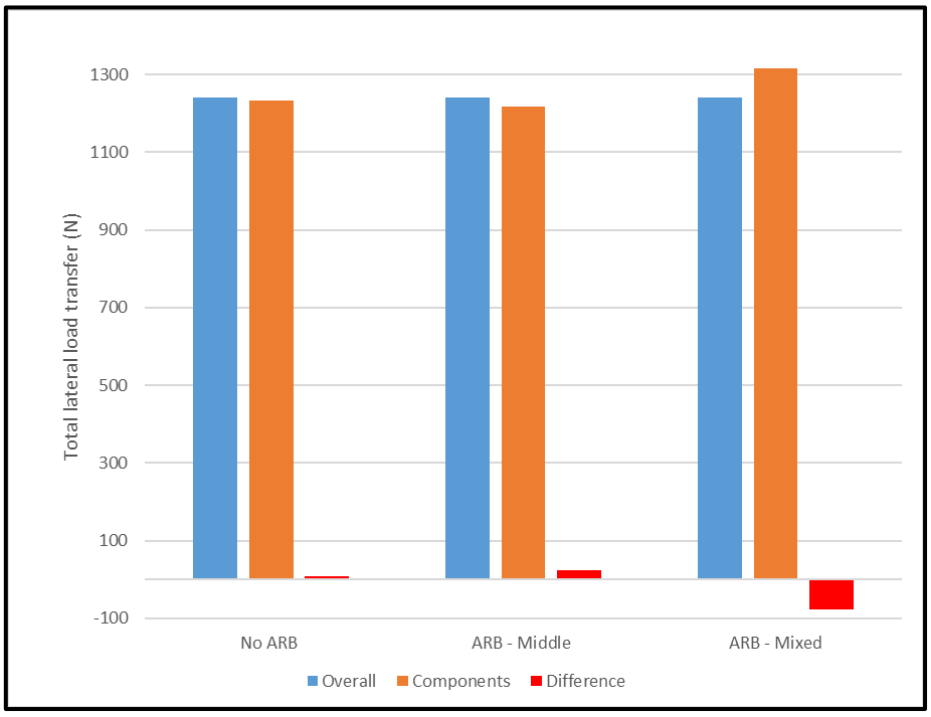

Figure 25 - Comparison between component and overall lateral load transfer

2.2.7 Antiroll Bar (ARB)

As discussed in section 2.2.6 load transfer is something that cannot be avoided and only be controlled. As the car negotiates a corner the weight of the car is transferred from all four wheels towards the outer wheels. If this transfer becomes too large, the body roll is such the inside spring is extended to a point from which it cannot extend anymore and once the down force on the inner wheel decreases enough, the wheel lifts off the ground.

Antiroll bars can be installed to counteract the rolling moment created, keeping weight on the inner wheels, preventing jacking. An antiroll bar acts as a torsional spring activated when one of the wheels

rebounds while the other one on the same axle compresses. Hence an antiroll bar has no effect on longitudinal load transfer during acceleration and braking. The W-FS18 car has adjustable antiroll bars at the front and the rear (Figure 26 and Figure 27). The effective stiffness of the ARB can be adjusted by changing the lever arm (labelled A in Figure 27). The design of the W-FS18 car does not allow the driver to make adjustments while driving but has to be made in the pit lane before a race.

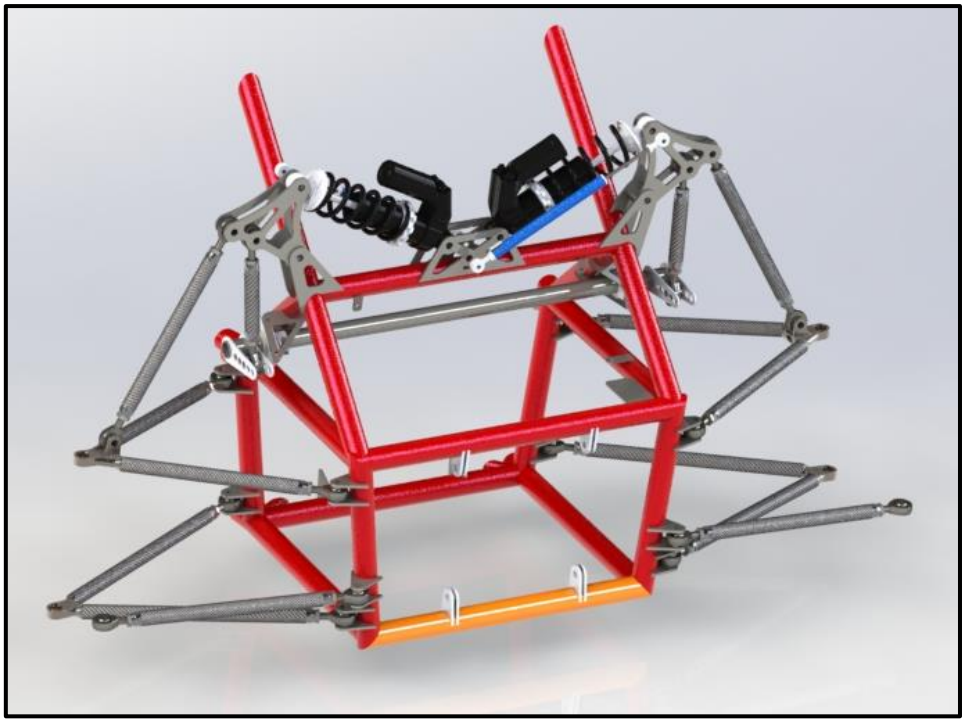

Figure 26 - Antiroll bar at the rear of W-FS18

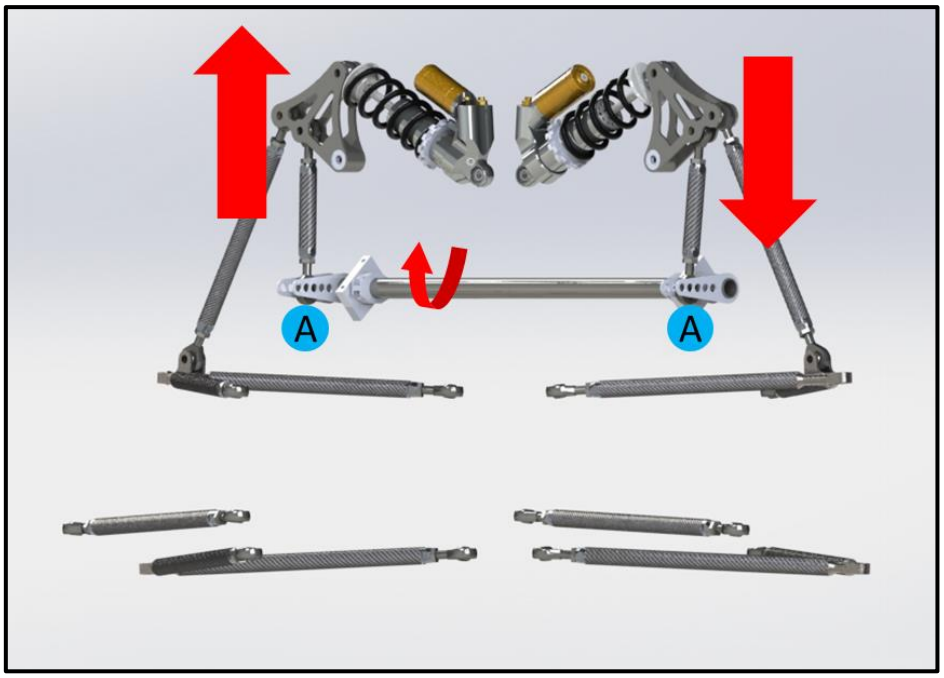

Figure 27 - Working of an antiroll bar

Figure 28 shows the difference in suspension travel for when the antiroll bar is connected (orange line) compared to it is not attached (blue line). It can be seen that when the ARB is not connected the wheel is much closer to being lifted off the ground. However, care needs to be taken as to not eliminate roll behaviour completely, as this will provide no feedback to the driver and make the car too stiff. This will result in the car behaving as it would have a solid axle, making suspension ineffective and levering the inner wheel off the ground regardless.

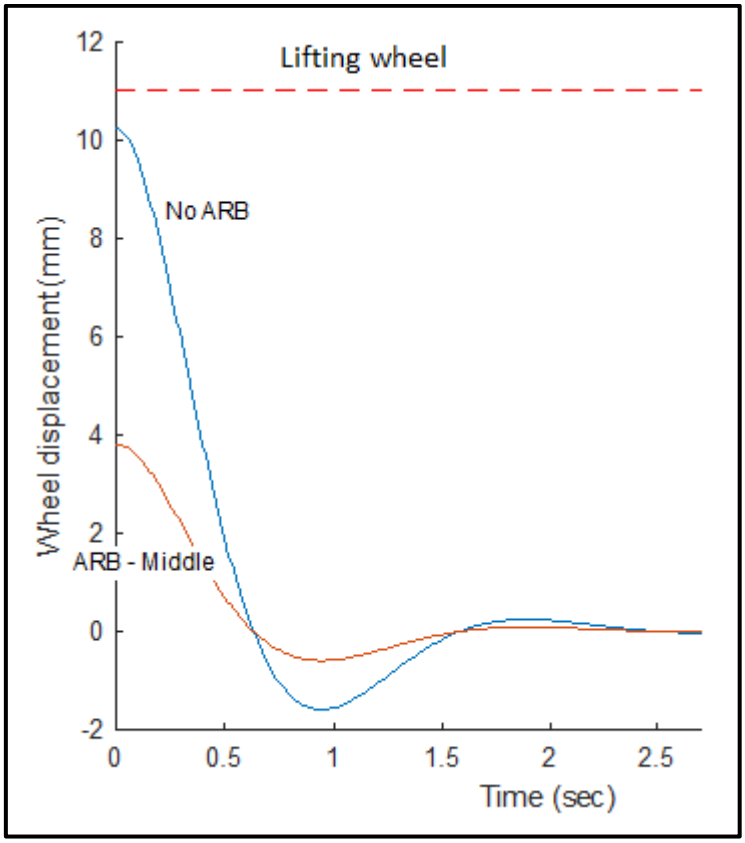

Figure 28 - Suspension travel with and without ARB

2.2.8 Roll Centre

The forces that develop in the tyres are transferred via the wheels, uprights and A-arms to the chassis. The roll centre can be defined as the imaginary point which the car rolls about. The position of the roll centre is highly influenced by the suspension geometry and therefore often varies between the front and the rear of the car. The imaginary line connecting the two centres is termed roll axis [4]. The position of the roll centre can be found by drawing two lines in line with the wishbones, the point at which the two lines meet is termed the instantaneous roll centre (MP). The tyre moves about the instantaneous roll centre so it is connected to the middle of the contact patch of the tyre by another line. Repeating this process for the other side, the roll centre is located at the intersection of the lines that go from the contact patch to the instantaneous roll centre. If the static roll centre is investigated

and the left and right hand suspension setup and weight distribution are the same, it is sufficient to do this for one side as the roll centre will then be located in the middle of the car (Figure 29).

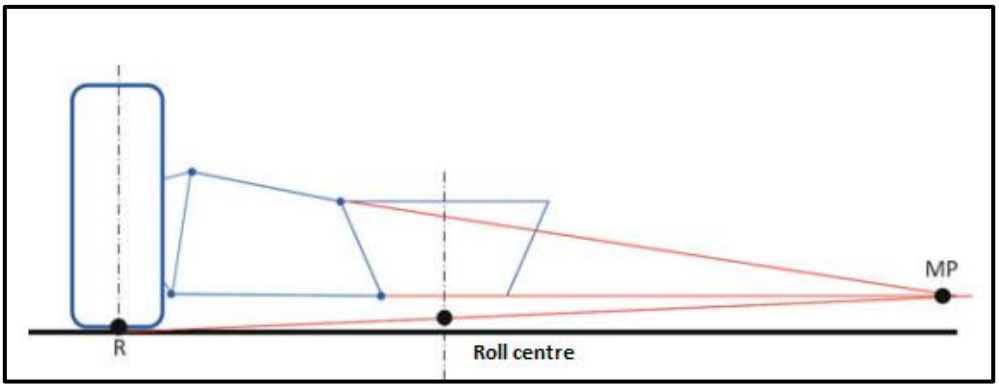

Figure 29 - Roll centre location for a double wishbone geometry

As the suspension compresses and rebounds a change in roll centre position will occur. If a suspension geometry is designed without consideration for this, the change might be large and the resulting change in handling behaviour can be sudden and unexpected. Care needs to be taken to minimise the movement of the roll centre as to avoid situations where the roll centre moves below the ground or above the centre of gravity as to not affect the loading scenario on the tyres unfavourably. In Figure 30 it can be seen that both the geometric (orange) and the sprung (grey) part of the load transfer are affected by the change in roll centre. Only the unsprung (blue) part of the lateral load transfer is unaffected by the location of the roll centre.

When the roll centre coincides with the centre of gravity, the sprung part of the load transfer becomes zero and geometric load transfer becomes maximum. However, this geometry is to be avoided as it creates no load transfer that is translated through the springs resulting in no rolling of the car as both the sprung and unsprung load transfers are directly applied to the tyres (i.e. no suspension deflection). This means that there is no feedback for the driver and it makes the car hard to drive as it feels like the car reacts unexpectedly to driver input. When the roll centre is on the ground, the geometric load transfer becomes zero. An interesting phenomenon occurs when the roll centre moves below the ground, the geometric load transfer becomes negative, whereas the sprung load transfer becomes maximum, creating a large rolling effect. With both of these scenarios, the load at the tyre is unfavourably influenced to reduce grip and should be avoided.

It can be noted that in this study the roll centre was not placed above the centre of gravity, as this is not a feasible option as this would reverse the direction of roll, resulting in a virtually undriveable car (Figure 31).

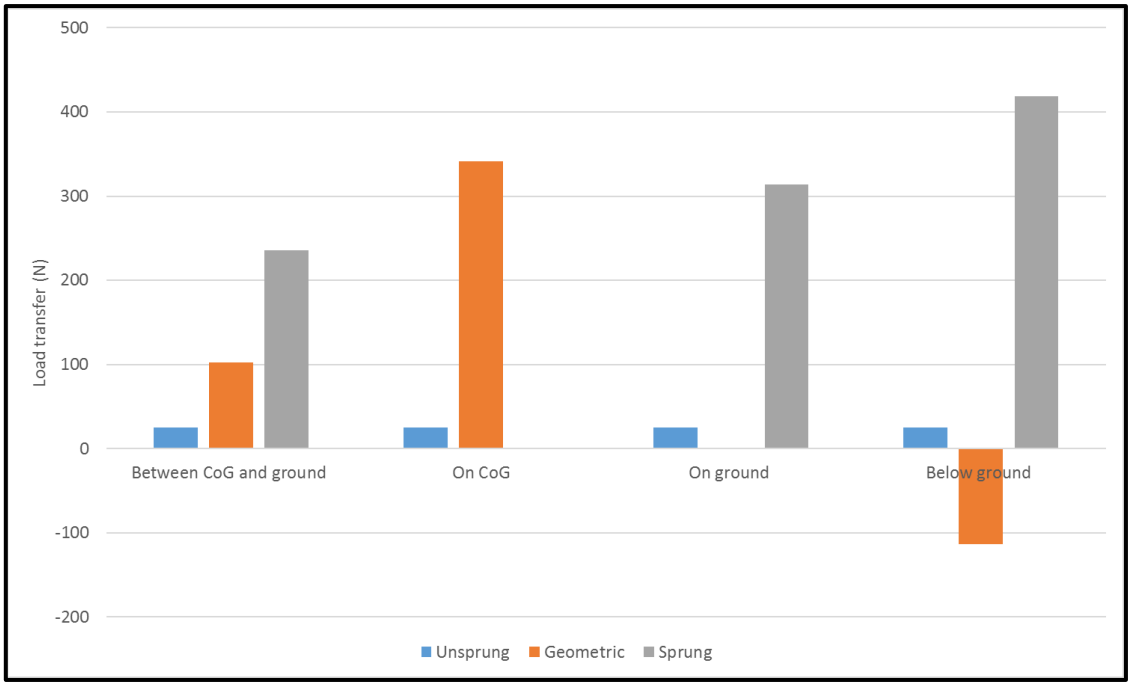

Figure 30 - Load transfer based on location of roll centre

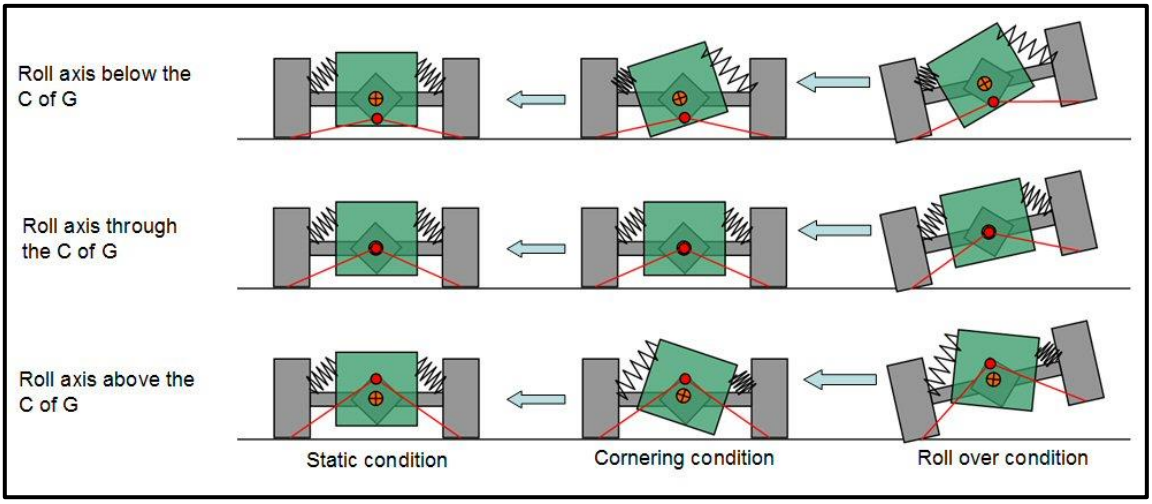

Figure 31 - Rolling behaviour for different roll centres [23]

Many cars often have a different roll centre height at the front and rear of the car. This is often due to geometric and packaging constraints, however, it can be designed to aid cornering behaviour. For a high roll centre (i.e. closer to COG of the car), the sprung part of the load transfer decreases. As previously mentioned, this is the only part of the load transfer that affects shock position and therefore body roll angle. A smaller roll angle at the rear means less positive camber gain, allowing for car yaw to generate more slip angle at the rear [3 p. 20], decreasing the chance of understeer [24]. Furthermore, as the rear tends to be heavier for race cars (engine at the rear), it is essential to reduce the amount it rolls as to avoid overloading the front outer wheel from load transfer from the rear to the front during body roll (through chassis twist, assuming an infinitely stiff chassis) [13] [25].

2.2.9 Spring and Dampers

Spring stiffness dictates the extent of movement e.g. roll, dive or squat, the chassis experiences (or how much compression or extension the suspension experiences) for an applied force, whereas the dampers influence the rate at which this change happens. For a number of years the Öhlins TTX25 shocks have been used by the team. These are mountain bike shocks designed for FSAE use with four way adjustable dampers. This means that high and low speed damping rates can be set independently for rebound and compression (Figure 32). A number of different spring rates are available and preload can be freely adjusted. In all following graphs spring rate is displayed in pounds per inch (lbs/in) as that is the convention in the automotive industry.

Figure 32 - Öhlins TTX25 [26]

The stiffer the spring, the less the spring deflects for a given force (Figure 34). As mentioned before, the car should have some movement (roll, squat and dive) to provide feedback to the driver as well as allowing for better contact between the tyre and the road over uneven surfaces. If the spring becomes too stiff, the car will effectively have no suspension, turning it into a go-kart. A common issue with go-karts is wheel lift as they have a solid axle not allowing the tyre to follow the road nicely and a small disturbance or bump will cause the tyre to lose contact with the road (Figure 33). However, too much movement will also cause the car to lose traction unnecessarily due to too much rolling.

Figure 33 - Go-Kart with no suspension

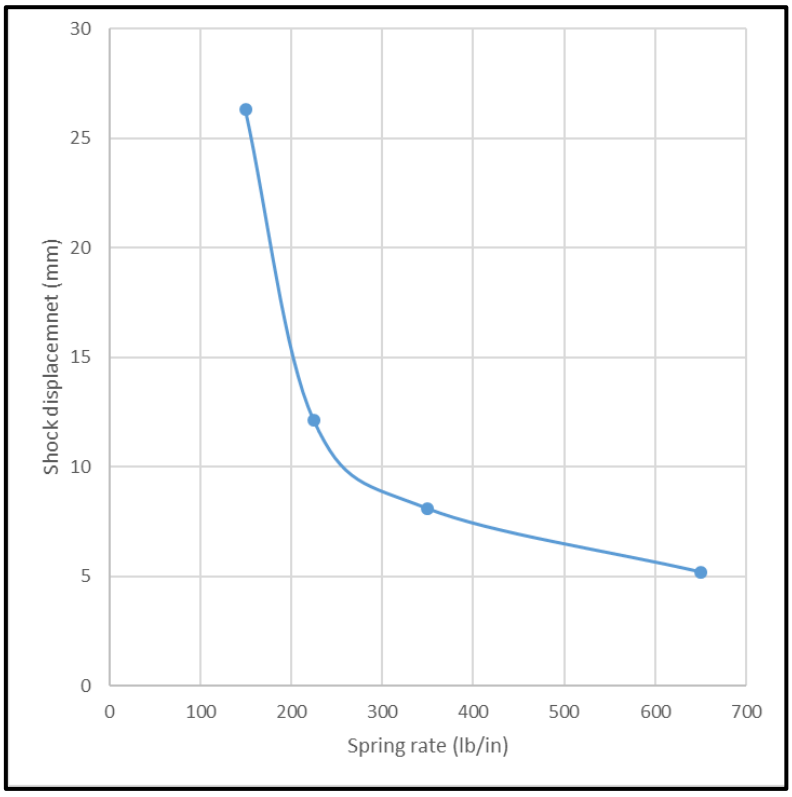

Figure 34 - Arbitrary suspension travel for different spring stiffness's in a 1.8g corner

Hydraulic dampers are most commonly used in racing as they can be specifically tuned depending on the track. Most dampers either have a single tube (monotube) or two (twin tube) (Figure 35). Both utilize a piston pushing damper fluid (most commonly oil) through valves which in turns pushes against a high pressure gas (often nitrogen). These valves can be adjusted depending on the complexity of the damper. Racing dampers are most commonly four way adjustable, meaning they have adjustments for high and low speed compression and rebound strokes.

Monotube dampers were invented in the 1950s and are longer than a twin tube design and a floating piston separates the oil from the gas in a single tube. As the suspension compresses, the piston pushes against the oil and the oil is forced through valves in the piston itself. Twin tubes are easier to manufacture and are more commonly used as a result [27].

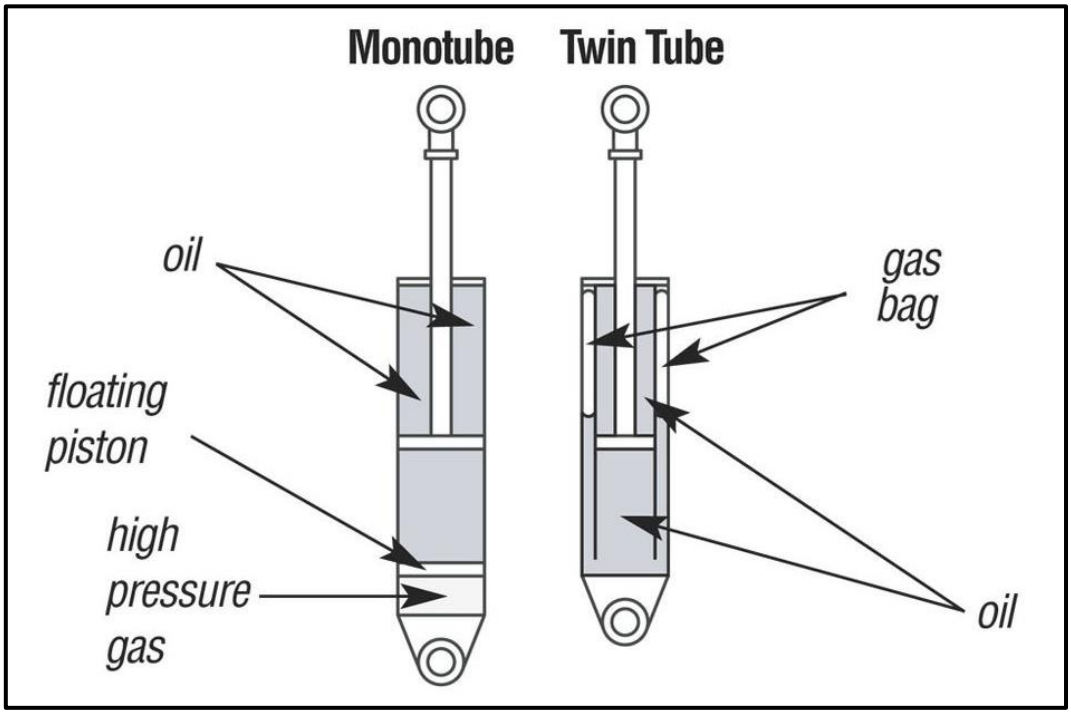

Figure 35 - Mono vs Twin tube damper design [27]

A schematic of a twin tube damper during a high speed compression (red flow) and rebound (blue flow line) strokes can be seen in Figure 36. As the suspension compresses, the piston forces oil from the inner tube into the outer one through a valve. As the suspension rebounds, the oil is sucked back into the inner tube through a different valve. The valve that opens depends on the speed of the input, i.e. low or high speed piston speed [27].

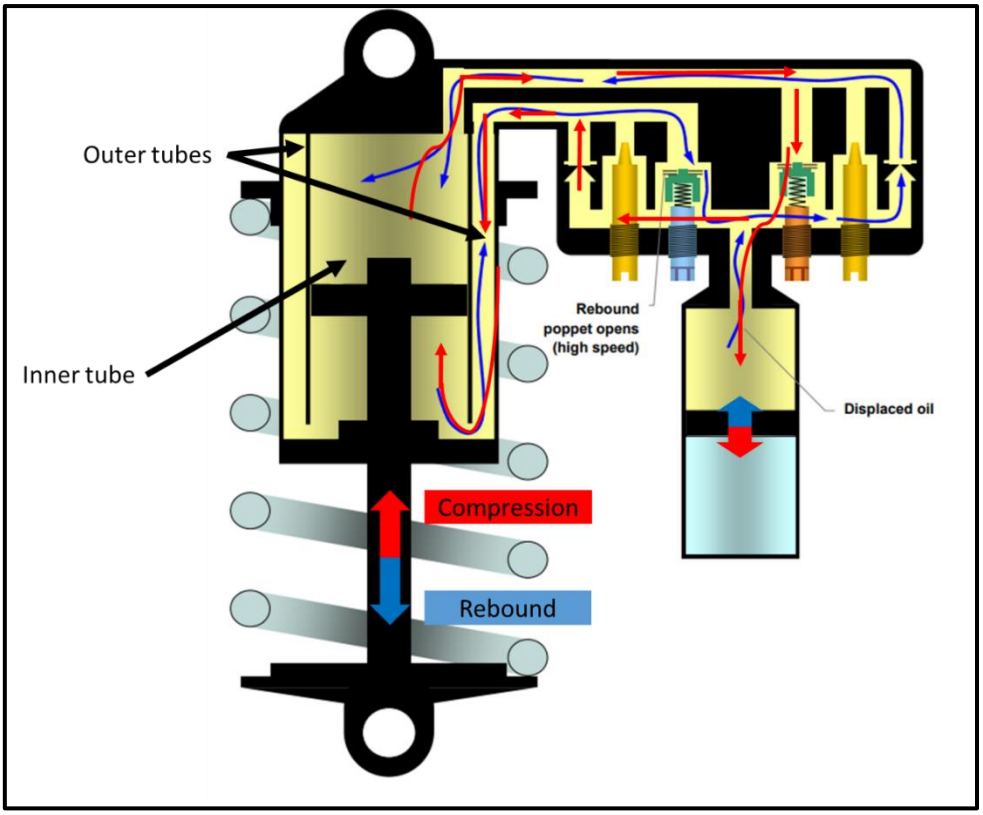

Figure 36 - Flow for a high speed compression (red) and rebound (blue) stroke in a twin tube damper [26]

Damping rates can be adjusted by changing the allowed flowrates through the valve. However, care has to be taken when damping rates are chosen as to not allow the system to be under or over damped (Figure 37). The damping ratio, Zita, is defined as the ratio between the chosen damping rate and the critical damping rate of the system. An undamped system (Zita=0) will theoretically oscillate forever (assuming no friction), whereas a critically damped system (Zita=1) will not oscillate at all. Both cases are not ideal as an undamped system will cause too much movement of the car and the other will not allow any feedback for the driver about how the car is behaving (i.e. the shock and suspension do not move).

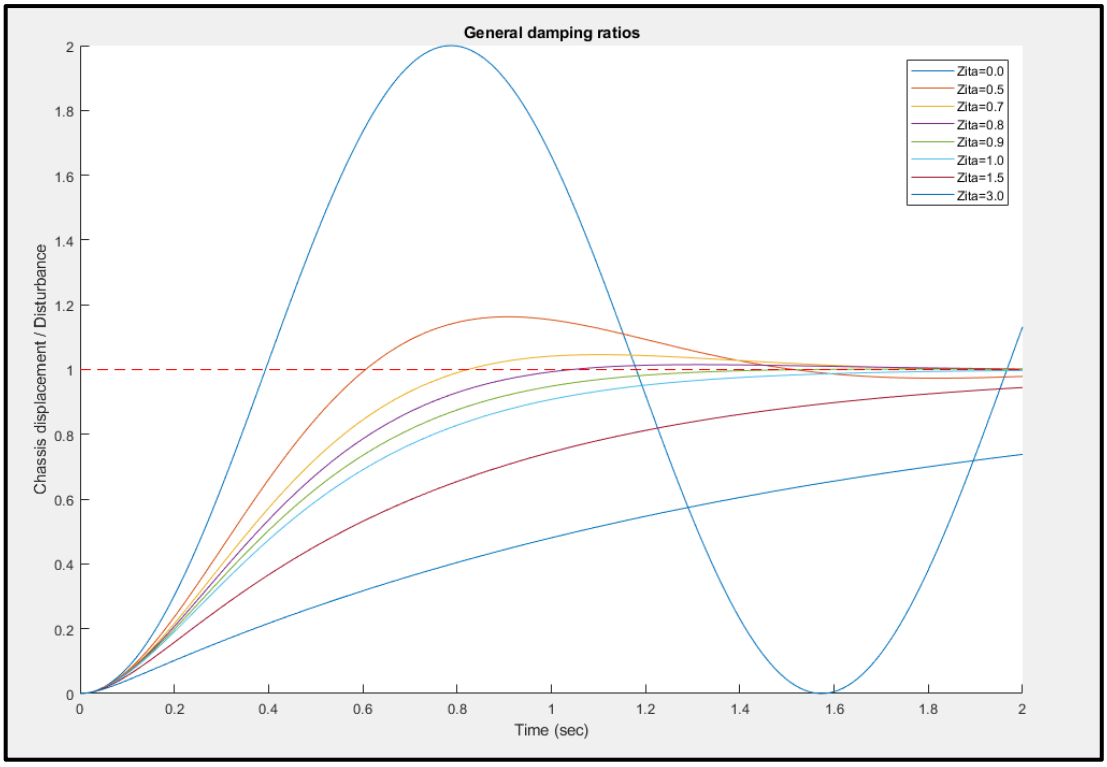

Figure 37 - Effect of damping rations on chassis displacement

Similarly to engines, dampers can be tested and tuned on a special dyno (Figure 38). These dynos oscillate the shock (without the spring) at different speeds and frequencies and measure the corresponding force to produce graphs (Figure 39) that can be used to find damping rates.

Figure 38 - Damper Dyno [28]

From Figure 39, the damping rate depending on the dampers settings can be defined. In order to find the damping rate, one first needs to identify the low and the high speed regions. This can be done by approximating the relationship between the velocity and the force as two linear straight line equations with two different gradients (damper rates). Looking at the purple line in Figure 39, the low speed damping rate can be found by the slope of the line up to approximately 25 mm/sec speed. The high speed damping will be the slope of the line upwards from 25 mm/sec. It should be noted that the knee point, the point at which low speed and high speed intersect, is slightly different for each setting of the damper.

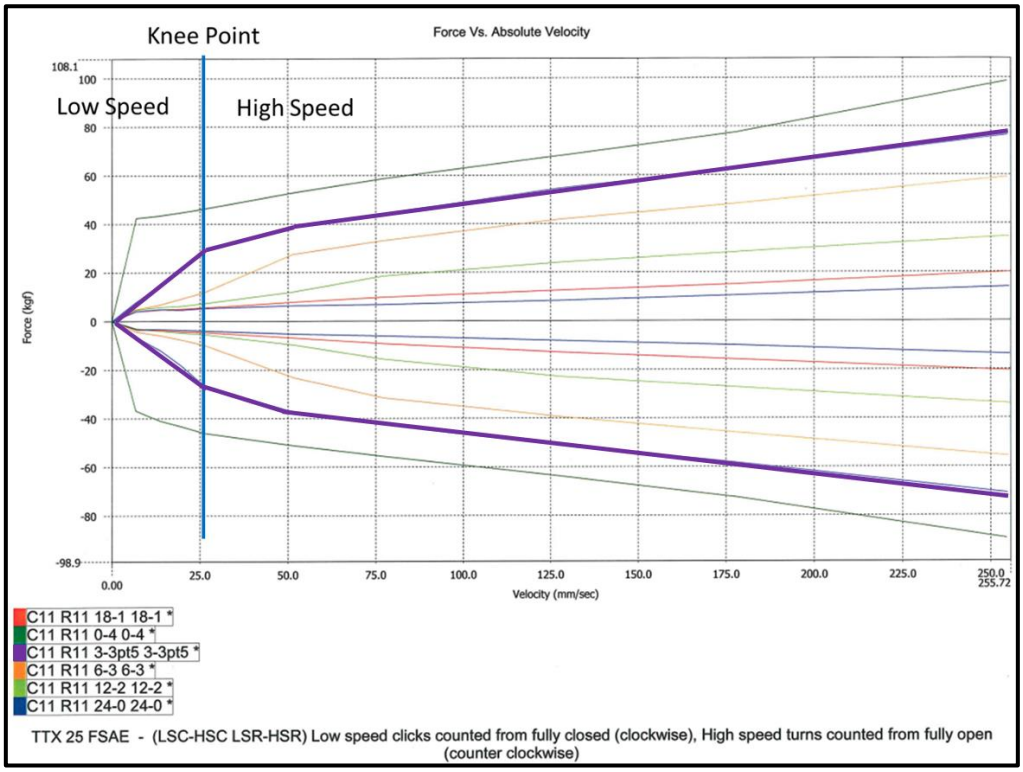

Figure 39 - Öhlins TTX25 Damper characteristics curve [26]

Finding the right amount of damping for the car will depend on the driver, track and wear of the tyres and can be difficult to dial in but time should be taken to do so as it is crucial to how the car behaves. When more damping is applied during compression, the transient response of the car is initially increased up to a point at which the shock effectively becomes locked. At that point, the suspension absorbs almost none of the force and the force is transmitted directly to the chassis, making the suspension system redundant (i.e. transforming it into a go-kart). Too little compressive damping will cause the car to react sloppily and become hard to control during cornering with road unevenness. A good compromise will enable the car to be driven to its limits in a controlled and predictable manner.

In the rebound direction, the same principal is true. Increasing the rebound damping will decrease the rate at which the chassis rolls during transient loading (i.e. slaloms). However, similarly as with the compressive damping, this can lead to locking out the suspension. This can result in the spring not allowing the wheel to return to the road [29].

In order to evaluate the effectiveness of the current damper setup, it is helpful to look at the range of damper speeds present throughout the track. This is most commonly done with a damper speed histogram (Figure 40). An ideal damper range follows a normal distribution (bell shape curve). The actual amount of damping necessary cannot be determined from this but it shows if the dampers on the car are balanced. An ideal damper setup dissipates an equal amount of energy in bump and rebound motion. Lighter coloured bars indicate the time spent in high speed damping [30]. The left histogram in Figure 40 shows badly distributed damper speeds. It can be seen that the wheel spends a lot more time in low speed bump than in rebound, the conclusion would be to either increase the low speed rebound or decrease the bump damping on that corner to even out the distribution. The right hand side of the graph shows fairly symmetrical damper characteristics in both bump and rebound.

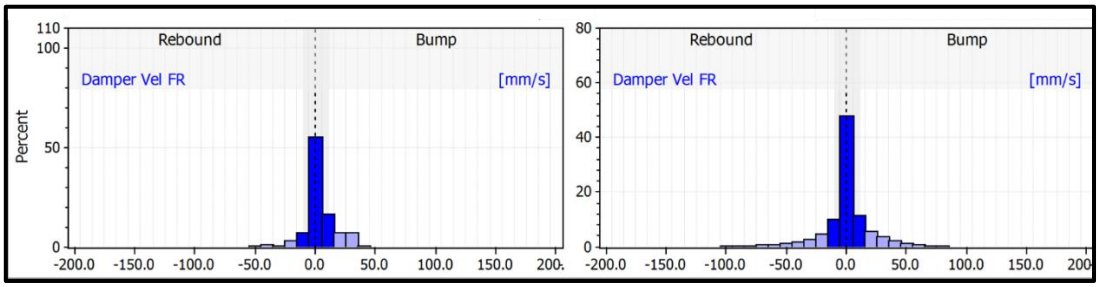

Figure 40 - Bad damper histogram (left) and good distribution (right)

If the bell curve is taken to be the ideal shape, more questions arise like the height of the peak and the width of the base. These depend greatly on the car and the track and can only be found through testing different setups and looking at other data to determine how the car behaves.

2.3 Current Suspension Models

The static and dynamic equations and principles mentioned in 2.2 can be applied to model the behaviour of a car in different scenarios (i.e. acceleration, braking and corner). Implementing computer aided calculations and code provides an easy way to check dynamic behaviour of different setups as well as investigating the effect of different parameters. Often simplifications have to be made in order to solve the system.

2.3.1 Quarter Model

This is by far the simplest model to implement as it only looks at one wheel at a time (Figure 41). In this case the only direction of motion is along the z-axis (vertical). This model, even though drastically simplified, can be used to give a basic understanding of the car as an oscillating system. With the two degrees of freedom (DOF) being the motion of the sprung and the unsprung mass, two differential equations can be used to solve the system [31].

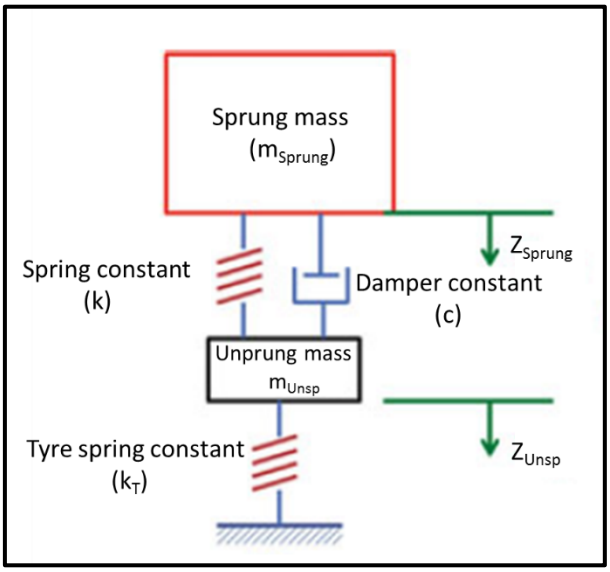

Figure 41 - Quarter car model [16 p. 92, (translated from German)]

$$m_{Sprung} * \ddot{z}_{Sprung} + k * \left(z_{Sprung} - z_{Unsp}\right) + c * \left(\dot{z}_{Sprung} - \dot{z}_{Unsp}\right) = 0 \quad (13)$$

$$m_{Unsp} * \ddot{z}_{Unsp} - k * \left(z_{Sprung} - z_{Unsp}\right) - c * \left(\dot{z}_{Sprung} - \dot{z}_{Unsp}\right) + k_T * z_{Unsp} = 0 \quad (14)$$

This model can be further simplified to one DOF by assuming a small unsprung mass which is usually the case with most racing cars. Furthermore, as the tyre and the spring are in series they can be combined into one spring with a total spring constant k_{Tot}.

$$k_{Tot} = \frac{k * k_T}{k + k_T} \quad (15)$$

Resulting in a simplified differential equation

$$m_{Sprung} * \ddot{z}_{Sprung} + k_{Tot} * z_{Sprung} + c * \dot{z}_{Sprung} = 0 \quad (16)$$

Rearranging and applying a Laplace transformation can be used to get equations for natural frequency and damping factor.

$$\omega_n = \sqrt{\frac{k_{Tot}}{m_{Sprung}}} \quad (17)$$

$$\delta = \frac{c}{2\omega_n * m_{Sprung}} \quad (18)$$

It is important to note that these equations relate to the wheel and a motion ratio might have to be used to relate the actual spring rate and damper rate to the wheel. Motion ratio defines how much the wheel is displaced compared to the spring (or vice versa). Allowable shock travel is often shorter than the expected wheel movement and motion ratios are needed, especially on rally cars, where bumps can be large. Motion ratios can be calculated for existing geometries by the use of trigonometry. As previously mentioned, a change in wheel angle to the ground occurs as the suspension travels (termed camber gain). This change in angle means that the motion ratio changes with travel. However, a well-designed suspension minimises camber gain and thereby change in motion ratio through travel.

Looking at only one wheel has obvious disadvantages, it is a hugely simplified model that does not consider slip angle, roll or pitch behaviour. However, it can still be useful for initial damper and spring rate selection [6].

2.3.2 Bicycle Model

As the name implies, the bicycle model considers two wheels, usually front and rear (Figure 42).

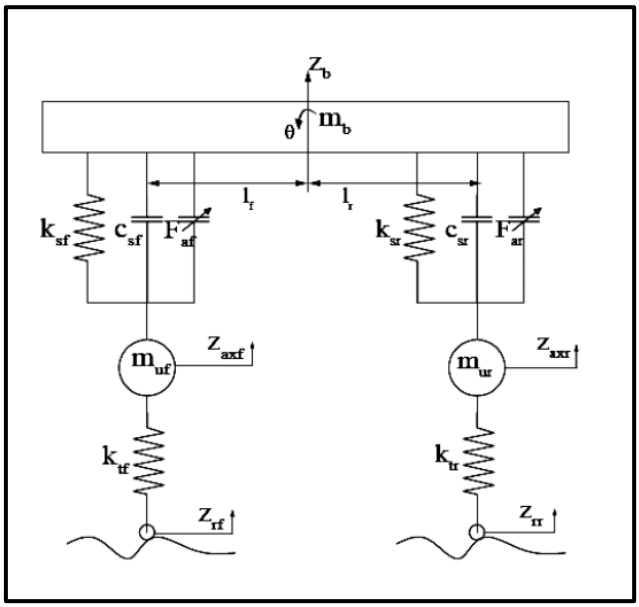

Figure 42 - Vibrational bicycle model [31 p. 169]

While this model can be used to analyse pitch behaviour of the car, it is not useful in considering any kind of rolling behaviour. Similarly to the quarter model, the equation of motions can be derived, where F denotes front and R rear.

$$m_{Sprung} * \ddot{z}_{Sprung} + k_F\left(z_{Sprung,F} - z_{Unsp,F}\right) + c_F\left(\dot{z}_{Sprung,F} - \dot{z}_{Unsp,F}\right) + k_R\left(z_{Sprung,R} - z_{Unsp,R}\right) + c_F * \dot{z}_{UnspR} = 0 \quad (19)$$

$$m_{Unsp,F} * \ddot{z}_{Unsp,F} - k_F\left(z_{Sprung,F} - z_{Unsp,F}\right) - c_F\left(\dot{z}_{Sprung,F} - \dot{z}_{Unsp,F}\right) + k_{T,F}(z_{Unsp,F} - z_{Bump,F}) = 0 \quad (20)$$

$$m_{Unsp,R} * \ddot{z}_{Unsp,R} - k_R\left(z_{Sprung,R} - z_{Unsp,R}\right) - c_R\left(\dot{z}_{Sprung,R} - \dot{z}_{Unsp,R}\right) + k_{T,R}(z_{Unsp,R} - z_{Bump,R}) = 0 \quad (21)$$

$$I_\theta \ddot{\theta} = t_R\left[-k_R\left(z_{Sprung,R} - z_{Unsp,R}\right) - c_R\left(\dot{z}_{Sprung,R} - \dot{z}_{Unsp,R}\right)\right] - t_F\left[-k_F\left(z_{Sprung,F} - z_{Unsp,F}\right) - c_F\left(\dot{z}_{Sprung,F} - \dot{z}_{Unsp,F}\right)\right] \quad (22)$$

$$\theta = \frac{z_{Sprung,F} - z_{Sprung,R}}{t_F + t_R} \quad (23)$$

I_θ, or pitch inertia, is a property that might not be known and depends on the design of the car. Many 3D CAD programs offer a function to determine inertia values along each axis. Once the car is built, this value can be verified by experiments.

Most frequently the bicycle model is used to analyse steering influence (Figure 43).

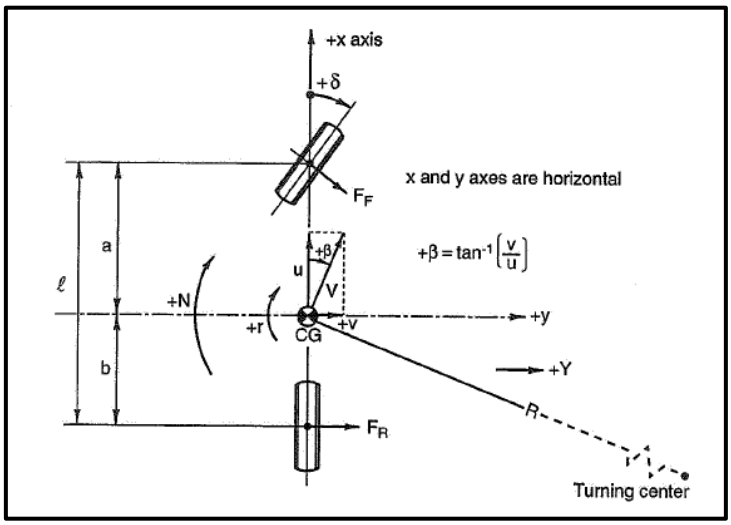

Figure 43 - Steering bicycle model [3 p. 127]

Slip angle and weight transfer caused by braking and acceleration can be considered when investigating steering forces. However, in terms of suspension behaviour it does not offer much more detail than the easy to implement quarter car model as it does not consider lateral load transfer through a corner. For an investigation into anti-dive and squat geometry however, this model can be helpful [6].

2.3.3 Full Car Model

Only the full car model considers steering effects and lateral and longitudinal load transfers (Figure 44).

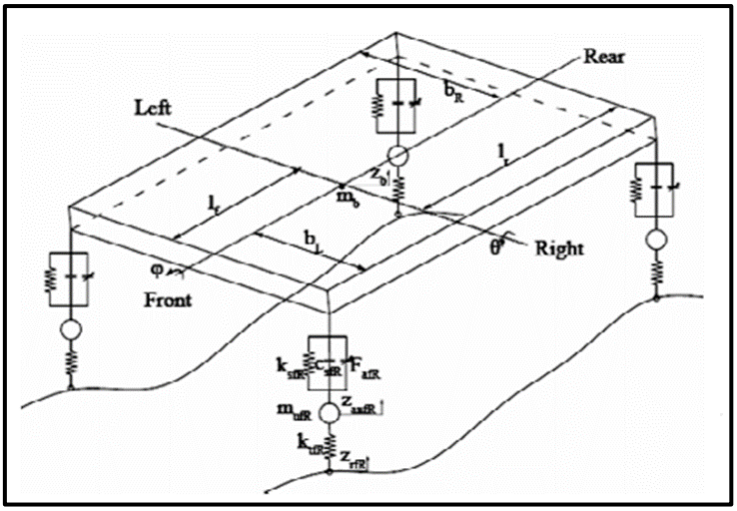

Figure 44 - Four wheel model [3 p. 118]

The four wheel or full car model most accurately models the actual behaviour of the car. However, when considering all variables, it will lead to a seven DOF system with many iterations necessary to solve the system, resulting in long processing times.

Research into a comparison between the full, half and quarter model shows virtually no discrepancy between the full and half model for a pitch scenario [31]. This is to be expected, as mentioned in 2.3.2, the bicycle model is very effective for a pitch motion. The quarter model is simplified to not consider dynamic load transfer and shows a larger discrepancy in the magnitude as well as the time occurrence of the displacement (Figure 45).

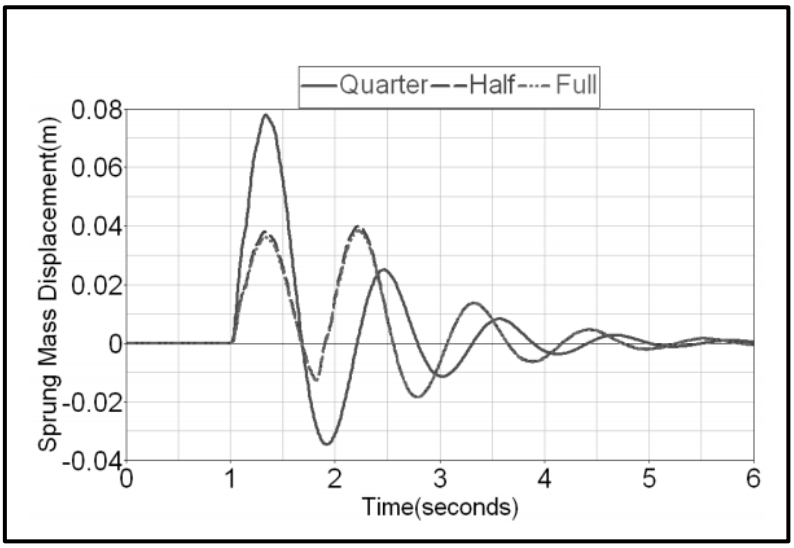

Figure 45 - Comparison of a quarter, bicycle and full car model during pitch [31 p. 173]

An expected discrepancy between the three models will show up when comparing them in a roll scenario (Figure 46). As expected, the discrepancy between the full and half model are now clearly visible. However, the actual magnitude difference is only 0.075 mm (~25% error).

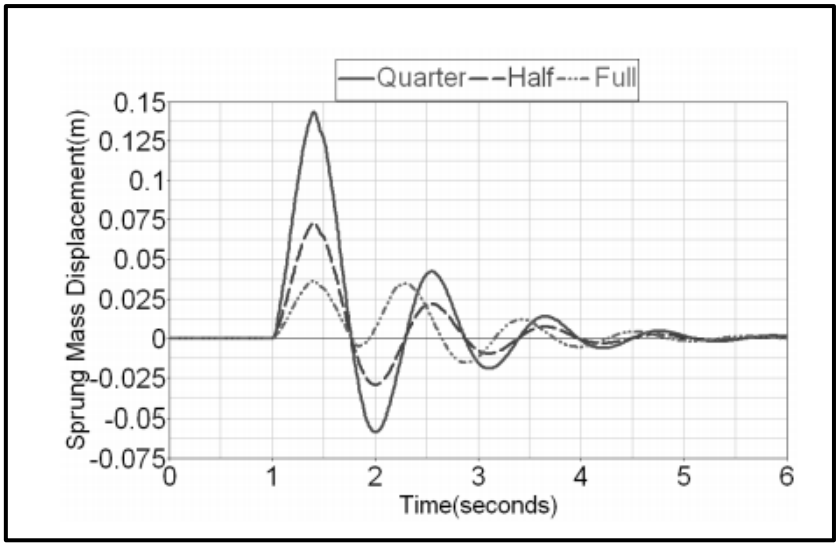

Figure 46 - Comparison of a quarter, bicycle and full car model during rolling [31 p. 173]

As for the quarter model, the natural frequency or ride frequency (ω_n) of the car can be calculated based on equation (17). This can be a good indicator of how the car is going to behave to inputs from both the driver and the road. If the car did not have any damping, this is the frequency that the car would continue to oscillate at. The higher the frequency, the harder and stiffer the ride will feel to the driver. A low frequency results in more mechanical grip but also in a car that is slow and sluggish to react to inputs by the driver. Often front and rear ride frequencies are chosen differently to decrease pitch. If the car hits a bump the front will get displaced first followed by the rear. This out of phase will create pitching towards the front of the car. If the rear was to have a larger frequency than the front, it would "catch up" with the displacement of the front, decreasing pitching (Figure 47) [32].

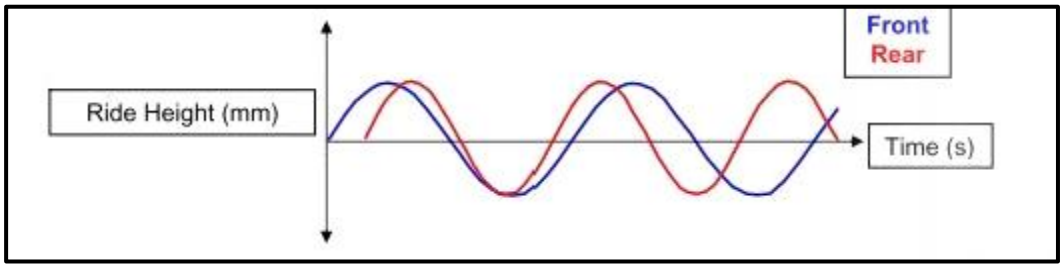

Figure 47 - Difference in ride frequency [29 Part 1]

The above theory was developed with passenger cars and comfort in mind, meaning low damping ratios. However, race cars often run high damping ratios, producing a ride with minimal wheel movement. It is not uncommon for race cars to have a higher front ride frequency to aid response of the car during corner entries (front wheel steered cars). Furthermore the increased mechanical grip at the rear aids grip during corner exit acceleration (rear wheel drive cars) [32].

2.4 Research Opportunity

It has to be noted that a lot of race teams heavily guard their suspension research and do not publish work and if so it tends to be outdated and irrelevant [33]. Most publications (such as [34] and [33]) focus on the design of the suspension rather than the tuning. The work is focused on the initial starting numbers such as ride frequency and initial damper rates [35], however, many of these values are not valid after the car is tested due to manufacturing discrepancies. There appears to be a gap in published research when it comes to tuning and optimising an already built suspension within its setup parameters (i.e. damper and antiroll bar adjustment). Furthermore, as multibody simulations become increasingly common, there is a potential to use software in conjunction with track data and simulation data from vibrational analysis using the models discussed in 2.3. Multibody simulation tools can be used to do many iterations at once, considering many degrees of freedom as well as the effect of driver capabilities.

The research in this thesis will focus on understanding the influence of different suspension parameters on car handling, track times and driver feedback. Furthermore, it will attempt to correlate theoretical models to data gathered on track. In order to develop meaningful models, it would be necessary to have access to a physical race car. Since 2006, the University of Waikato has a Formula SAE team that designs and manufactures a single seater race car every year (Figure 48).

Due to the build of the FSAE car being a fourth year engineering project, completed in one year, most teams are dissolved at the end of each year and a new team starts fresh the next year. This means that much of the information of how the car handles and problem areas that were identified never get passed down to the next team. Furthermore, due to the short design, manufacture and testing time, most years the car does not get tested and therefore tuned properly. 2019 offered a unique opportunity to look further into the vehicle dynamics of the car manufactured by WESMO in 2018, W-FS18, as two people who were part of the 2018 team stayed at the university and were able to provide valuable information.

Figure 48 - University of Waikato's SAE car - W-FS18

W-FS18 did well at the 2018 competition held at Winton Motor Raceway, outside Melbourne in Australia, placing third in the acceleration event and completing skidpad 400th of a second slower than the fastest car. However, the autocross and endurance event showed the gaps in the suspension tuning, finishing autocross 12 seconds slower than the fastest combustion car and not finishing endurance due to a failed wheel hub. As endurance and autocross are the dynamic events worth the most points, even though the car did well in all other events, the team scored a midrange 12th place overall finish. If the team had the time and resources to spend more time tuning the suspension of the car, it is believed that the car could have performed much better. Therefore, this research was the ideal opportunity to take a deeper look into what the suspension issues with the 2018 car were and remedy it. Furthermore, the other aim of this research was to develop models that were easy to use and populate with data specific to any SAE car and could be passed on to other WESMO teams.

Chapter 3 - Methodology

The research plan (Figure 49) involved developing a theoretical vehicle dynamics model which calculated suspension position, load transfer, damping rates and traction based on inputs such as geometry and accelerations in the lateral, longitudinal and vertical directions. Tyre data, provided by the FSAE Tire Test Consortium, was used to obtain traction coefficients to calculate traction. Multiple scenarios were compared using coding and graphing software. The numerical information was then used as part of a multibody simulation which modelled the car's behaviour during roll and ride. Data gathered from the University of Waikato W-FS18 car was used to validate and improve these theoretical models. Once the theoretical and practical data were correlated, they were used to obtain recommendations for improving the car behaviour and improve lap times.

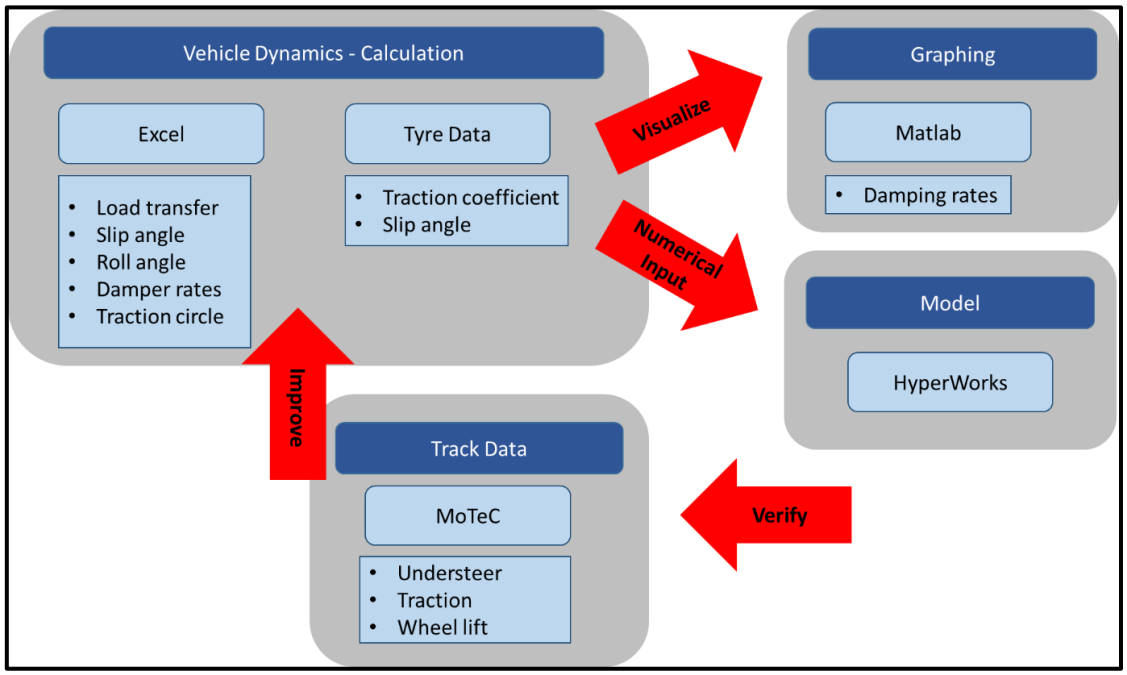

Figure 49 - Research flow chart

3.1 W-FS18 Geometry

To draw any meaningful conclusions from theoretical calculations, simulations or track data, it is necessary to know the geometric properties of the physical car. Even when care is taken during the manufacture of the chassis, the CAD dimensions and the physical car will not match perfectly and measurements have to be performed. These measurements include the COG location as well as weight distribution. For these measurements, the car was placed on digital corner scales with fuel and a driver. Static corner weights were recorded and used to obtain an axle distribution. To find the COG location, the ARBs were disconnected and the springs replaced by solid rods of the same length as the shocks. The rear of the car was then jacked up by a known distance. From the corner weights when the car

was on an angle and the known height, the COG location was found using moment equilibrium in Figure 50 and 51 and the equations below.

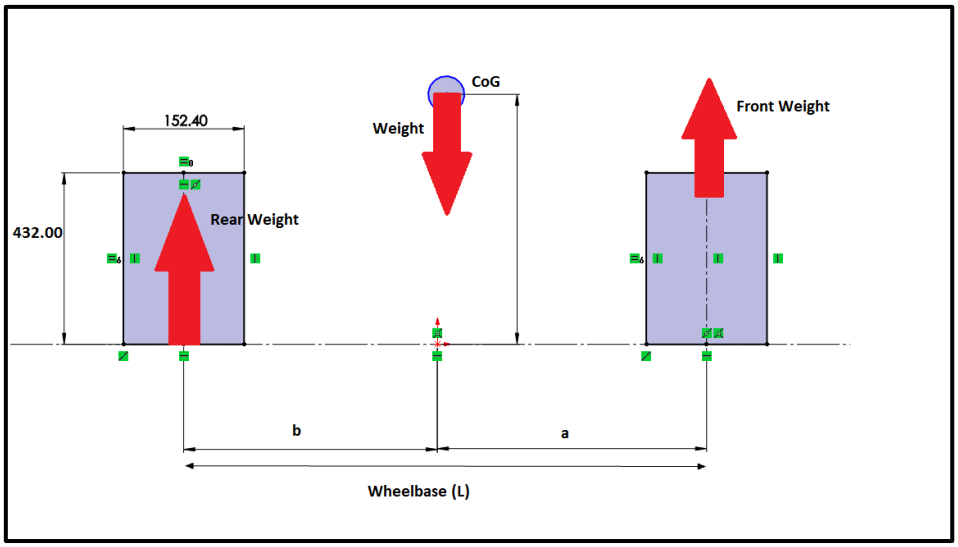

Figure 50 - Static scale weights

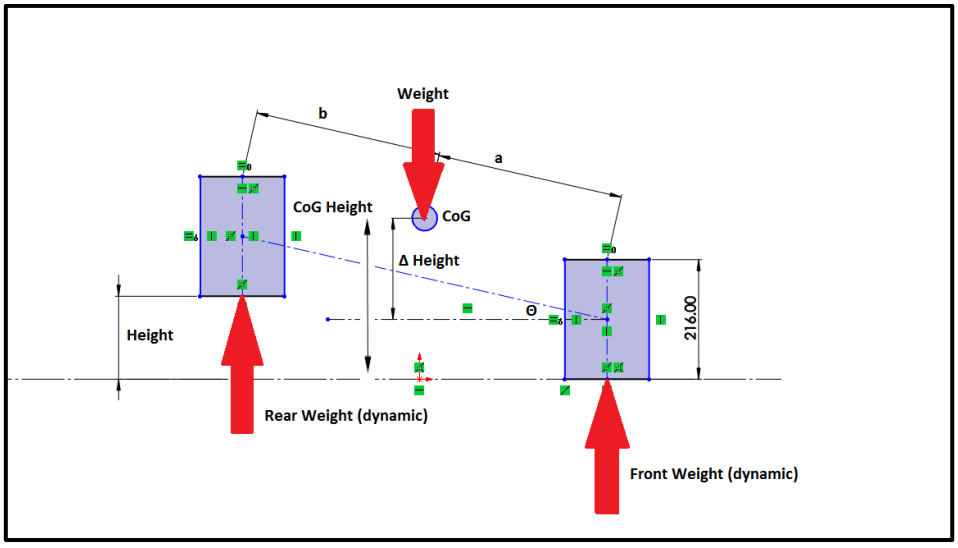

Figure 51 - Dynamic scale weights

$$a = \frac{Weight_{Rear} * L}{Weight_{total}} \quad (24)$$

$$b = L - a \quad (25)$$

Once the rear of the car was jacked up to a known height h, trigonometry and moment equilibrium was applied to Figure 51.

$$\theta = \sin^{-1}(\frac{h}{L}) \quad (26)$$

$$CoG\ height = \frac{Weight_{Front,dynamic} * L - Weight_{total} * b}{Weight_{total} * \tan\theta} + Tyre\ Radius \quad (27)$$

Using equation (27) and measurements taken from the W-FS18 car, the centre of gravity was found to be 296 mm above the ground and half way between the front and the rear (i.e. 50/50 weight distribution, see Table 3). Refer to Appendix A 1 and A 2 for the full derivation of the equations as well as the measurements of the W-FS18 car. Other measurements included wheelbase and track width which were measured with a tape measure (refer to Appendix A 3 for a list of full vehicle parameters). It is important to note that the car does not utilise antidive or -squat geometry and the effect of pitch centre on longitudinal load transfer can be neglected. Furthermore, an average height for the roll centre was used. Table 4 shows the difference in height between the front and rear roll centre.

Table 3 - Summary parameters W-FS1s8

Weight – Overall	261.9 – no driver	kg
Weight distribution	50/50	-
Wheelbase	1575	mm
Distance Front – COG, a	787.5	mm
Distance Rear – COG, b	787.5	mm
COG height	296	mm
Track Width – Front	1100	mm
Track Width – Rear	1050	mm
Static Roll Centre – Average	72	mm

Table 4 - Roll centre height from ground for W-FS18

Suspension Position	Roll centre height – Front (mm)	Roll centre height – Rear (mm)
Neutral	94.09	50.1
+ 25 mm	53.97	8.54
-25 mm	137.43	93.34

It is unusual for the car to have a lower rear roll centre. Due to packaging constraints on the 2018 car, this roll centre was chosen as the most feasible, as a higher roll centre resulted in a large vertical and lateral movement of the roll centre. Figure 52 shows the current rear wishbone mounting on W-FS18. It can be seen that there is no way to mount the suspension points higher or lower to produce a higher

roll centre without having to add chassis members. Due to rule constraints this was not an option. Furthermore the wheel side of the wishbones could also not be altered due to packaging issues with the wishbones hitting the wheel through the expected travel of the suspension.

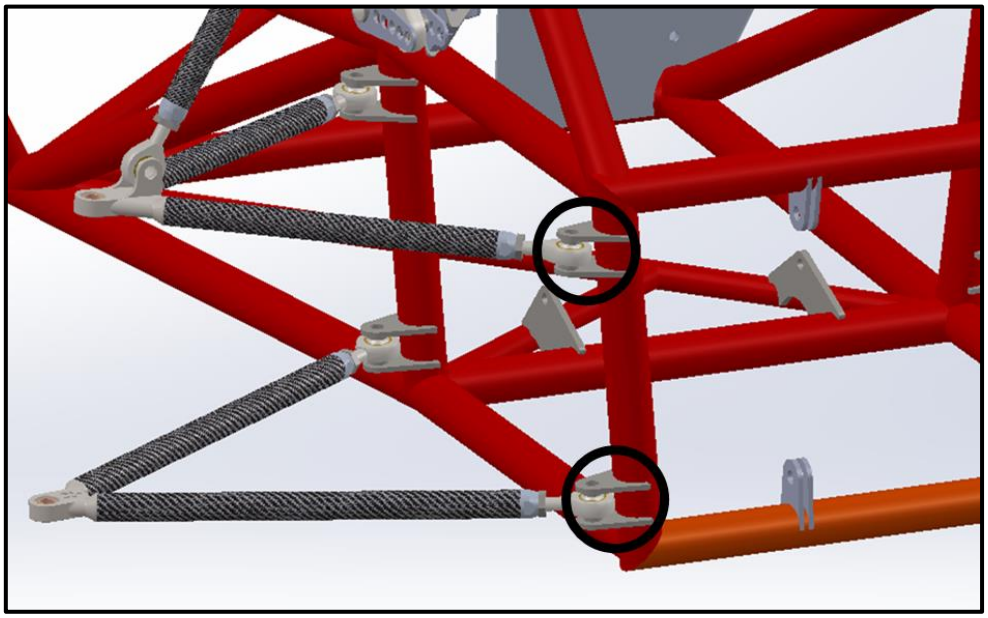

Figure 52 - 2018 Packaging constraint for roll centre [36]

Other parameters that initially had to be determined and adjusted were toe, caster and camber angles. In order to allow for optimum setup a wheel alignment machine at the local garage, Wally Elders Garage Ltd, was used (Figure 53). The camber at the rear on the left and right side of the car was similar (~ -1.5°). The front wheels were more unequal, varying from -1.23° to -2.15°. However, as further analysis later showed (section 4.2), the effect of 1° of camber change on tyre properties is negligible. As long as the toe on the left and right of the car is similar, no unexpected behaviour will occur, i.e. the car behaves the same in a left- and right-hand corner and does not pull to one side. Toe angle affects steering behaviour more than suspension, however, it does affect slip angle which can cause under- and oversteer. Caster angle is affected by suspension geometry which was already fixed and mostly affects steering forces [7].

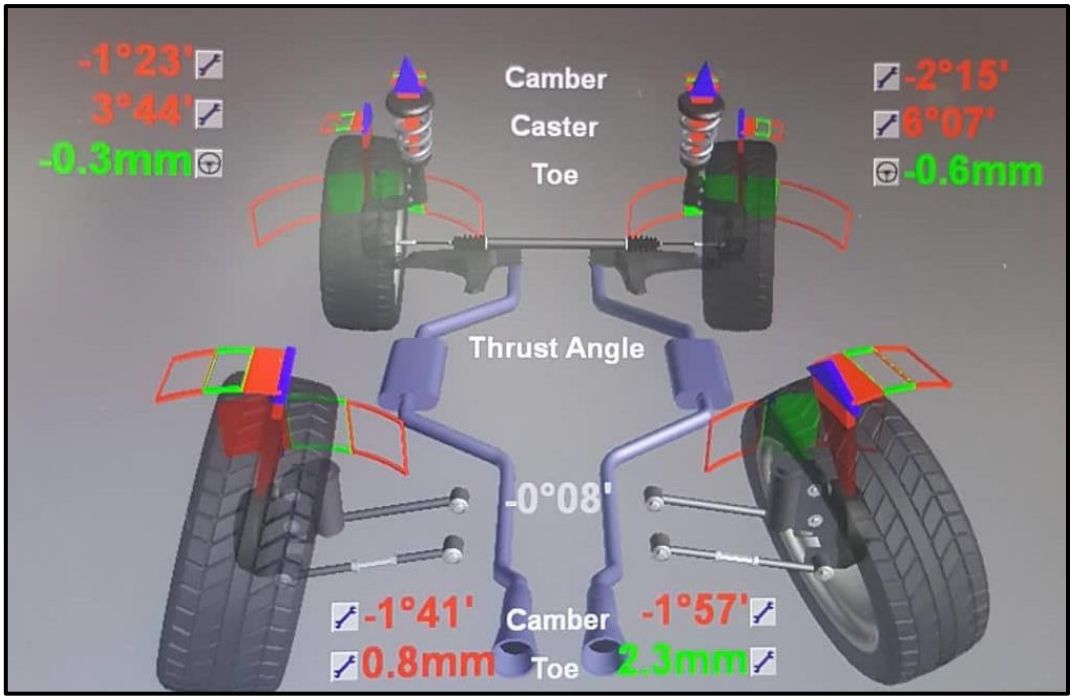

Figure 53 - Wheel alignment [37]

3.2 Data Acquisition

A data acquisition system uses electronic memory to store a number of defined variables as a function of time or position, while the car is on track. This data can then be downloaded and analysed [30 p. 5]. To log data, sensors need to be installed, these often include speed, linear position sensors as well as an accelerometer to measure acceleration in 3D. Data gathered by these sensors can be extremely helpful when analysing the performance of the car and the driver. Engine vitals can be used to diagnose problems in the tune or the fuel delivery system, suspension data can give information on how the car rolls and steering and braking data can help improve driver performance [30].

The W-FS18 was equipped with a MoTeC CDL3 data logger, mounted at the rear (Figure 54).

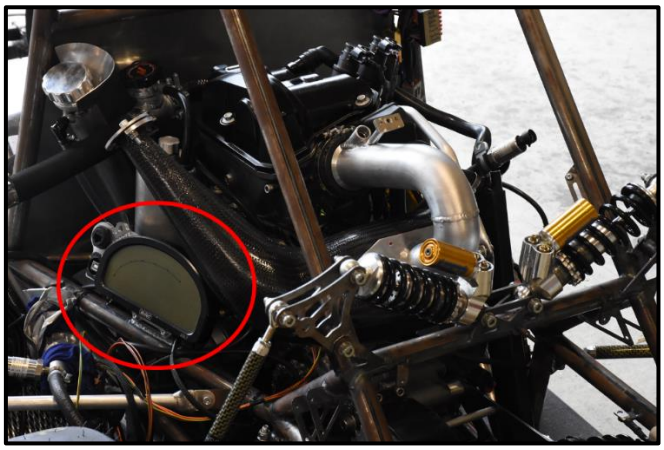

Figure 54 - MoTeC CDL3 Dash Data logger

Between the MoTeC data logger and the Link ECU (for engine sensors only), a number of channels were logged at a rate of up to 500 Hz (Table 5).

Table 5 - Logged channels on W-FS18

GPS Time	G Force Lat	Engine Temp	Lap Number
GPS Latitude	G Force Long	Air Temp Inlet	Drive Speed
GPS Longitude	G Force Vert	Bat Volts ECU	Lap Distance
GPS Speed	Display Next Line	Fuel Inj Timing	Trip Distance
GPS Heading	Traction Enable Switch	Ign Advance	Odometer
GPS Date	Wheel Speed FL	Cam Pos L Inlet	Wheel Slip (Percent)
GPS Sats Used	Wheel Speed FR	Cam Pos R Inlet	Lap Gain/Loss Running
GPS Altitude	Wheel Speed RL	Lambda 1	Lap Gain/Loss Final
Engine RPM	Wheel Speed RR	Fuel Pres	Reference Lap Time
Manifold Pres	Ground Speed	Eng Oil Pres	Brake Bias Setting
Baro Pres	Gear	Susp Pos FL	Engine Run Time
Throttle Pos	Lap Time	Susp Pos FR	Min Eng Oil Pres
Fuel Inj Duty	Running Lap Time	Susp Pos RL	Log Time Remaining
Fuel Actual PW	Beacon	Susp Pos RR	Logging Running
Bat Volts SDL	Light 2	Steering Angle	CPU Usage
SDL Temp Brake	Eng Hours 1	Brake Pres Front	Pres Rear

It is important to note where certain sensors are located as this can explain certain errors or irregularities in the data gathered (Figure 55). The linear position sensors are mounted on the front and rear shocks. The front sensor is mounted differently to the shock compared to the rear, measuring the deflection of the spring to the mounting point of the pushrod rather than the actual shock itself (right photo). This is due to the length of the sensors themselves being longer than the shocks and packaging constraints. Care was taken to apply the appropriate motion ratio to the logged front position data gathered (Figure 56). It can be seen that front and rear springs as well as the rear linear potentiometer have the same motion ratio (0.79 spring travel per wheel travel). Only the front sensor is different due to the mounting (0.77 spring travel per wheel travel).

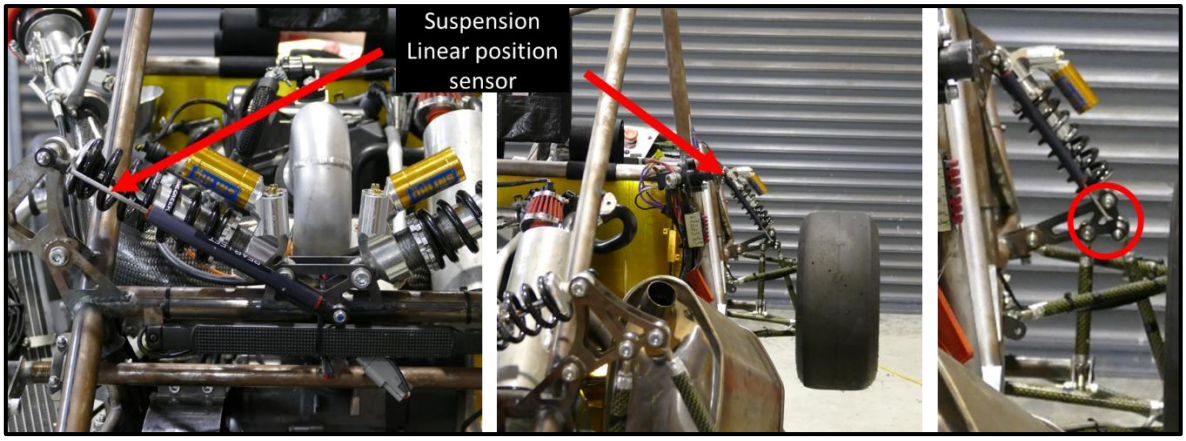

Figure 55 - Linear position sensors rear (left) and front (middle and right)

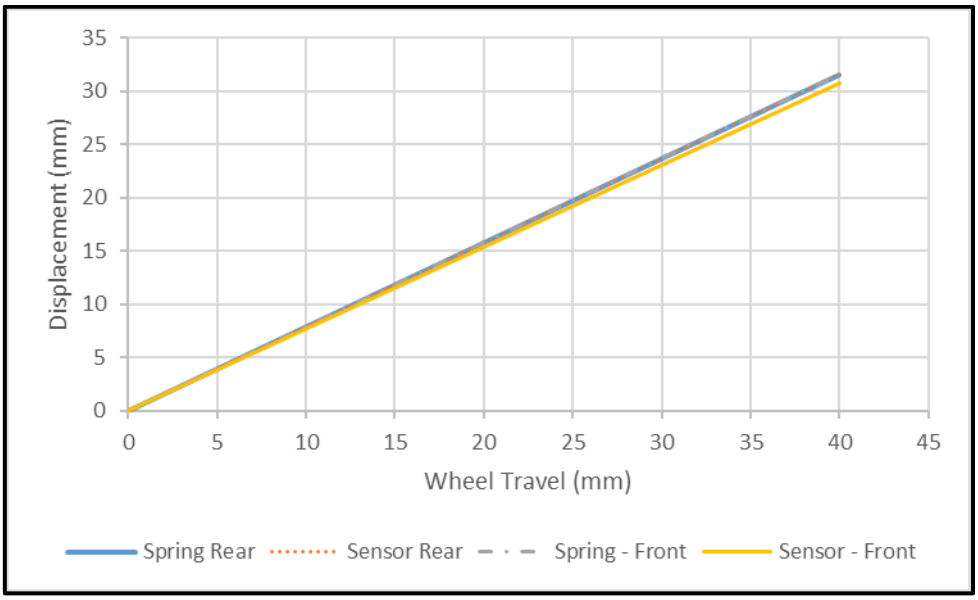

Figure 56 - Effect of motion ratio on shock and sensor displacement

As the wheel moves through its travel the motion ratio changes as angles and perpendicular distances change. However, if the wheel displacement is small and the motion ratio was designed with this in mind, the change can be minimised and often is small enough to be neglected. Figure 57 shows the change in motion ratio for the W-FS18 car. It can be seen that the change in motion ratio is small for small wheel displacements. In section 4.2 it will be shown that the average wheel displacement was 5 mm, resulting in no remarkable change in motion ratio.

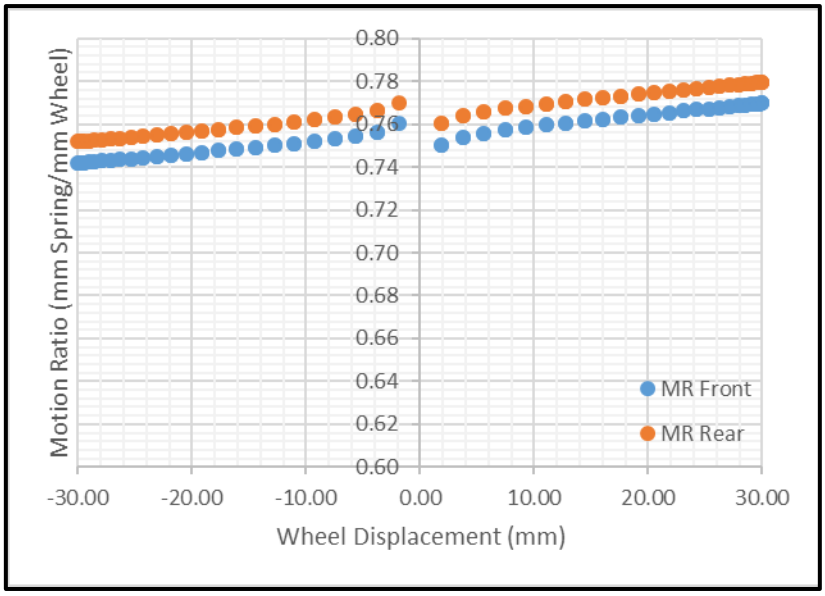

Figure 57 - Change in motion ratio through wheel travel for W-FS18

Due to the number of logged signals, there was a large amount of data that needed to be analysed to evaluate the performance of the car. This was done using MoTeC i2 Pro software which is capable of displaying data in various forms such as Figure 58. Furthermore, custom channels that process logged data (termed math channels in MoTeC) were created, for example, differentiating the shock position (measured with the linear position sensors) in respect to time, to show shock velocity.

Figure 58 - MoTeC Display of damper velocity and shock position

The sensor that measures steering angle is a linear potentiometer (displacement sensor), it therefore logs rack travel rather than steering angle (Figure 59). A relationship between turning angle of the wheels and rack travel was found by placing the front wheel of the W-FS18 car on a piece of plastic

and turned through its full steering lock while recording rack travel (Figure 60). This was repeated for the right and left side of the car, no discrepancy was found.

Figure 59 - W-FS18 Steering with linear potentiometer

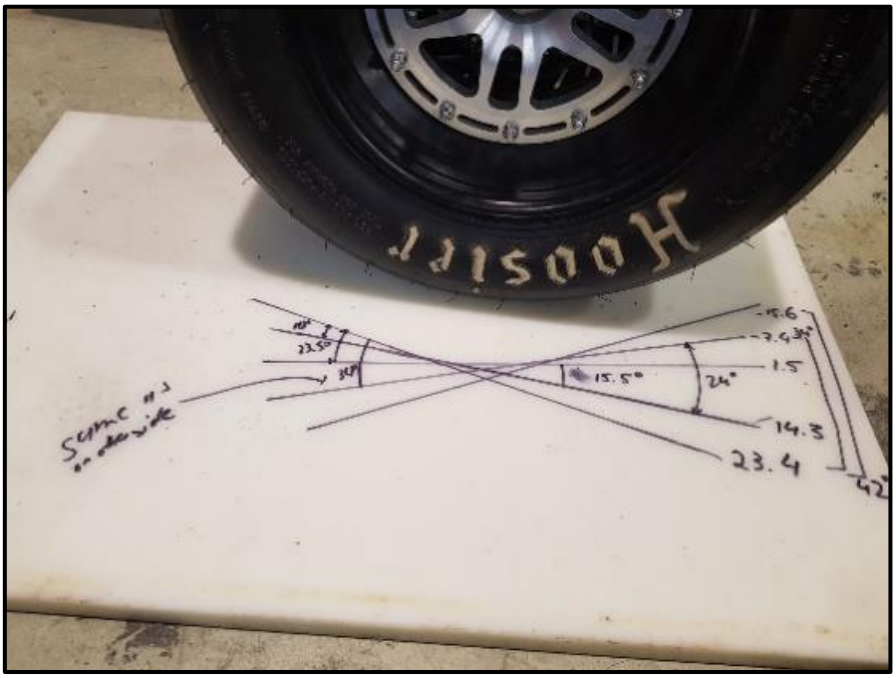

Figure 60 - Steering angle measurement

Plotting rack position versus the wheels angle gave an equation that was used to convert rack travel into a steering angle at the wheel (Figure 61). The line does not pass through the origin due to not being able to zero the sensor with the wheels perfectly straight.

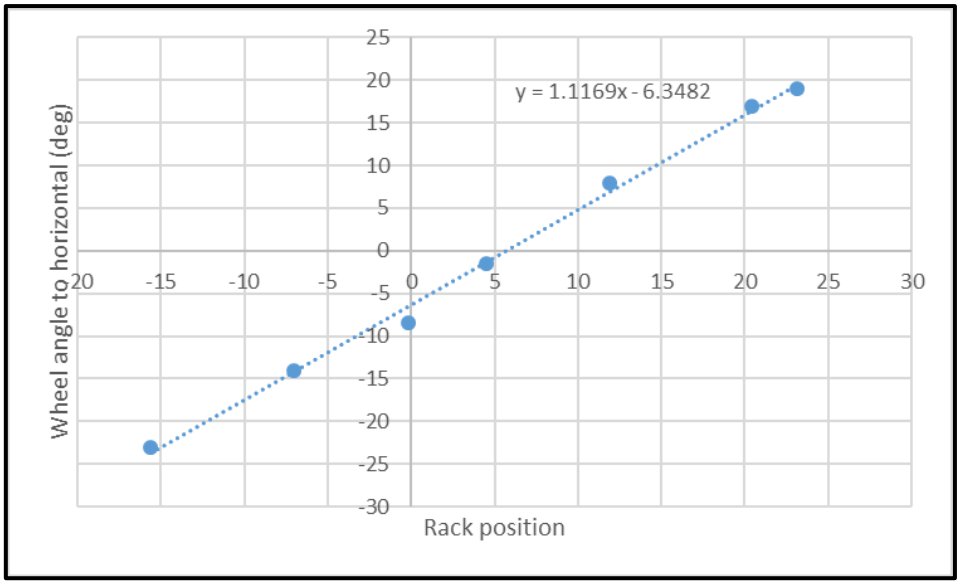

Figure 61 - Relationship between rack travel and steering angle at the wheel

The MoTeC dash logger contains an accelerometer sensor that measures lateral, longitudinal and vertical acceleration. This was mounted at the rear of the W-FS18 car on the left hand side, however it is important to note that it was not mounted in line with the car's longitudinal axis, nor perpendicular to the lateral axis. This resulted in the need of math channels to adjust the logged accelerations to correct them. Using vector addition, the corrected lateral and longitudinal accelerations were found (Figure 62). Refer to Appendix A 4 for the trigonometric functions used to resolve this vector addition.

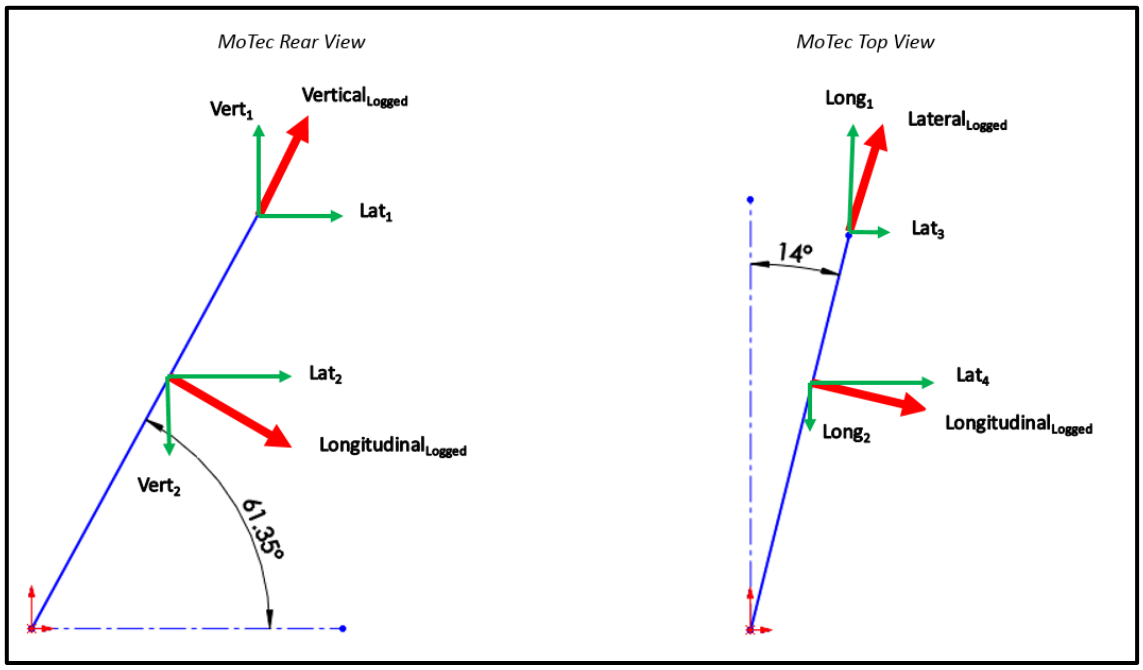

Figure 62 - MoTeC logger placement

Summing up the partial lateral accelerations gave the corrected overall lateral acceleration. The longitudinal and vertical accelerations were also found in a similar manner.

$$a_{Lat,tot} = a_{Lat,1} + a_{Lat,2} + a_{Lat,3} + a_{Lat,4} \quad (28)$$

$$a_{Long,tot} = a_{Long,1} - a_{Long,2} \quad (29)$$

$$a_{Vert,tot} = a_{Vert,1} - a_{Vert,2} \quad (30)$$

3.3 Calculations

Basic calculations can be used to get a quick, simplified idea of how different setups affect the behaviour of the car. However, as they are highly simplified, the results are expected to have a large error percentage. The equations and physical principles were explained in section 2.2.

A big part of the calculations, which is also used in other modelling methods, is the analysis of tyre data. Calspan Tire Research Facility (TIRF) carried out extensive testing of tyre properties [17].

During these tests a road is simulated by a stainless steel belt covered in a material that mirrors the frictional properties of a road. The tyre is controlled by a drive system which allows for tyre pressure, downforce, castor, camber, slip angle, wheel speed and slip ratio (wheel speed divided by road speed) to be controlled. A six-component strain gauge is used to obtain forces and moments at the wheel drive shaft. The system is capable of changing up to three variables during a run and logs data at up to 2000 Hz [17]. For a full list of properties measured refer to Appendix A 5. The Tire Test Consortium data for the Hoosier tyres that the W-FS18 car has at both front and rear (18.0x6.0-10 Road Racing C2000 R25B) has been made available and was used in the current research. The measured data was plotted in many different ways to obtain friction coefficients which are an important part to understand and maximise the grip potential of the car. The calculation of these traction coefficients will be discussed in detail in section 4.2.1.

Figure 63 - Tyre testing machine [17]

3.4 Matlab

Matlab is one of the simplest and most versatile programs that can be used to implement frequency analysis based on quarter, bicycle and full car models. It was decided that a dynamic model for a full car going around track would require too much specific data like a power and torque curve for the engine as well as a thermodynamic model for the tyres to predict temperatures around the track. This amount of data would make the model slow to run and require extensive computational power. The full car model was still used to obtain data for steady state loading, for instance a curve with a constant lateral and longitudinal acceleration was analysed as well as constant braking and acceleration scenarios. This was used to help fine tune antiroll bar settings as well as narrow down the choice of spring rates. In order to visualize different damper rates, a quarter model was implemented. With both models, various geometric and physical properties were adjusted and the effect on grip analysed. Longitudinal and lateral acceleration were also specified and different scenarios represented. However, due to processing times due to increased complexity of the model, the number of free variables was limited, for example the effect of change in tyre temperature and the resultant increase in pressure, was neglected.

3.5 HyperWorks

HyperWorks is a multibody simulation software. Multibody dynamics simulations (MBD) have become increasingly popular in recent years. Due to their complexity they allow for in-depth design and dynamic analysis. In this research it was used to create a multibody of the W-FS18 suspension. The initial design work was done in SolidWorks and then imported into HyperWorks. Within the software, each point was then defined with its degrees of freedom with the use of different joints, for example the spherical bearing in the A-Arms of the suspension was modelled by a ball joint with 360° of rotational freedom (Figure 64).

An entire car, including engine and drivetrain, can be modelled this way, based on coordinates from the CAD model. HyperWorks allows for a variety of pre-programmed simulations to be run, these include static roll and pitch analysis as well as more dynamic scenarios like a constant radius turn. Furthermore, an intelligent driver can be specified, i.e. novice up to advanced driver, which will affect the racing line the driver takes. Tyre properties can be specified depending on pressure, camber, slip angle and temperature, making the model highly customisable due to the number of variables considered.

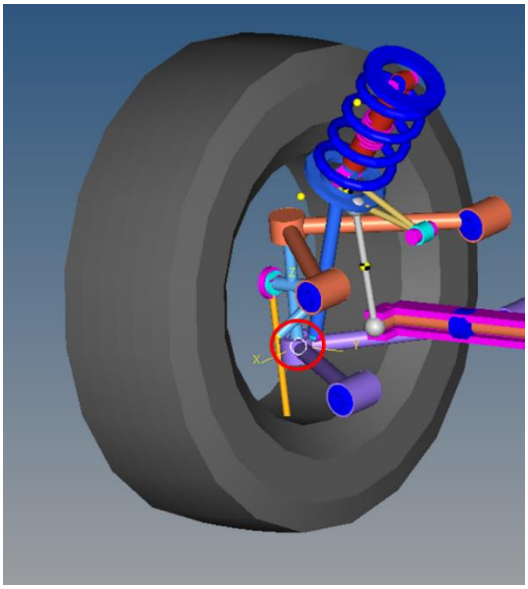

Figure 64 - Spherical bearing representation in HyperWorks

In this research HyperWorks has been used to verify the validity of assumptions like minimal camber gain through rolling and steering. Furthermore, the roll analysis was used to visualise the effect of different ARB stiffnesses on the roll behaviour.

3.6 Track Data

3.6.1 Physical Testing

Track testing was carried out at the "Kartsport Hamilton" go-kart track in Hamilton, New Zealand. In order to obtain comparable results over various testing days, one track setup was used (Figure 65).

The track consisted of a slalom at the start straight, a hair pin turn, a chicane as well as a minimum radius corner (7.5 m). Red arrows in Figure 65 a represent the placement and direction of cones. Numbers between cones indicate the steps between each set of cones. The entire track length was found to be approximately 365m long, depending on the drive line the driver took.

After the initial testing day, it was noticed that the minimum radius corner was too tight and the driver was hitting the curb in order to negotiate it and it was decided to open up the corner. Furthermore, in order to be as consistent as possible one driver was used for all track days. The driver was not given information about setup changes (refer to Appendix A 6 for all setups tested) and whether or not it would improve or worsen the car behaviour so as to not influence their opinion. The driver was given a few setting laps to get used to the new suspension settings and then was told to push the car to its maximum. The number of setting laps were determined based on data gathered and driver feedback. Lap times were compared in order to determine a point at which the driver had become consistent for each setup. This was typically between three or four laps.

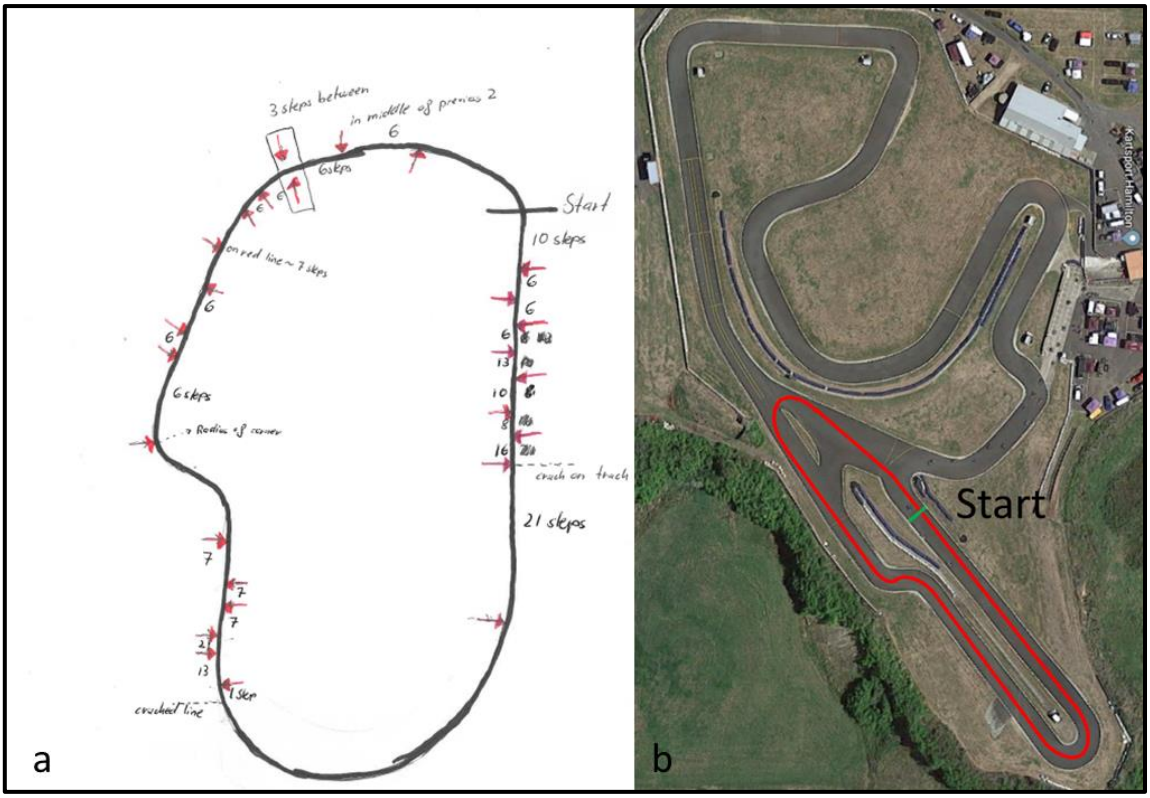

Figure 65 - Test track

To compare data gathered on the car with simulation data it was vital that the testing occurred when the track was completely dry, as no data for the tyre was available for when the tyre is wet. A total of ten track days were completed of which two could not be used as the car either broke or it started raining soon into the testing, rendering the data unusable. All data channels mentioned in section 3.2 in Table 5 are logged as soon as engine revs beyond idle.

3.6.2 MoTeC

In order to use the data logged to tune the suspension for grip as well as use it to validate any of the theoretical models, it had to be manipulated mathematically to show data that was not logged directly. As mentioned in section 3.2, math channels can be created to achieve this.

An initial judgment of the roll and pitch behaviour of the car was made by looking at the body angle of the car in each scenario. These were calculated from the respective suspension positions ($x_{xx,yy}$), the track width, wheelbase and motion ratio (MR_{xx}), assuming a stiff chassis. The W-FS18 torsional rigidity was 2400 Nm/° which is well within the recommended 2000 – 2500 Nm/° for this assumption to be valid [36]. Motion ratio was defined shock displacement divided by wheel displacement. Care needs to be taken as some literature [3] defines it as wheel displacement divided by shock travel and the equations then need to be adjusted accordingly.

$$\alpha_{Roll,Front} = \tan^{-1}\left(\frac{x_{Left,Front} - x_{Right,Front}}{Track_{Front} * MR_{Front}}\right) * \frac{180}{\pi} \quad (31)$$

$$\alpha_{Roll,Rear} = \tan^{-1}\left(\frac{x_{Left,Rear} - x_{Right,Rear}}{Track_{Rear} * MR_{Rear}}\right) * \frac{180}{\pi} \quad (32)$$

$$\alpha_{Pitch} = \tan^{-1}\left(\frac{\frac{Avg(x_{Left,Front}, x_{Right,Front})}{MR_{Front}} - \frac{Avg(x_{Left,Rear}, x_{Right,Rear})}{MR_{Rear}}}{Wheelbase}\right) * \frac{180}{\pi} \quad (33)$$

The car should have a certain amount of roll per lateral acceleration as it provides the driver with feedback. Most literature suggests about 0.7 °/g lateral acceleration [15].

As useful as it is knowing how much the car rolls or pitches in different scenarios (under different lateral and longitudinal accelerations), it is more helpful looking at how much the car rolls per acceleration (termed roll gradient (RG) and pitch gradient (PG)).

$$RG_{Front} = \frac{\alpha_{Roll,Front}}{a_{Lateral}} \quad (34)$$

$$RG_{Rear} = \frac{\alpha_{Roll,Rear}}{a_{Lateral}} \quad (35)$$

$$PG_{Rear} = \frac{\alpha_{Pitch}}{a_{Long}} \quad (36)$$

Another indication of the behaviour of the car is the slip angle of each tyre (α). These can be calculated based on tyre properties like cornering stiffness (c_α) and suspension geometries (refer to Appendix A 7 for the derivation of the equation below).

$$\alpha_{Rear} = \frac{F_{Z,Dynamic,Rear}}{c_{\alpha,Rear} * g} * a_{Lat} \quad (37)$$

$$\alpha_{Front} = \frac{F_{Z,Dynamic,Front}}{c_{\alpha,Front} * g} * a_{Lat} \quad (38)$$

The difference in slip angle between the front and rear was used as to indicate under- and oversteer behaviour. If the front slip angle was higher than the rear, the car understeers. The front swings away from the direction the car is going in, causing a larger turning radius. During oversteer the rear slip angle is higher, causing a smaller radius turn.

If the Ackermann angle as well as the angle of the front outside wheel are known, the understeer angle can be determined. To calculate the Ackermann angle, the angle that the wheel needs to be at to negotiate the corner, only the wheelbase and corner radius (R) need to be known (Figure 66). The radius in turn can be calculated by knowing speed and acceleration (39).

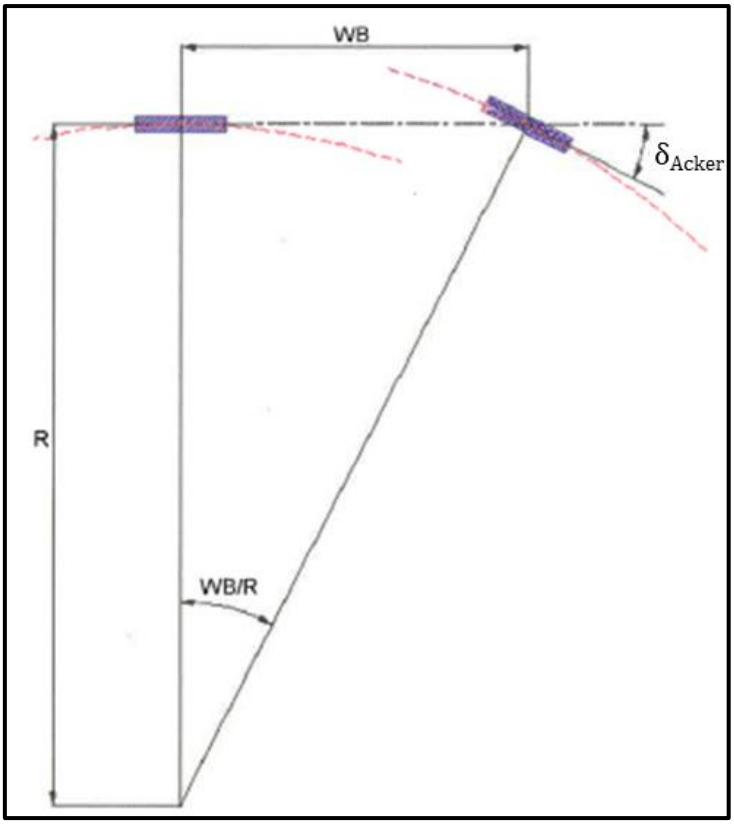

Figure 66 - Understeer angle based on corner radius

$$\delta_{Acker} = \frac{Wheelbase}{R} \quad (39)$$

$$R = \frac{V^2}{a_{Lat}} \quad (40)$$

It can be noted that equation (39) does not have a trigonometric function even though δ_{Acker} is an angle, measured in radians or degree. This is due to the approximation that tanΘ is Θ for angles smaller than 15°.

The following relations can be implemented:

Steered angle = Ackermann angle => Neutral steer

Steered angle < Ackermann angle => Oversteer

Steered angle > Ackermann angle => Understeer

The main goal of the car suspension is to optimise grip. It is therefore useful to look at the grip during different scenarios, i.e. under acceleration, braking and cornering to identify areas that need attention. The easiest way to visualise grip was the traction circle which shows lateral and longitudinal accelerations (Figure 67). Theoretical pure maximum lateral and longitudinal accelerations of the tyre and car were calculated (more detail on how these can be calculated in section 4.2.1). These were

used to plot a theoretical traction circle that then was overlaid with track data gathered. A comparison between them was used to identify scenarios were the driver can push the car harder as it still has traction left. The traction circle was also used to identify scenarios where the car loses traction and the driver has to slow down. Knowing the specific scenario when the loss of traction occurs, allows for specific tuning for that particular scenario.

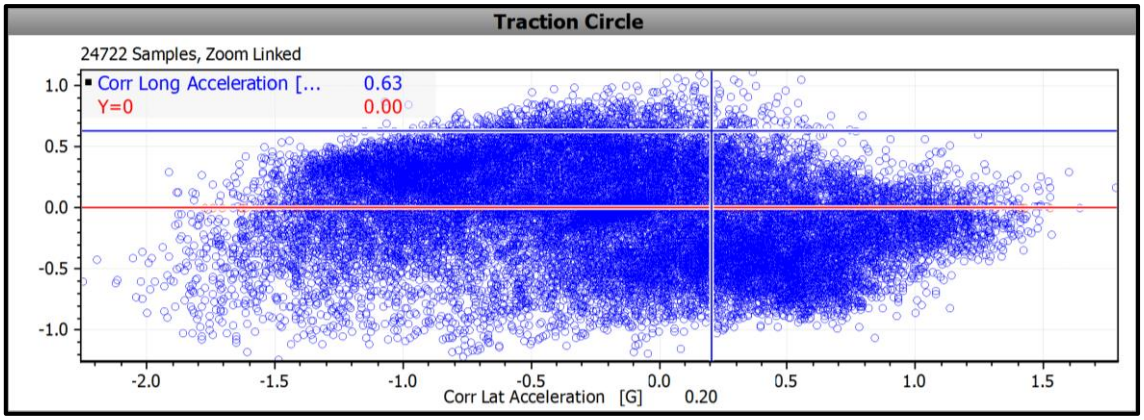

Figure 67 - W-FS18 Traction circle for endurance at competition

However, the traction circle does not show the full potential of what the tyre can be pushed to, a theoretical ellipse can be plotted over to show the theoretical limits of the tyre. An easier way to visualize the grip during transient loading (combined lateral and longitudinal acceleration) is by implementing grip factors. The grip factor of the tyre is the vector sum of lateral and longitudinal acceleration plotted against distance. Different conditions can be used to split the overall grip factor into braking, acceleration and cornering scenarios. During braking the longitudinal acceleration is negative so the braking grip factor is displayed when the longitudinal acceleration drops below -0.75 g whereas an acceleration is triggered when the acceleration reaches 0.75 g and a cornering scenario is defined as more than 0.5 g lateral acceleration. These boundary values are car and track dependant and need to be varied in order to obtain meaningful results. In the case of W-FS18, these values were estimated based on the traction circles from competition. It can be concluded that the larger the area under the curve for each grip factor, the better the car grips during that specific scenario. Average values for each factor can be helpful when trying to quantify grip levels between setups.

Chapter 4 - Results and Discussion

The aim of this research was to investigate the effect of different suspension setup parameters on the handling characteristics of a single seater race car, W-FS18, built by the School of Engineering student team at the University of Waikato in 2018. Furthermore, theoretical models made were verified and improved with the help of data gathered while the car was on track.

This chapter will present the theoretical as well as the experimental data, explain where there was correlation, what assumptions were made and where and why the models differed and ultimately makes suggestions on how to change the current W-FS18 suspension setup to improve lap times.

4.1 Initial Track Testing

4.1.1 Shock Data

Visual analysis of the car during track and skidpad testing revealed an obvious issue with the setup as it often lifted both inner wheels during cornering (Figure 68) even though the lateral acceleration was less than 1 g and well below the theoretical maximum (<1.8 g lateral acceleration).

Figure 68 - W-FS18 lifting inner wheels off the ground during 2018 skidpad testing

Track data analysis supported this initial conclusion. Investigation of a damper histogram showed a great asymmetry between bump and rebound damper velocities (Figure 69). Especially the front left (FL – red) damper can be seen to have a great difference between the time spent in bump and rebound for speeds between 10 mm/s and 20 mm/s. The bin that connects bump and rebound speeds is termed the zero bin and can be used to draw conclusions about the relative suspension stiffness of the corners [30]. The front left zero bin reached about 38% whereas the front right reached up to 48%. The rear was similar with 58% and 56%. In order to even the stiffness at the front, dampers needed to be checked to ensure they were set symmetrical between the left and right. If not, a difference in tyre

pressure could cause the difference. If tyres pressures and the original setup were found to be the same, asymmetrical damper settings might have to be used to create a balanced car and the affected shocks should be examined for faults (more in section 4.3).

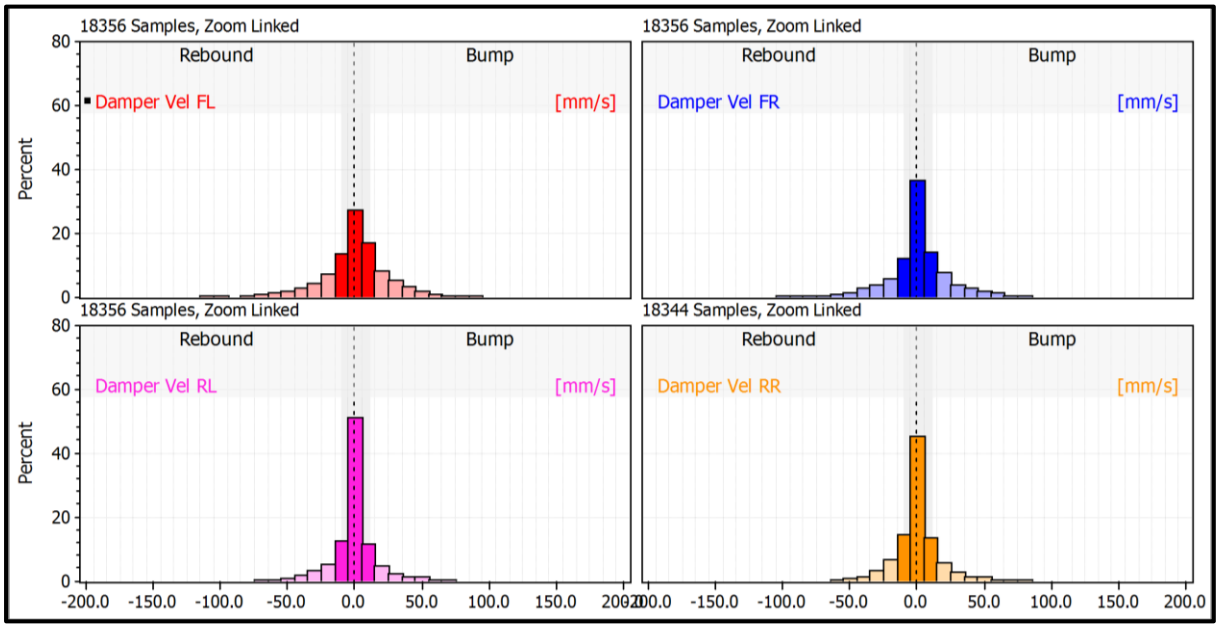

Figure 69 - Asymmetrical damper histogram from the 2018 competition for W-FS18

Apart from the obvious asymmetry and the non-normal distribution, average speeds and time percent spent in each stage were investigated. From Table 6 it can be seen that for high speed damping there was no large difference between bump and rebound (14% at most). However, the difference in time spent in bump and rebound for the low speed was large (up to 75%), especially for both the rear dampers, indicating a non-balanced car.

Table 6 - Damper speed analysis for the 2018 competition for W-FS18

		Bump (%)	Rebound (%)	% Difference	Average (%)
Front – Left (FL)	Lo%	27.4	25.7	-6.6	26.6
	Hi%	25.0	21.9	-14.2	23.5
Front – Right (FR)	Lo%	32.6	28.5	-14.4	30.6
	Hi%	20.4	18.5	-10.3	19.5
Rear – Left (RL)	Lo%	45.3	25.8	-75.6	35.6
	Hi%	13.7	15.2	9.9	14.5
Rear – Right (RR)	Lo%	43.4	25.4	-70.9	34.4
	Hi%	15.3	15.9	3.8	15.6

4.1.2 Driver Analysis

During testing for the W-FS18 car different suspension settings were tested (refer to Appendix A 6), mainly focused around the stiffness of the front antiroll bar. One driver was used for all three setups. The first setup had the front ARB at the middle setting, setup 2 at the softest and setup 3 removed the front ARB completely. It can be seen that no ARB at the front had the fastest lap times (Figure 70) and therefore was the setup used for any consecutive testing.

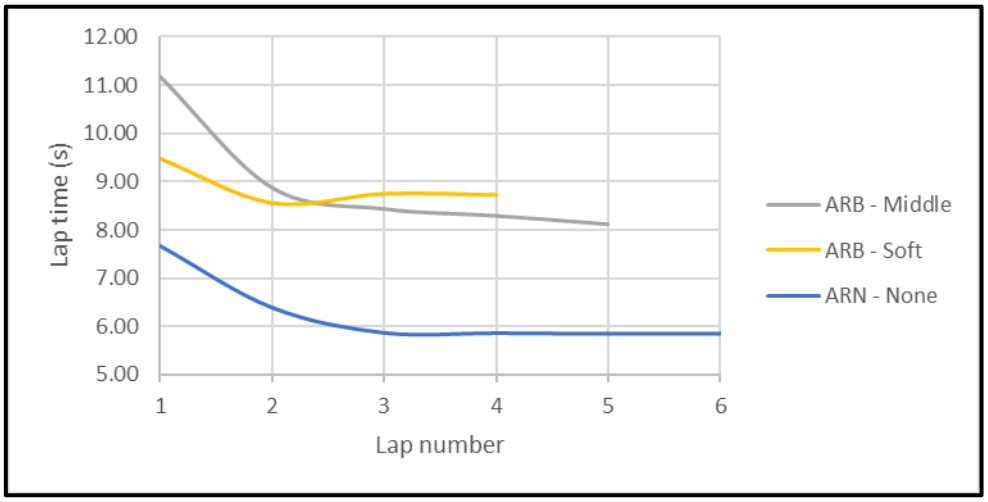

Figure 70 - Setup comparison for skidpad

In 2018, this was taken as the ideal setting and nothing else was examined due to time constraints between finishing the car, testing and shipping the car to Australia for competition. To select drivers for the skidpad at the competition, different people were tested in the car. During skidpad the drivers drive a circle (inner radius 7.5 m) twice in the clockwise and twice in the anticlockwise direction. In this case the setup was kept at setup 3 and the only variance was the driver. Figure 71 shows how the different drivers performed for a number of laps. It can be seen that the first lap was always the slowest which was expected as the driver is new to how the car reacts. As the driver became used to the handling the lap times dropped quickly and started to stabilise after about three or four laps. The only driver that was found to be inconsistent with lap times was Driver 3 (orange trace). His lap times fluctuated severely even after nine laps. Drivers 2 and 5 (the two blue lines) were faster than the rest, posting initial times faster than the best of the other drivers. It could be argued that Driver 2 had more practice as he was the driver used for initial setup testing.

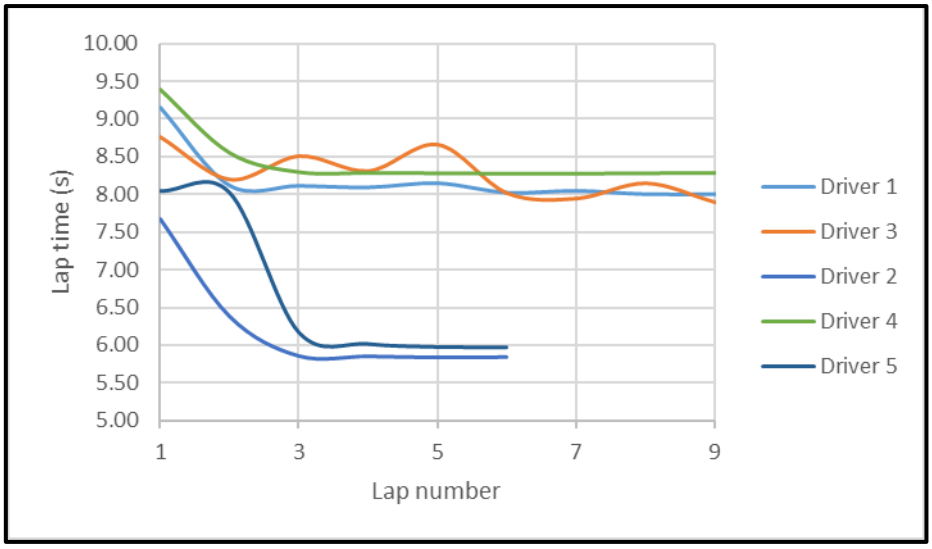

Figure 71 - Driver comparison for skidpad

Driver 4 (green line) was seen to be one of the most consistent drivers, posting times only varying within 0.02 s for the last five runs. He was chosen as the driver to complete all the testing for this research. This can further be justified by looking at the standard deviation in Table 7. He had the smallest deviation over the last three laps whereas Driver 3 has the largest. However, it should be noted that he had the smallest overall deviation, meaning his times did not fluctuate as much overall, i.e. times did not improve greatly between his first and last run, whereas Driver 5 had the largest standard deviation, i.e. greatest improvement.

Table 7 - Standard deviation for different drivers during skidpad testing in 2018

Standard Deviation in seconds					
Driver	**Driver 1**	**Driver 2**	**Driver 3**	**Driver 4**	**Driver 5**
All laps	0.73	1.47	0.62	0.74	2.07
Last 3 laps	0.05	0.02	0.26	0.01	0.05

Comparing the fastest times any of the drivers achieved (5.85 for one round) to the fastest overall time for skidpad for the combustion cars at the 2018 competition (5.083 for one round), it is clear to see that the team could gain points by maximising the grip and reducing lap times.

To establish if the car was reliable enough to tune the suspension and achieve consistent results, track data was analysed and drivers were talked to at length. From driver feedback it was established that the car did not bump steer or change behaviour drastically during a corner, both good indicators that the car would behave as expected to any setup changes. The data verified that no typical bump steer

indicators were present as the steering sensors did not show sudden motions in steering position while the car went over a bump.

4.2 Dynamics and Tyre Data

4.2.1 Effect of traction coefficient

The main purpose of a race car's suspension is to maximise the contact between tyre and road so it is only logical to start any investigation at the tyres contact patch and examine the traction.

To maximise tyre grip so the car has better traction around corners and greater cornering speed, it is necessary to know lateral and longitudinal forces developed at the tyre's contact patch as well as the friction (or traction) coefficients. However, these coefficients depend on the downforce exerted on the tyre as well as the tyre pressure, camber and slip angle.

Tyre temperature and pressure were recorded while different drivers completed twelve circles each on the skidpad track. The maximum average change in pressure was found to be 1 PSI after three complete rounds of skidpad testing and tyre temperature increased by 9 to 20 °C (Table 8).

Table 8 - Change in temperature and pressure after skidpad runs

Average - Total		
	Front Left - FL	Front Right - FR
ΔTemp (°C)	9.00	17.61
ΔPressure (PSI)	0.58	0.58
	Rear Left - RL	Rear Right - RR
ΔTemp (°C)	12.22	19.25
ΔPressure (PSI)	0.50	1.00

The tyre data provided by the Tire Test Consortium used tyre pressures of 10, 12 and 14 PSI (refer to Appendix A 8 for sample graphs). As the maximum tyre pressure change experienced by the car was only 1 PSI the effect of tyre pressure on friction coefficients could be neglected. If this analysis was to be applied to the endurance race (22 km long) this initial assumption would have to be revisited, but it certainly holds for short circuits.

Another assumption was to neglect the effect of tyre camber gain (how much the camber changes due to suspension geometry when the tyre is moving up or down relative to the car due the tyre rolling over a bump, braking or acceleration or when the car rolls during cornering) during ride. The W-FS18 suspension was designed to minimise camber gain during bound and rebound. A multibody simulation showed the camber change was only 0.043° per mm of wheel travel (Figure 72). The typical wheel

displacement during a race averaged about 5 mm travel with a maximum of 17 mm (for data refer to Appendix A 9). Therefore the tyre camber change was only 0.2° on average and 0.7° at maximum.

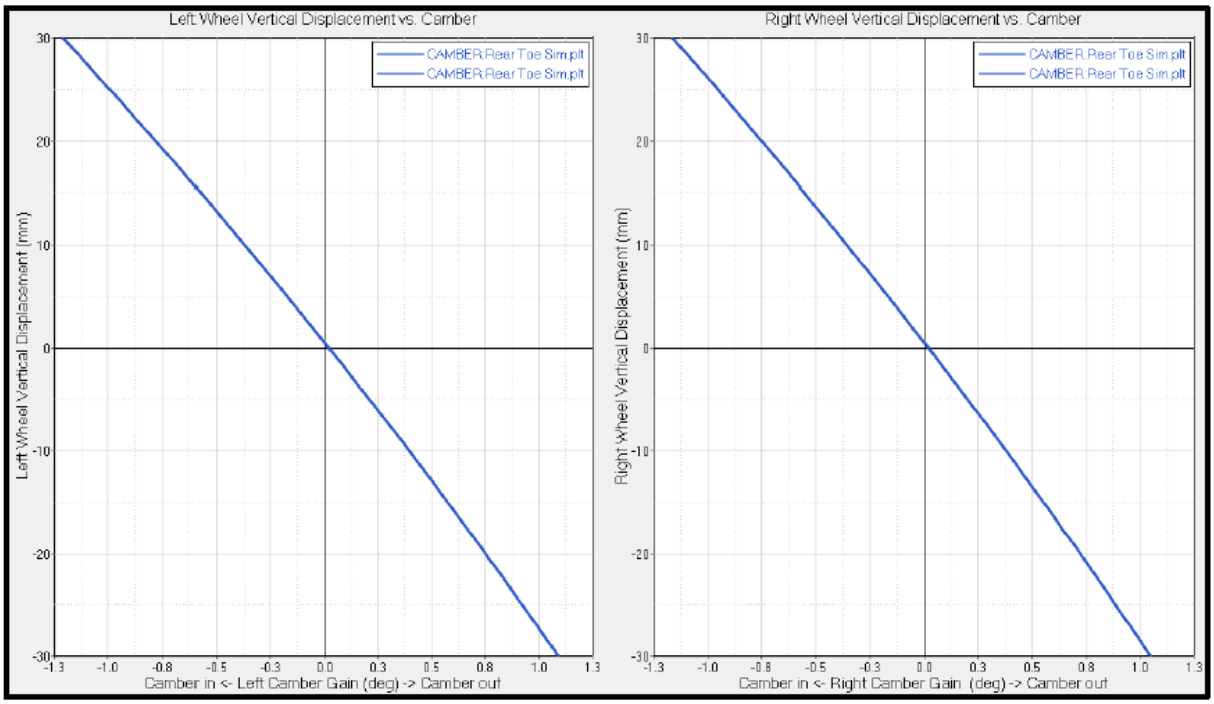

Figure 72 - Camber gain through the suspension travel from HyperWorks [38]

Typical wheel down force values for the W-FS18 car vary between 15 to 1,380 N during a corner, depending on the wheel (refer to Appendix A 10 for a full list of vertical loads). Using the Tire Test Consortium data and neglecting changes in tyre pressure and chamber, the lateral traction coefficient vs down force was plotted with a tyre static camber of 2° and pressure of 10 PSI (Figure 73) for 0° and 5° slip angle (angle of the plane of the tyre from the longitudinal axis of the car). Under no sweep, the maximum lateral traction coefficient was 0.4 at 1000 N downforce, while under sweep the traction coefficient ranges from 2.2 at 1400 N downforce (i.e. generating a lateral force of 3000 N) to 3 at 200 N downforce (i.e. a lateral force of 600 N).

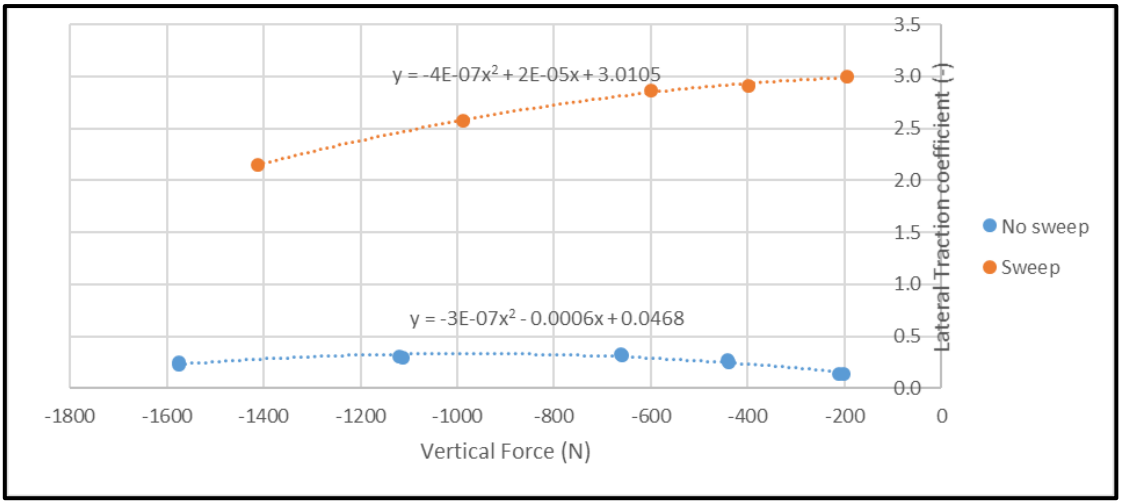

Figure 73 - Lateral traction coefficient vs down force

Keeping in mind that the front wheels of the W-FS18 car achieved a maximum slip angle of 6° (Figure 74) the effects of slip angle and down force on the lateral traction coefficient from the Tire Test Consortium data (Figure 75) were investigated. For a down force of 200 N, the maximum lateral traction was achieved at 8°, whereas for higher downforces, maximum lateral traction was achieved at 10-12°. After the maximum was reached, the coefficient drops due to the tyre not being able to support the load at the large slip angle and starting to slide. The red box in Figure 75 indicates the operating zone of W-FS18. Within this range the change in traction coefficient was approximately linear for downforces between 1300 to 1900 N, while for the 200 N and 600 N downforces, the curve is S-shaped. This means that for the outside wheels which experience most of the downforce during cornering and provide the majority of the traction, the lateral traction coefficient can be predicted using a simple linear relationship.

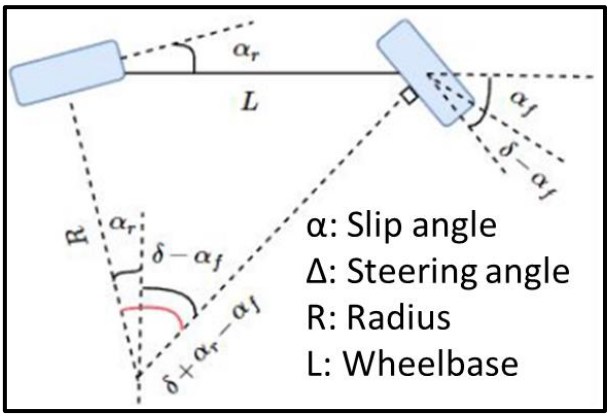

Figure 74 - Slip and steering angle

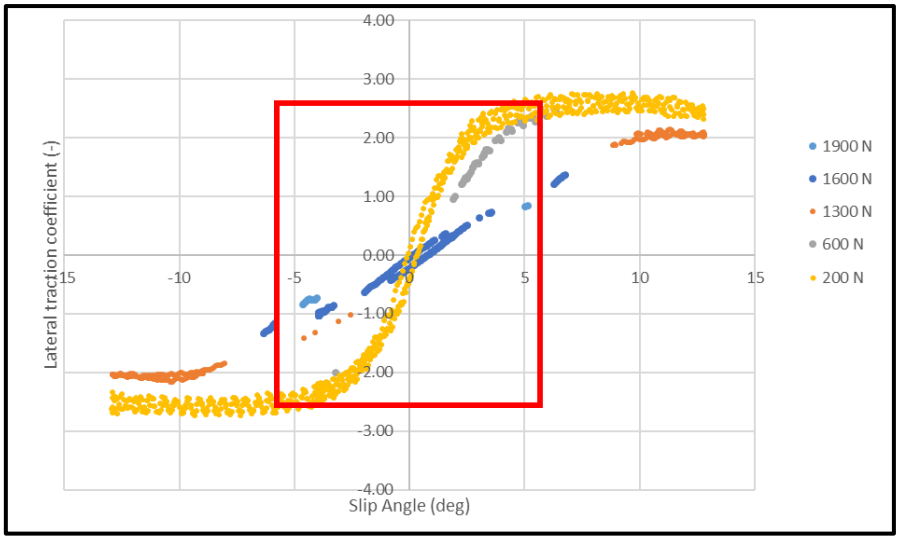

Figure 75 - Lateral traction for different slip angles

Tyre pressure will affect the traction and slip behaviour of the car. Using Tire Test Consortium data, the effect of tyre pressure and slip angle on lateral force generated was examined at a camber of 2° and a downforce of 1100 N (Figure 76). The tyre with the lowest pressure (red trace) produced the lowest lateral traction, whereas the higher pressures up to 12 PSI showed higher lateral loads. The highest tyre pressure (14 PSI, grey trace) was too inelastic to allow enough deformation to maximise grip. The lowest pressure trace has a deformation at around 5-6° slip angle when the tyre is returning to 0° slip angle, likely due to the tyre contact patch having a slightly higher slip angle than the overall tyre because the tyre is not rigid enough. This difference in slip angle causes the tyre to "flop over" at some point which appears to occur at 5-6° slip angle.

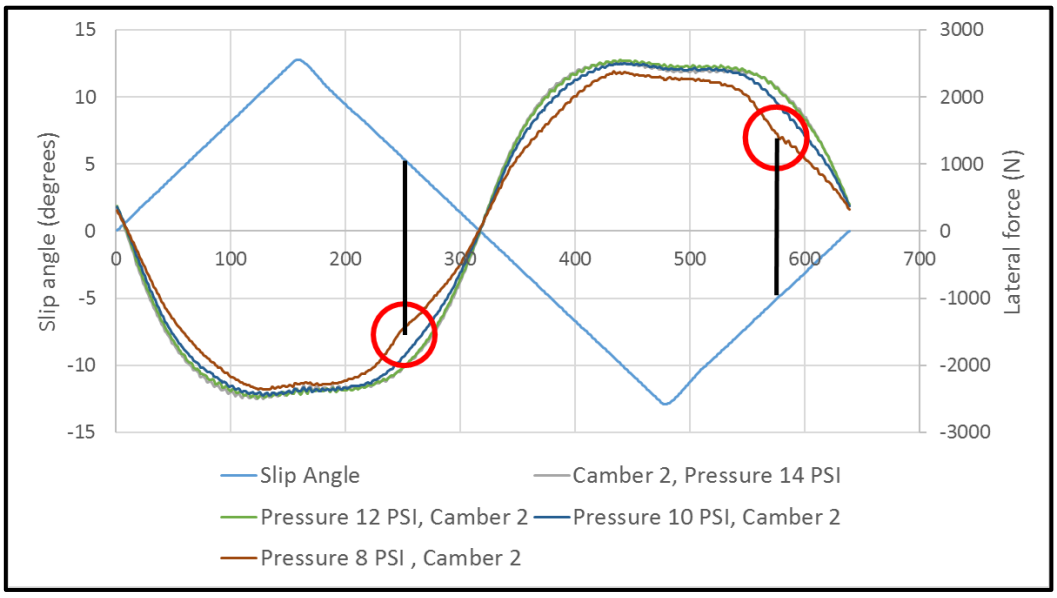

Figure 76 - Lateral load and slip angle comparison for a swept run for different tyre pressures under the same down force and camber angles

Figure 77 shows that the effect of camber on down force and slip angle is small. All four camber lines follow the same shape and peak at roughly the same slip angle (between 13° and 12°). The camber angles investigated varied from 0° up to 3° in the positive direction (i.e. the top of the tyre points towards the right, refer to Figure 15 for the coordinate system). When a negative lateral load is applied (towards the left), a large positive camber reduced the lateral load thereby reducing the traction coefficient. However, when the lateral load was positive (applied to the right, Figure 78) a large camber increased the traction coefficient. However, overall it can be said that for a small camber gain (<1°), the effect it has on traction coefficient and lateral force can be neglected. The difference between lateral force for 2° and 3° camber is 130 N at the most, considering the down force, this results in a difference of 0.03 for the lateral traction. Larger camber angles were not tested. Camber gain through steering was neglected as well. This assumption was verified in section 4.4.

It is interesting to note that in the region where the lateral load is negative (left) the difference between the cambered tyre and the non-cambered tyre is more noticeable than on the right side of the graph, where the lateral load is positive. The positive lateral load combined with the positive camber mimics a negatively cambered tyre on the outside of a corner. The down force will try and straighten the tyre and increase the contact patch size to the size of a non-cambered tyre. The near zero size difference in contact patch means that the lateral load created will not vary as much. The negative lateral load on the left side of the graph does the opposite. The down force pushes the cambered tyre further in that direction, thereby decreasing the size of the contact patch and lateral load further.

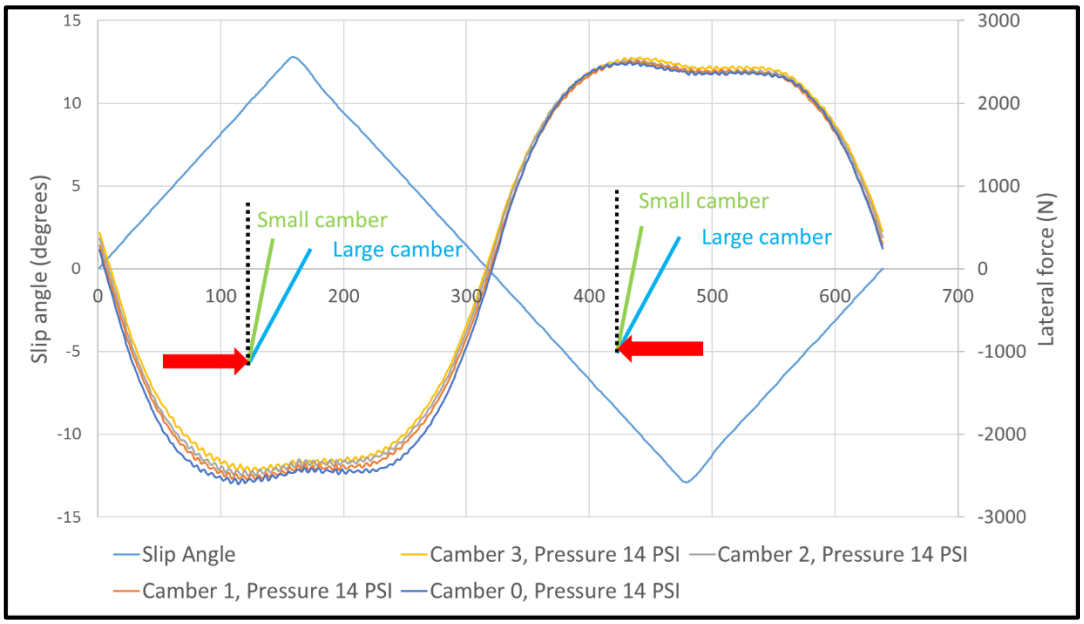

Figure 77 - Lateral load and slip angle comparison for a swept run for different camber angles under the same down force and tyre pressure

Figure 78 - Positive camber with positive lateral force applied

A similar process as for the lateral traction was used to obtain equations for longitudinal traction coefficients during braking and acceleration (Figure 79 and Figure 80). Slip angle did not affect the longitudinal coefficient to the same extent as the lateral scenarios. This was expected as it is the slip angle that generates lateral loads, which should be near zero for acceleration and braking. However, it is clear to see that during cornering slip angles affect traction properties and cannot be neglected. Based on equation (37) and (38) slip angle can be calculated if the cornering stiffness of the tyre is known. Cornering stiffness is the tyre's ability to resist deformation under lateral load [3] and can be defined as the slope of the lateral load versus slip angle for small slip angles where the graph appears linear (Figure 81).

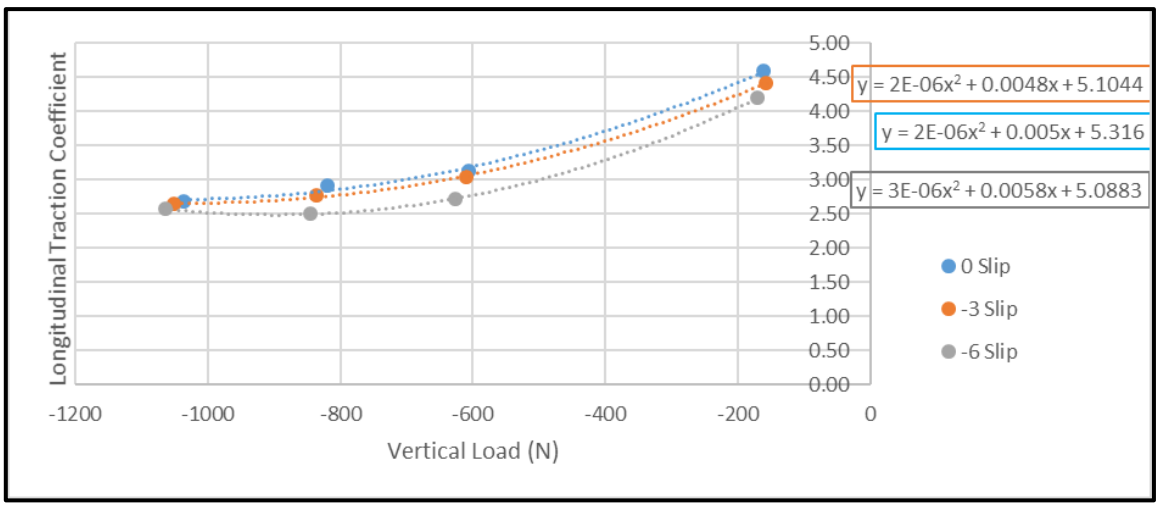

Figure 79 - Acceleration traction coefficient

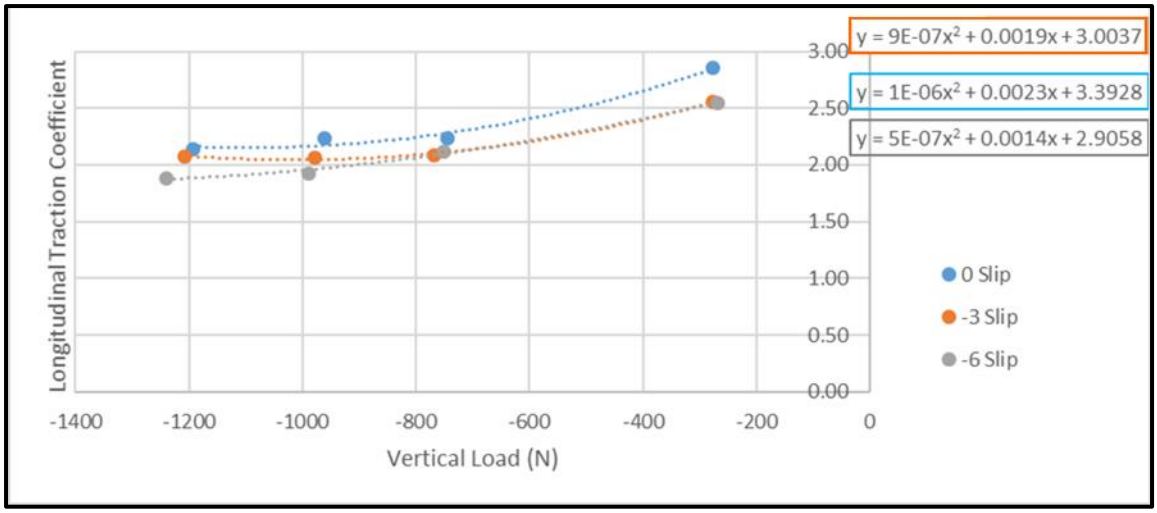

Figure 80 - Braking traction coefficient

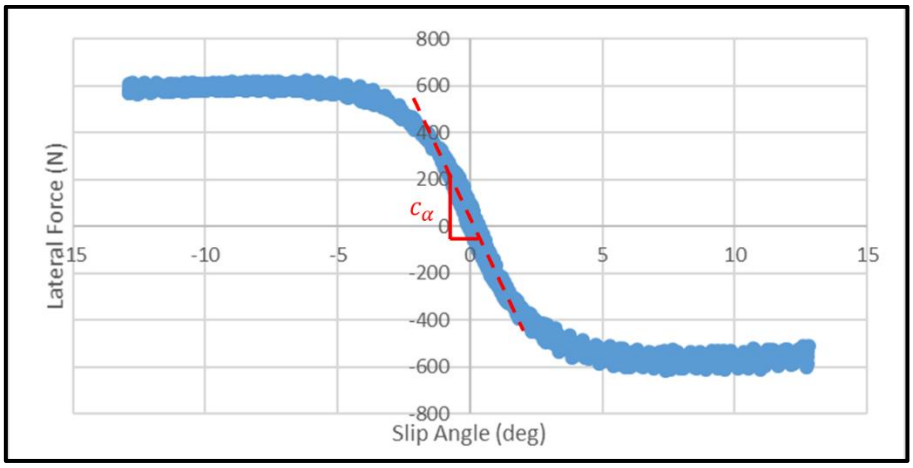

Figure 81 - Cornering stiffness for arbitrary down force

Repeating this for various down forces (for a given pressure and camber) gave an equation from which cornering stiffness was calculated for any vertical load. The tyre data provided by the Tire Test Consortium already provided cornering stiffness for various down forces so a graph could be plotted from these numbers (Figure 82).

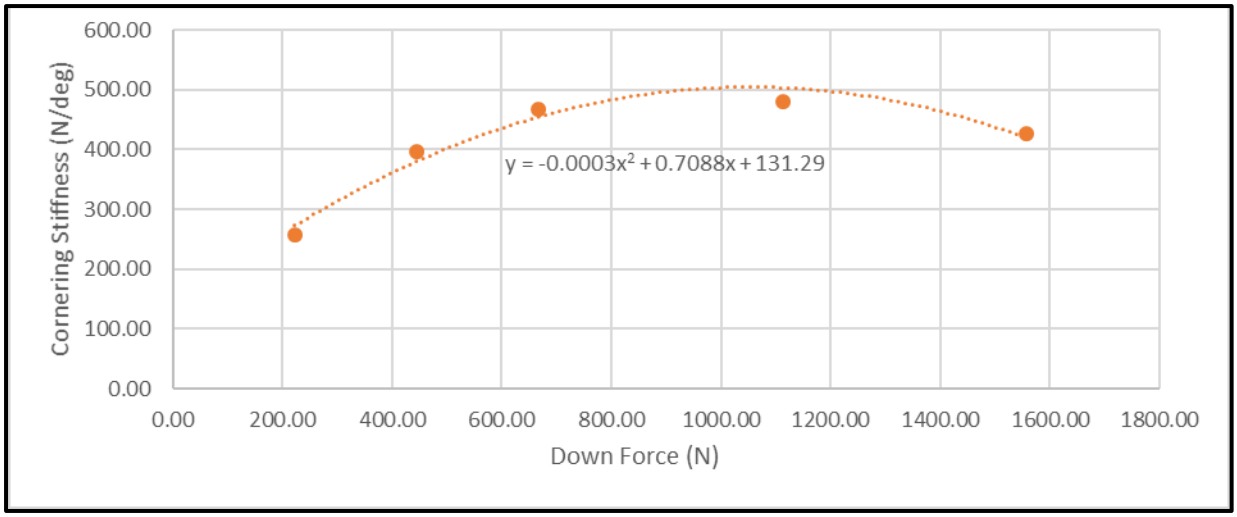

Figure 82 - Cornering stiffness based on down force

The last parameter that needs to be known to calculate slip angle is the lateral or longitudinal acceleration. It is helpful to look at the maximum acceleration the car can withstand without losing traction.

W-FS18 has adjustable antiroll bars, meaning that the amount of roll and hence the maximum lateral acceleration would be affected by the stiffness setting. Four different settings were tested and calculated: no ARB, at the softest, in the middle and the stiffest setting (same setting at the front and rear), the corresponding stiffness can be found in Table 9. The difference in stiffness from front and rear on the same setting is due to the difference in length and motion ratio.

Table 9 - W-FS18 ARB stiffness for different settings

Stiffness (Nm/°)	None	Soft	Middle	Stiff
Front	0	2421.1	5447.6	9684.5
Rear	0	2959.9	6659.8	11,839.6

The suspension geometry and spring rates of W-FS18 were used to calculate the lateral and longitudinal accelerations to lift the inner front and rear wheel (Table 10). The acceleration was calculated by considering both lateral and longitudinal load transfer. As previously mentioned the suspension travel was small and therefore camber gain was neglected.

The loss of traction was determined by two conditions: The load transfer away from the wheel was larger than the vertical force required to lift the wheel; and the suspension travel was large enough for the shock to reach maximum extension, locking it and thereby levering the wheel off the ground. This enabled a traction circle to be drawn for the limits of the car, showing the drivers how far they can push the car without losing traction.

Table 10 - Accelerations to lift wheels

	Front	Rear		
Roll to lift				
Upwards force to lift inner wheel	684.25	713.68	N	
Lateral acceleration to lift wheel	1.71	1.98	g	No ARB
	1.88	1.80		ARB Middle
	1.87	1.81		ARB Softest
	1.89	1.79		ARB Hardest
Acceleration to lift				
Upwards force to lift inner wheel	684.25	713.68	N	
Longitudinal acceleration to lift	2.57	-	g	
Braking to lift				
Upwards force to lift inner wheel	684.2475	713.6775	N	
Longitudinal acceleration to lift	-	2.68	g	

During a corner the jacking forces, body roll angle and suspension travel depend on the stiffness of the antiroll bar (ARB). The current setup of the W-FS18 is with the ARB in the middle position, resulting in a maximum possible lateral acceleration of 1.8 g. For acceleration and braking, the maximum acceleration can be seen to be 2.6 g and 2.7 g respectively. With these acceleration values it is possible to plot a traction circle that shows the limits of the car with the current suspension setup (Figure 83).

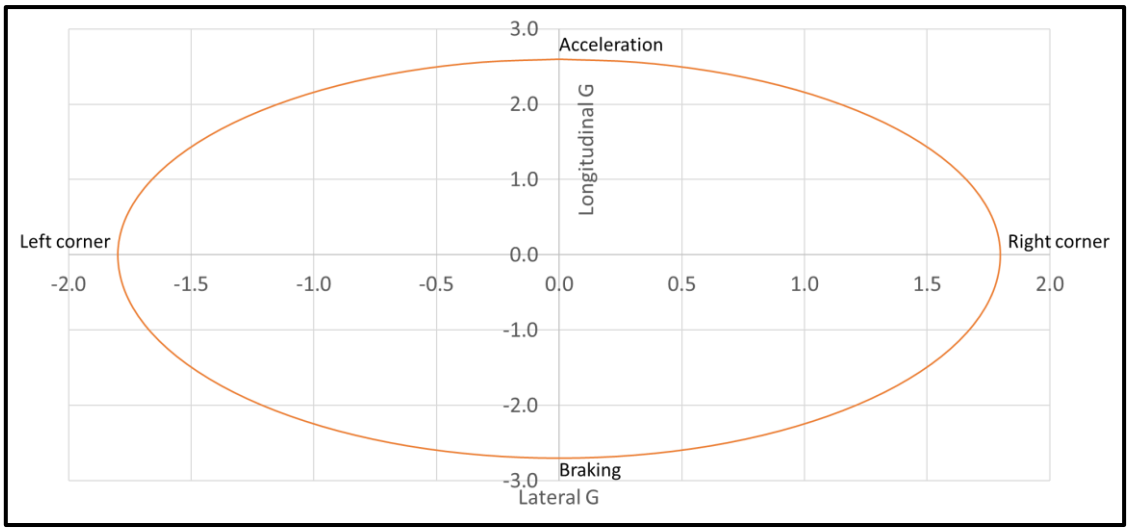

Figure 83 - Traction circle for current W-FS18 setup

This traction circle (or ellipse) can be used to determine maximum combined lateral and longitudinal acceleration, for example at a corner exit when the car still experiences lateral loading but also longitudinal loads due to the driver accelerating.

The maximum lateral accelerations vary with ARB settings and therefore the traction circle will as well (Figure 84 and Figure 85). This is to be expected as the ARB adds roll stiffness to the car. No ARB resulted in the lowest lateral acceleration as the maximum load transfer is exceeded earlier. However, it is interesting to note that the hardest ARB setting did not produce the most lateral acceleration, instead, the softest setting did. This is due to the ARB being too stiff at the hardest setting, resulting in it mimicking the behaviour of a solid axle, jacking the inner wheel off the ground earlier than expected.

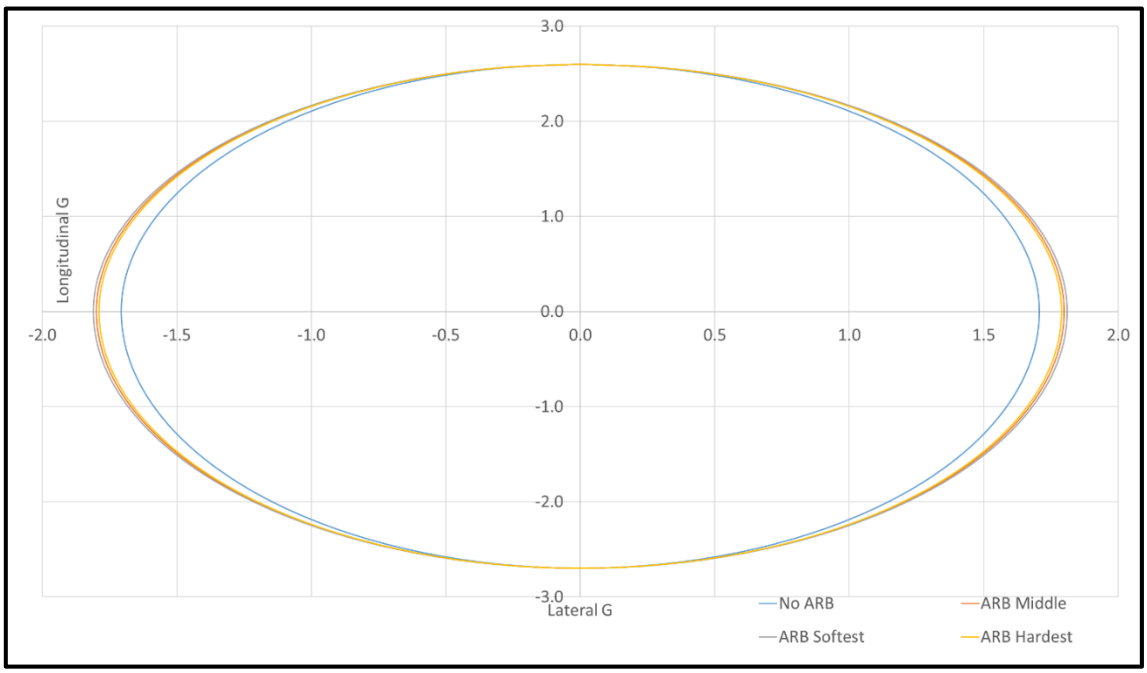

Figure 84 - Traction circle for different ARB settings

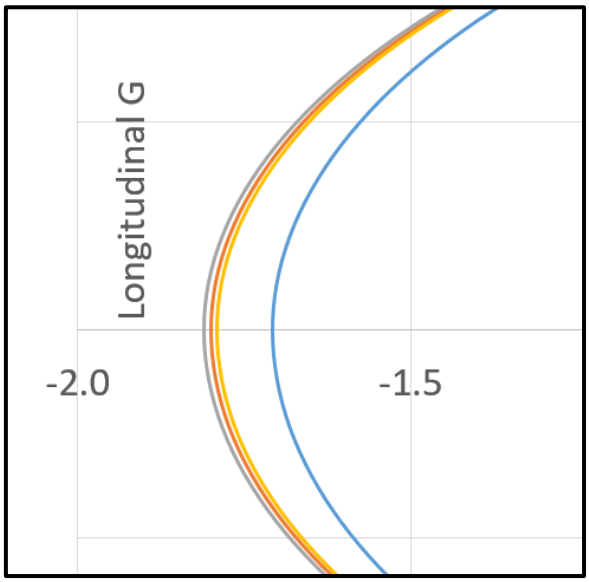

Figure 85 - Zoomed traction circle for different ARB settings

Different spring rates are another setup change that affects the traction circle (Figure 86). Even though spring rates do not affect the overall load transfer, they affect the roll stiffness of the car and thereby affecting the contribution of the sprung mass to the jacking forces. For this case the ARB was kept constant at its middle setting.

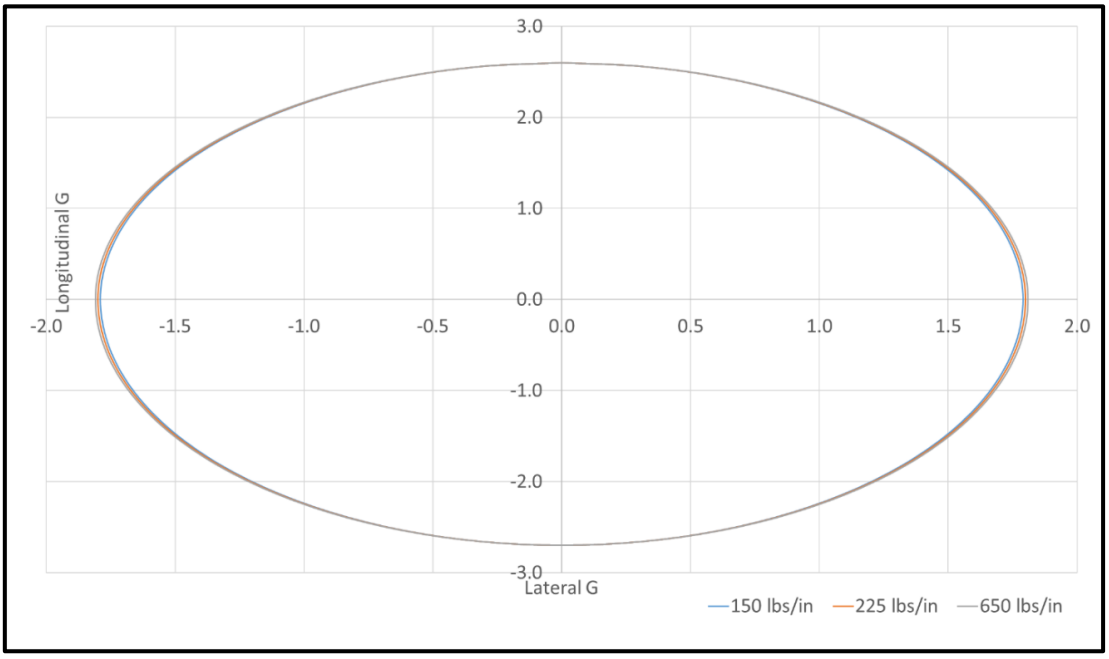

Figure 86 - Traction circle for different spring rates

Figure 87 shows a zoomed in section of Figure 86 during a pure left hand corner (no longitudinal acceleration). It can be seen that there is a small difference between the different spring rates. The effect of spring rate on the traction circle was going to be investigated on the W-FS18 car, however due one of the hubs failing, this could not be done (more detail in section 4.5).

Both front and rear spring rates were varied in the model to explore the effect of spring rate on traction. The stiffer the spring the more lateral acceleration is possible before the tyre loses contact with the road. However, this is only feasible to a certain degree as when the springs become too stiff the car barely produces roll, creating less feedback for the driver as well as creating an uncomfortable ride.

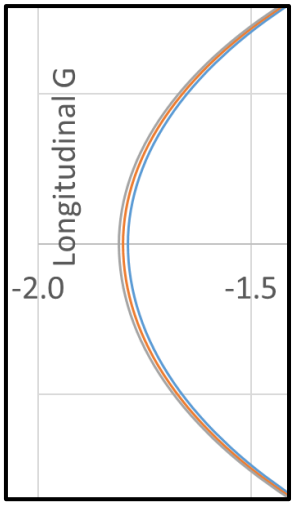

Figure 87 - Zoomed traction circle for different spring rates

Most cars will run different spring rates at the front and rear of the car to create balance and prevent under- or oversteer. This is due to the difference in weight distribution, track width and often roll centre height. The difference in roll centre height (refer to Table 4 in section 3.1 for W-FS18 roll centre heights) will mean that the car rolls about a different point, creating a different characteristic at the rear compared to the front of the car. Different spring rates or ARB settings can help to even out this effect and aid cornering behaviour.

Comparing a soft spring at the front and a stiff one at the rear (blue line) to the opposite (orange line) (Figure 88), it can be seen that the softer spring at the rear allows for a greater lateral acceleration. When comparing the maximum acceleration values for the unequal springs to Figure 86, it can be seen that the softer spring at the front results in the front wheel lifting at a lower acceleration than if the same spring was used on the front and rear. A stiffer spring at the front however allows for more acceleration (Table 11). This difference is due to the shorter track width in the rear, higher unsprung weight in the rear wheels due to the tripod joints and drive shaft, and lower roll centre at the rear. The calculations for all the traction circles assumed a 50/50 weight distribution between the front and the rear wheels similar to the W-FS18 car. Changing the spring rates did not affect the maximum longitudinal acceleration or braking as this is based on an overall equilibrium of moments (Equation (5)).

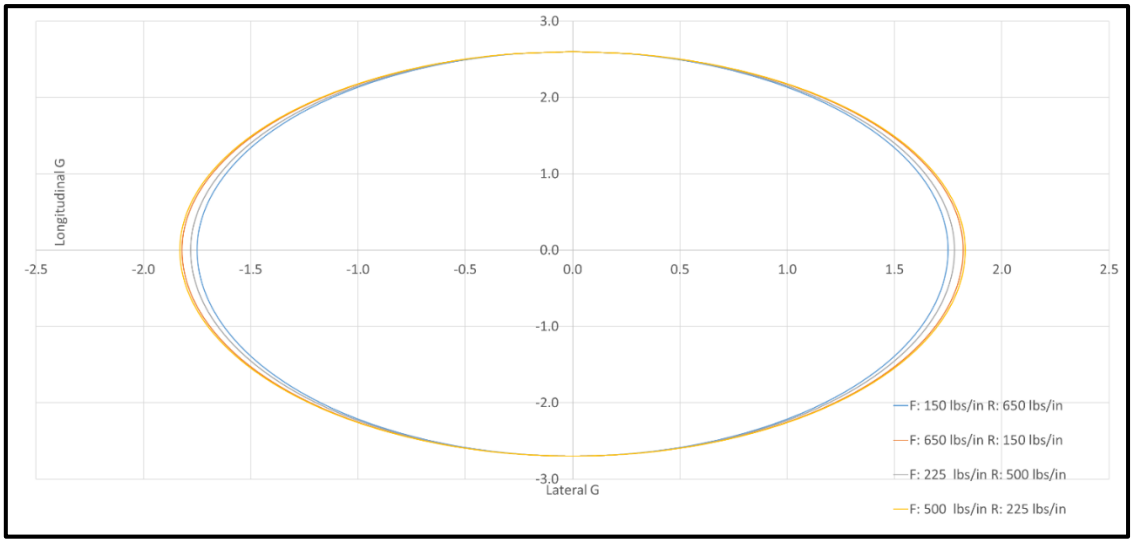

Figure 88 - Traction circle for unequal springs

Table 11 - Lateral acceleration to lift wheels for different spring rates

Spring Rate – Front (lbs/in)	**Spring Rate – Rear (lbs/in)**	**Lateral Acceleration to lift**
150	150	1.79 g (rear lifts)
150	650	1.75 g (front lifts)
650	150	1.82 g (rear lifts)

Changing the weight distribution will also affect the traction due to the load transfer distribution changing. This change affected both lateral and longitudinal traction (Figure 89). As the down force increases, both the lateral and longitudinal traction coefficients decrease (Figure 73 in 4.2.1), thereby decreasing the overall traction and reducing the maximum lateral acceleration possible. This is especially notable for the 10/90 and 90/10 F/R weight distributions (green and orange in Figure 89). With 90% weight distribution on the front wheels, the maximum acceleration reaches 4.4 g, whereas during braking the maximum deceleration is only 0.4 g. The opposite is true for 90% weight distribution towards the rear (i.e. high braking but low positive acceleration). A 50/50 weight distribution (light blue line) produces the greatest lateral acceleration of 1.8 g due to distributing the weight evenly between front and rear of the car.

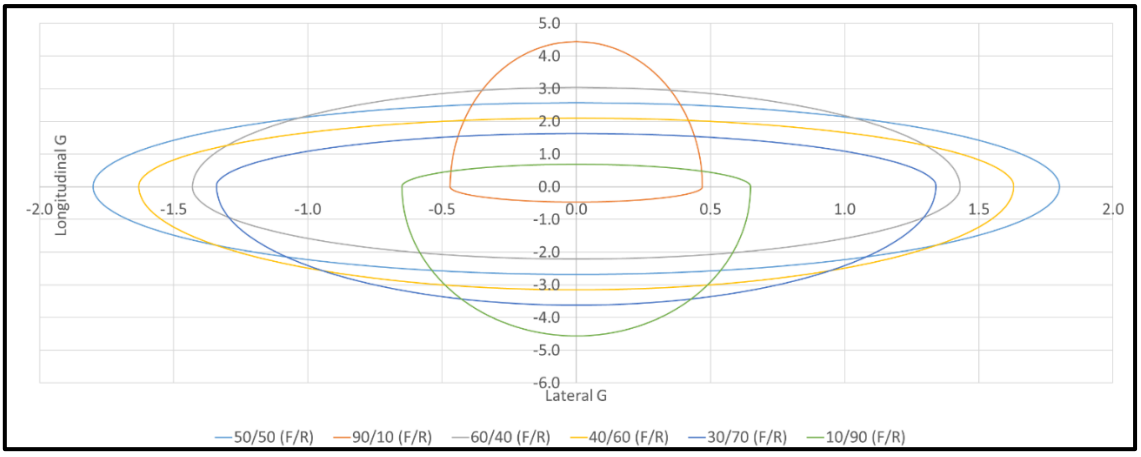

Figure 89 - Traction circle for different weight distributions

4.2.2 Effect of spring rates

The assumption of neglecting camber gain for calculating the traction coefficient only holds as long as the change in camber and overall suspension travel is small. The suspension travel of the W-FS18 car was small (5 mm average) and the dynamic change in camber was only 0.2° with a maximum lateral and longitudinal accelerations of 1.5 g and 2 g respectively. A stiffer spring further reduced suspension travel while even the softest spring (150 lbs/in or 26 N/mm) only resulted in 10 mm travel resulting in a camber gain of 0.43° (Figure 90). To reach at least 1° of camber gain the suspension travel would need to be 23.26 mm, which using soft springs (150 lbs/in) would require a lateral acceleration of 3.5 g and 4.7 g longitudinally. However, these accelerations are not feasible for the W-FS18 car due to the types of tyres used, suspension geometry, track width, roll centre and centre of mass. Therefore the effect of dynamic camber change on traction for the W-FS18 car can be neglected.

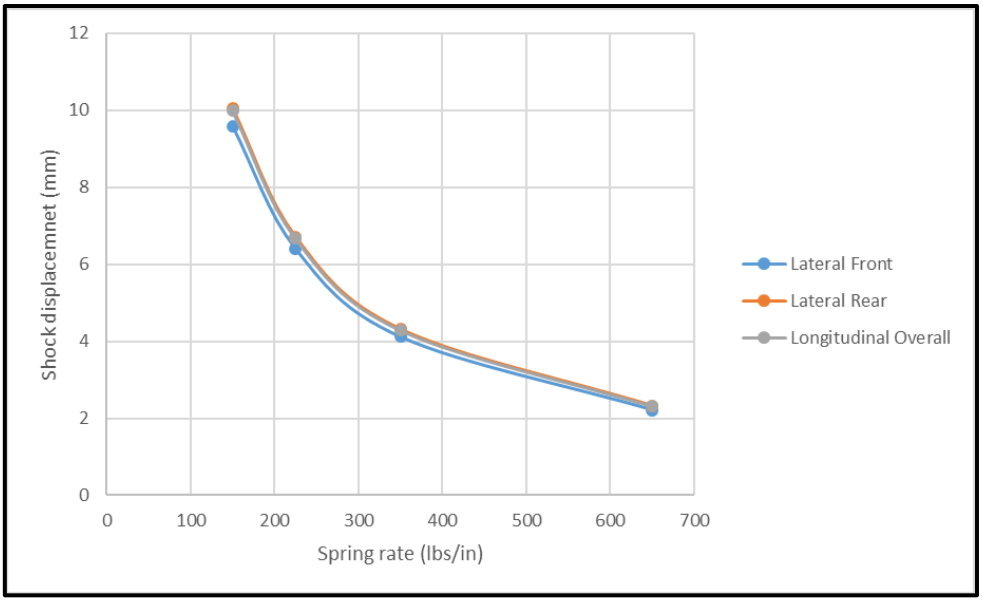

Figure 90 - Suspension travel for different spring rates

Increasing spring rates will increase the ride frequency of the car, i.e. the ride is not as soft, reducing driver comfort (Figure 91). As stated in section 2.3.3, a stiffer car allows for a quicker transient response of the car during cornering, braking and acceleration, whereas a lower frequency allows for more mechanical grip. Different combinations of front and rear springs will produce different ride frequencies as well as different frequency gains from front to rear. Most road cars have a higher rear ride frequency gain to eliminate pogoing after riding over a bump, however, this is not necessarily true for race cars. Often the rear in a race car has a lower ride frequency to improve response of the car during corner entry and improved grip for acceleration out of the corner.

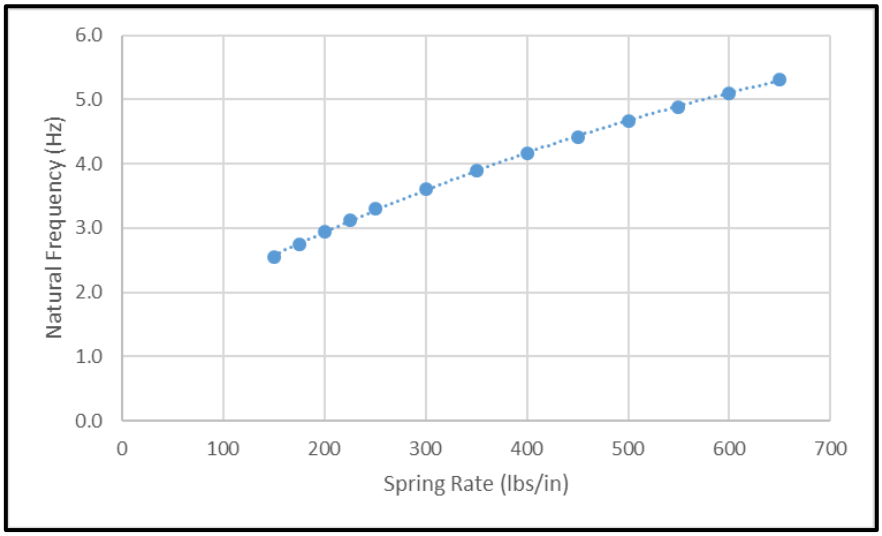

Figure 91 - Effect of spring rates on ride frequency

Comparing ride frequencies for different spring combinations (Table 12), a soft spring at the front (150 lbs/in) and a stiff one at the rear (650 lbs/in) create a large gain in frequency at the rear (over 100%). A setup like this will react very differently at the front of the car compared to the rear to bumps and driver input. The front of the car will be sluggish to turn into a corner whereas the rear will be very responsive to any kind of input and will tend to “kick” out whenever there is a small unevenness (i.e. bump or curb) on the road. The opposite will be true for a stiff front and a soft rear (50% rear frequency loss). Ideally, the front and rear frequencies will be similar (~10% difference in frequency) but still create a rear gain or loss depending on the type of track and road surface. For a corner heavy course, the front should be stiff and the rear soft to aid steering input and grip during cornering. On bumpy road surfaces, such as gravel roads, the rear should have a higher frequency compared to the front to avoid excessive pitching.

Currently W-FS18 runs 225 lbs/in springs at both the front and rear. Considering suspension travel from Figure 90 and ride frequency from Table 12 as well as the increase of traction for a stiffer front

from Figure 88 it would be advisable to run the 225 lbs/in springs at the rear and the 250 lbs/in springs at the front. This would aid overall traction as well as responsiveness during corner entry.

Table 12 - Ride frequency gain for different combination of springs

Spring rate (lbs/in)		Frequency (Hz)		
Front	**Rear**	**Front**	**Rear**	**Rear Gain (%)**
150	150	2.55	2.55	0
350	350	3.90	3.90	0
650	650	5.31	5.31	0
150	650	2.55	5.31	108.01
650	150	5.31	2.55	-51.93
250	500	3.30	4.66	41.42
500	250	4.66	3.30	-29.29
225	250	3.13	3.30	5.44
250	225	3.30	3.13	-5.16

As previously mentioned (Figure 90), different spring rates affect the displacement of the shock. Shock displacement can be used to calculate the roll angle of the body of the car (Figure 92), based on equations (32) and (33). However, as mentioned in 2.2.6, it is important to note that only the sprung mass load transfer affects the shock displacement and thereby roll angle.

Figure 92 - Body roll angle

Softer springs with more travel will allow for greater body roll (Figure 93). A certain amount of body roll is desirable as otherwise the driver does not get good feedback from the car during a corner. However, too much roll will lift the inside wheel off the ground prematurely by “locking” the suspension out, effectively creating a go-kart with no suspension that tripods around the corner as soon as the down force on it decreases further.

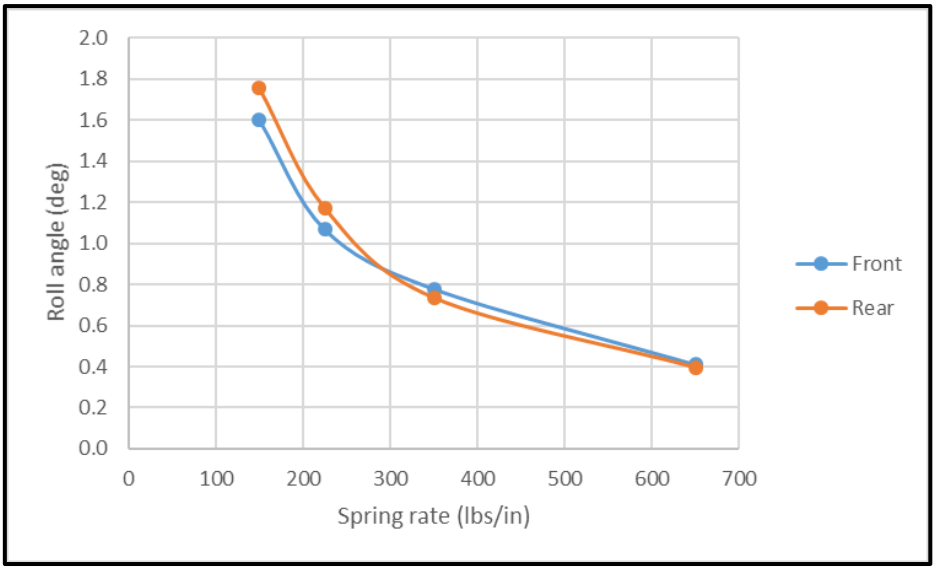

Figure 93 - Effect of spring rate on roll angle

As expected, the stiffer the spring the less deflection and thereby the less angle is developed. Often it can be helpful to not just look at the roll angle itself but rather the roll gradient, which is the roll angle per g of lateral acceleration (Figure 94).

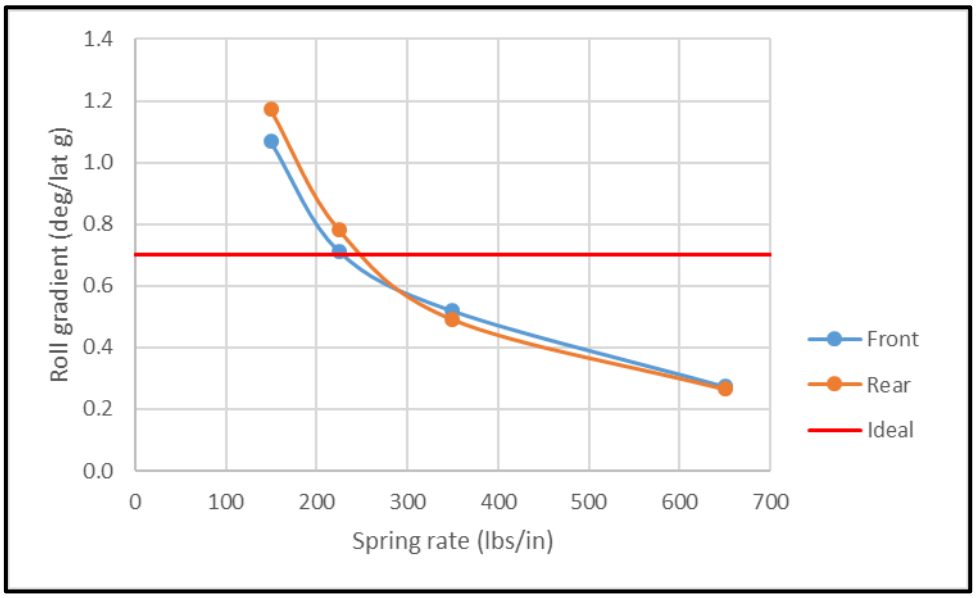

Figure 94 - Roll gradient for different spring rates

The theoretical ideal value of 0.7 °/g lateral acceleration [29] can be achieved with 225 lbs/in springs at the front and 250 lbs/in at the rear. However, as previously mentioned to aid steering the front should have stiffer springs. Considering this, it might be better to have 225 lbs/in at the rear and decrease the roll gradient with the help of an antiroll bar as Figure 94 is based on an antiroll bar at the middle setting for both front and rear.

4.2.3 Effect of damping rates

As mentioned in section 2.2.8, too much damping can lead to the shock being "locked" out, resulting in a go-kart like car with effectively no suspension. Each shock on the W-FS18 car has high and low speed damper settings, resulting in 288 different possible settings for one corner of the car. This high number of possibilities (~600 million for four corners) makes calculating the exact point at which the suspension becomes "locked" nearly impossible. This means that a theoretical damping rate can initially be chosen when the car is designed, however due to manufacturing discrepancies, different track characteristics and driver preference the rate will most likely have to be adjusted after on track testing.

From research [31] it was found that the most accurate model would be one that considers both lateral and longitudinal load transfer, i.e. a full car model and not just one or two corners. Due to a need to repeat and adjust damper numbers quickly and easily compare trends, a full car suspension model was implemented in Matlab (refer to Appendix A 11 to A 13).

However, due to complexity, processing times as well as the number of specific engine data (i.e. power and torque curves), only a steady state system was implemented. This meant both lateral and longitudinal accelerations could be specified but were assumed to be constant through the simulation, i.e. steady state cornering. Furthermore, Matlab was used as a visual graphing tool to display the effect of different damping rates for a certain displacement which was used to validate the calculations. In Figure 95 the chassis displacement for one corner during a 10 mm bump can be seen. Different low speed compression and rebound (LSC and LSR) as well as high speed compression and rebound (HSC and HSR) were plotted. For a damping ratio of 1.0, the equation for displacement becomes undeterminable (division by zero) and instead is plotted for 1.001. Without consideration for damper velocity this graph does not give much more information other than what is expected from damper theory mentioned in 2.2.8. However, it does validate the model as the model behaves as expected.

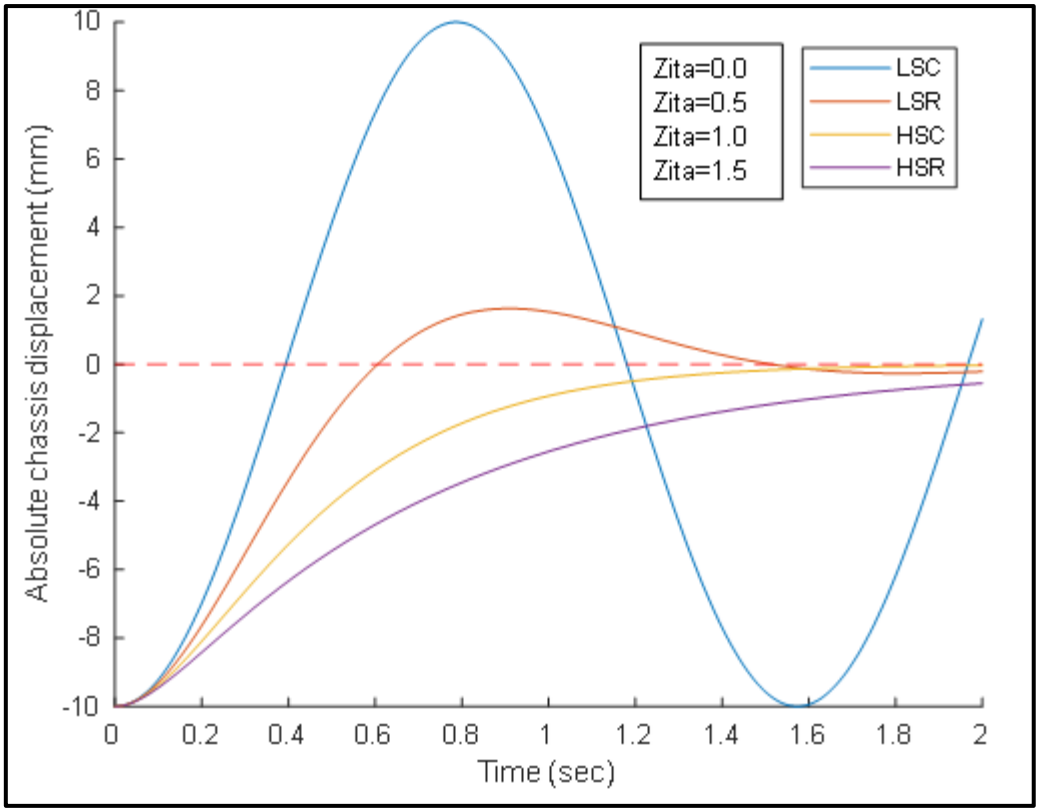

Figure 95 - Chassis displacement for 10 mm bump

The model was adapted to show the damper speed (equivalent to chassis speed. A loop was created initially calculating the damper speed based on the low speed ratio. If the calculated speed was higher than the low speed for compression or rebound (LSR or LSC) the calculation was repeated with the appropriate high speed ratio. The validity of this was investigated with track data and will be discussed in greater detail in section 4.3.4. Figure 96 shows the absolute damper velocities during a constant velocity (no longitudinal acceleration) and 1.3 g lateral acceleration corner. To be able to check the validity of the model with track data, damping ratios were chosen that could be tested in real life. As can be seen, the damper on the front outside wheel has the highest velocity at 32 mm/s, indicating that the damper is well into the high speed region. Furthermore, the damper velocities vary between the inside and outside. This is due to the difference in damping ratio between compression and rebound which results in the inner wheels settling down faster than the outside. This is favourable as the inner wheels are more likely to lose traction as they are in rebound and the load transfer is to the outer wheel.

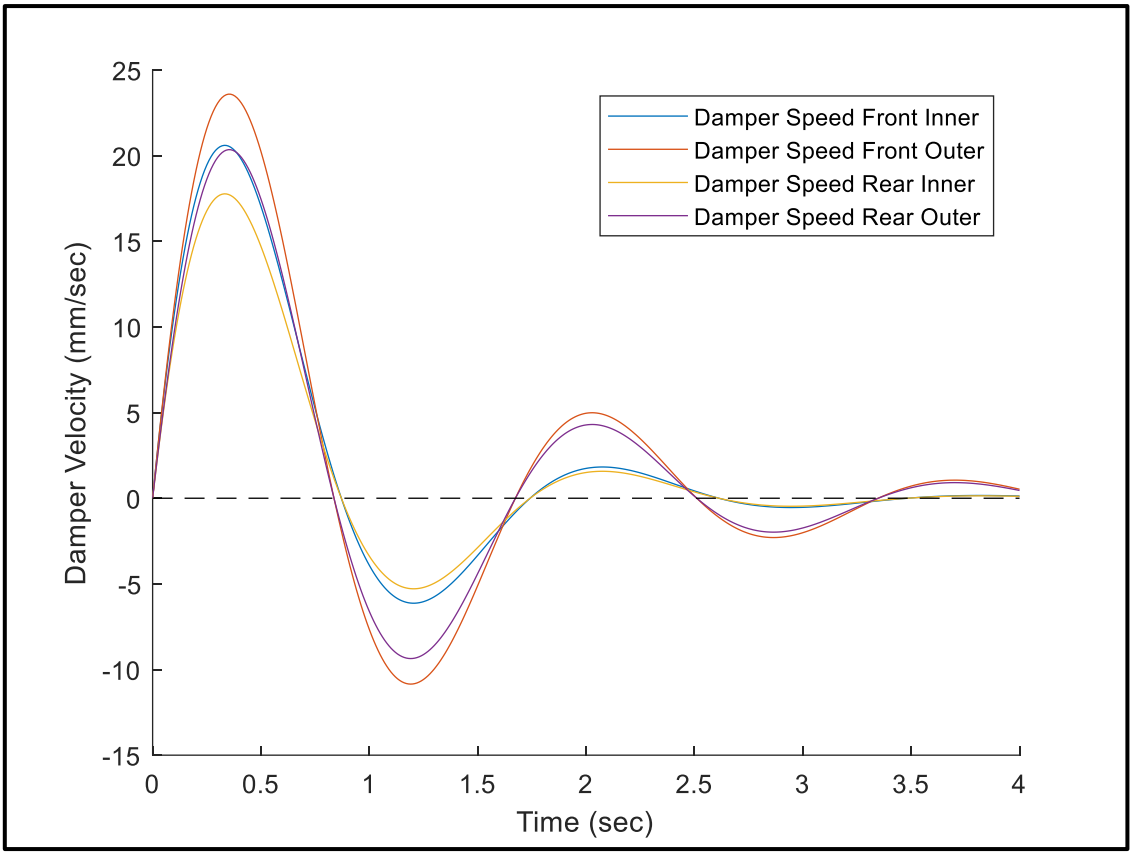

Figure 96 - Damper velocity for a constant velocity 1.3g corner

Damping ratios affect how quickly the wheel returns to its original position after a disturbance but not the initial displacement itself. A large fast bump might not cause the car to lose traction if the damping rates are chosen so the wheel returns quickly to the ground and does not oscillate past the point at which the car loses grip. In Figure 97, Matlab was used to plot this for a 30 mm disturbance. The red dotted line indicates the displacement at which the wheel will lift off the ground for the current suspension setup. If the initial displacement is quick it is possible for the car to not lose traction if the wheel is allowed to return to the ground and be loaded again. This can be seen to be the case with the damping ratio of 0.6 for which the damper (equivalent to chassis) displacement returns to below the lifting threshold within 0.4 seconds. For a damping ratio of 0.2 this occurs even quicker although it overshoots the threshold again in the rebound region and should therefore be avoided. The overdamped system with a ratio of 1.5 takes longer to return to equilibrium, meaning the tyre is unloaded for longer than necessary. This threshold as well as the damping ratio will vary not only from car to car but also between setups. This theoretical model has shown that the ideal ratio for the W-FS18 car will be about 0.6. This was be verified with track testing and driver feedback in section 4.5.

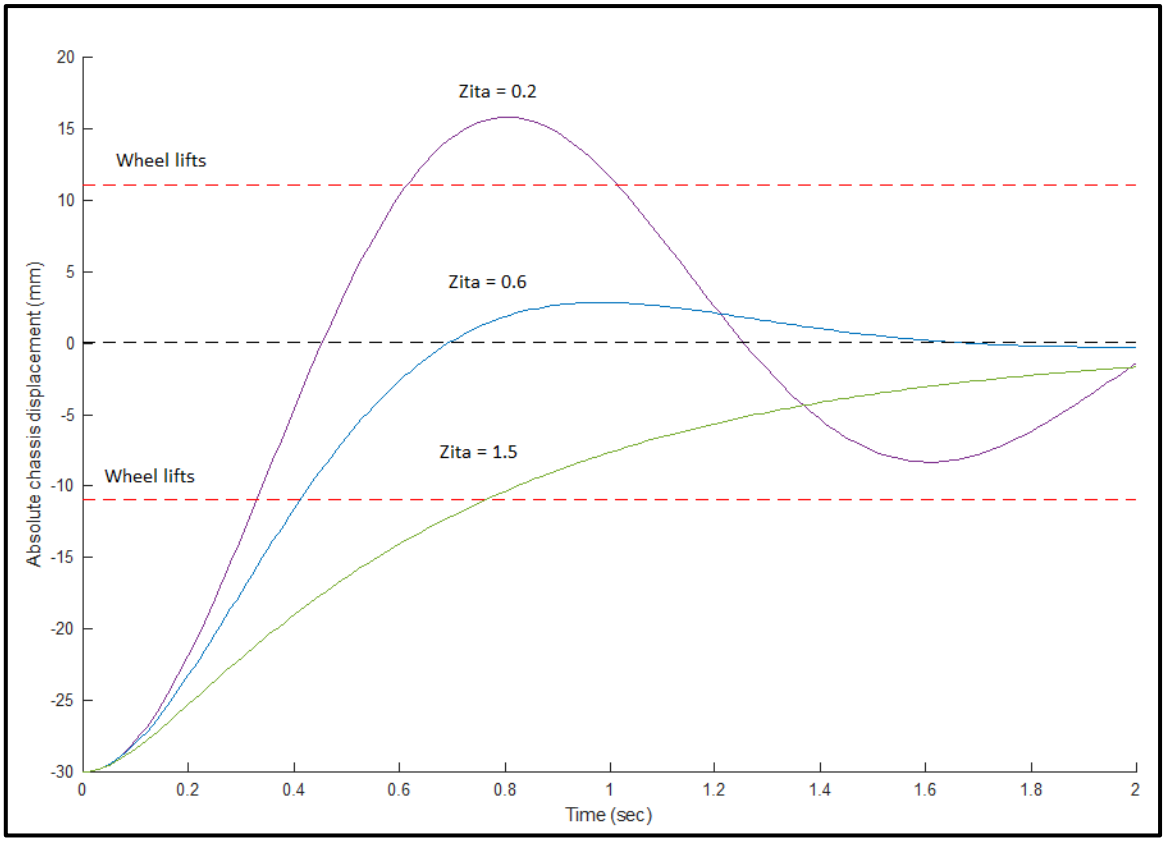

Figure 97 - Wheel lift for a 30 mm disturbance

4.3 Track Data

The calculations and conclusions above are based on theory and mathematical models. As previously mentioned, the car had a number of sensors that continuously logged data, including shock position, wheel speed and engine vitals (Refer to Table 5 in section 3.2 for a list of all logged channels on the W-FS18 car). This data could be used to verify the accuracy of the theoretical models as well as the assumptions made.

4.3.1 Diagnosing loss of traction

In section 4.2 different traction circles were plotted for various setup changes, such as different ARB settings, spring rates and weight distributions. With the accelerometer in the MoTeC a traction circle of what the car actually achieved was plotted (Figure 98). This can be helpful for the driver to know how much further they can safely push the car during cornering, braking and accelerating.

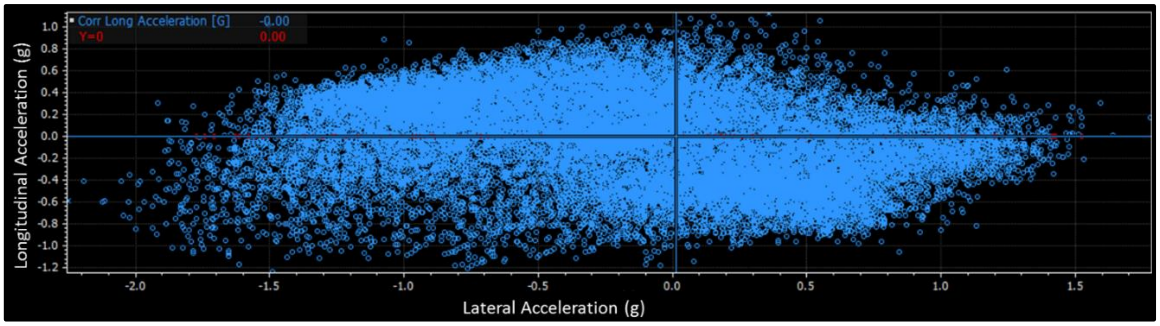

Figure 98 - Traction circle of W-FS18 with no ARB at front and 2nd softest at rear, 50/50 weight split and 225 lbs/in springs

When the logged data is overlaid with the theoretical maximum accelerations, it can be seen that during longitudinal accelerations there is still plenty of grip left that the driver can push for (Figure 99). However, laterally it can be noticed that during a left hand corner the acceleration actually exceeds the theoretical maximum. Furthermore, it is interesting to note that the acceleration during left hand corners is greater than in the right hand corners. This is due to the nature of the track though. Investigating the GPS data logged during the race, it can be seen that most big corners are right hand turns, explaining the pure lateral accelerations during right turns. All left corners were found to be slalom corners, creating a transient loading case as the driver has to brake while turning. This can be seen in the traction circle as most points that are outside the theoretical limit are under these conditions. Of particular interest is the circled corner as the car comes out of a right hand corner before turning into a left hand slalom, making it more likely to lose traction (Figure 100).

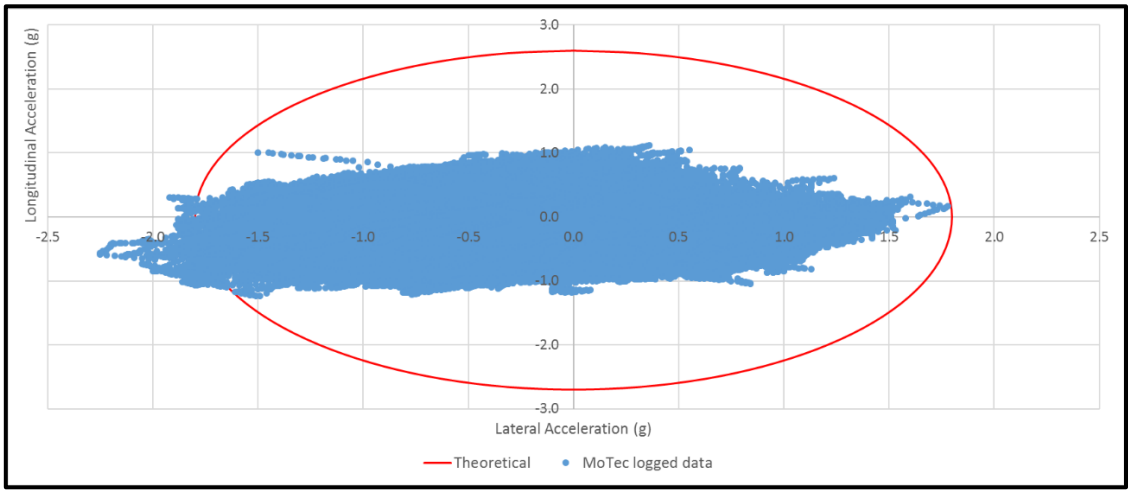

Figure 99 - Comparison between logged and theoretical data

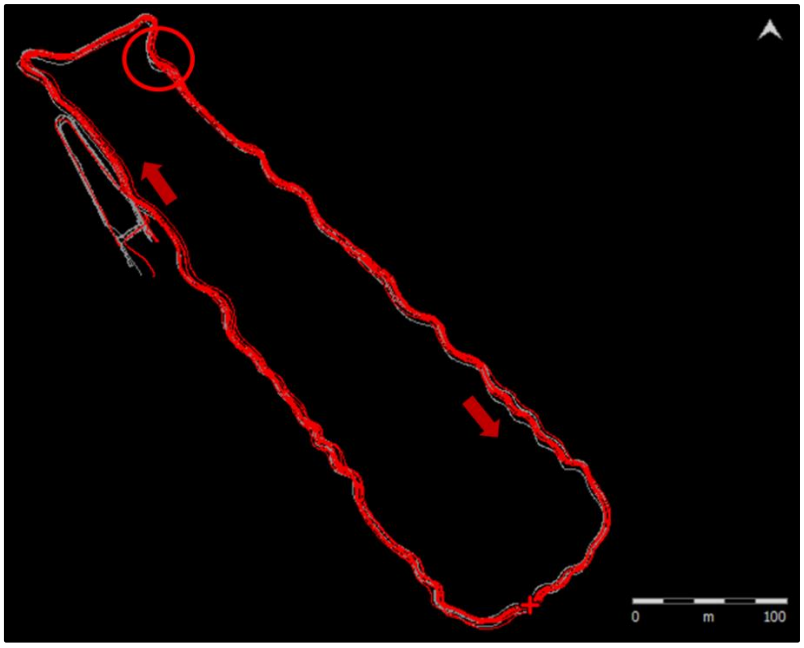

Figure 100 - Track setup

Regardless of the corner during which the loss of traction occurs, Figure 99 clearly indicates that the car is losing traction. Once this observation is validated, the cause for the loss of traction and a solution can be found. In order to validate this, logged wheel speeds can be investigated. If the car loses traction, the wheel speed should drop quickly. In this case, during a left corner, it is expected that the left wheels (inside) would lift (Figure 101). The front left wheel (red line) shows a significant drop in speed, compared to the other three wheels. This is a clear indication of the inner wheel lifting during lateral and braking accelerations. As soon as the tyre regains contact with the surface, it gains traction and thereby speed. From the time scale, it can be seen that the tyre loses contact for approximately 50 ms. Even for a short period of time the loss of grip can result in serious understeer behaviour of the car.

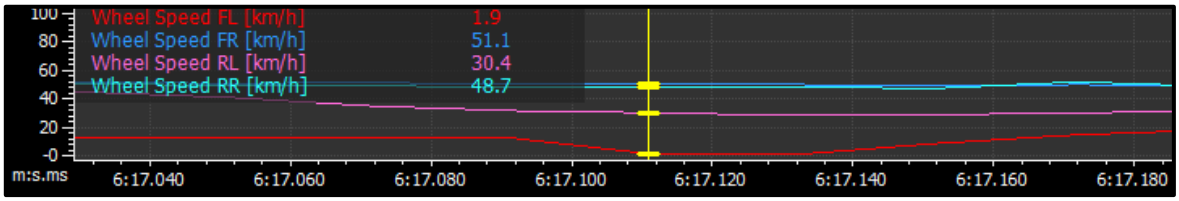

Figure 101 - Wheel speeds for loss of traction

To find a solution to the loss of traction aside from the driver slowing down, the sensor data should be used to its full potential. The circled chicane from Figure 100 can be split into a right hand corner leading into left hand slalom. During the right hand corner, the car does not lose traction (Figure 102).

The yellow cursor shows numerical values at the midpoint of the right hand corner. Throttle position (graph D) shows that the driver is not accelerating but starting to brake, indicated by the increase in

brake pressure (graph E). The wheel speeds are all non-zero and have not lost traction yet (graph B). The purple line represents the angle of the tyre at the ground (graph F) and can be seen to be nearly at full lock (based on Figure 60). From the suspension potentiometers (graph C), the car does not roll evenly, i.e. left and right hand shock displacements are uneven, which could be due to different damper settings for the left and right.

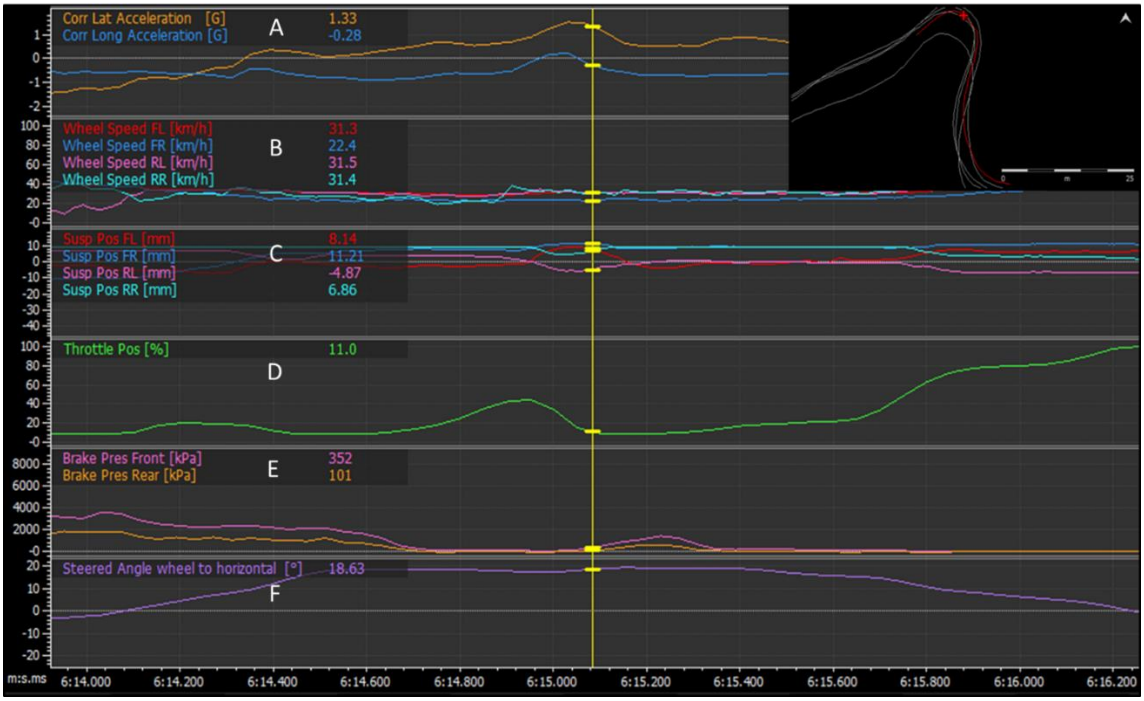

Figure 102 - Right hand corner analysis

The damper velocities for the front left and right are vastly different (Figure 103) even though the dampers are set to the same setting (set evenly before the run). The dampers on W-FS18 were rebuilt and serviced in 2017 but not used until 2018. However, the shocks are designed as mountain bike shocks and are therefore serviced by a bike shop. Bikes do not rely on two shocks displaying the exact same damping properties as front and rear shocks are often set to different damper settings. A car, however, is reliant on both shocks on the same axle displaying the same properties for a certain setting. Unfortunately, the discrepancy between left and right damping was noticed too late to rebuild the shocks and correct this. This difference in damping could be one of the causes for the car losing traction and lifting wheels. The dampers were set to an asymmetric setting to try and compensate for this.

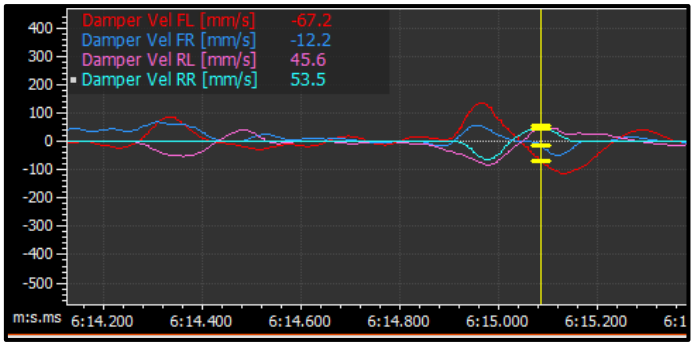

Figure 103 - Damper velocities

Once the driver goes past the apex of the corner, they started accelerating towards the left slalom corner (Figure 104). The driver is at full throttle (graph D) and has started to turn the steering wheel the other way, indicated by the now negative wheel angle (graph F). The driver is preparing to start braking, shown by the increase in brake pressure (graph E). The wheel speeds are greater at the rear as the brake bias allows for more braking of the front (graph B). However, the speed of the front left wheel has started to decrease rapidly, indicating it is starting to lift. Furthermore, the shock travel for that wheel has become constant at 15.56 mm, indicating that the spring is fully extended and the wheel is off the ground (graph C).

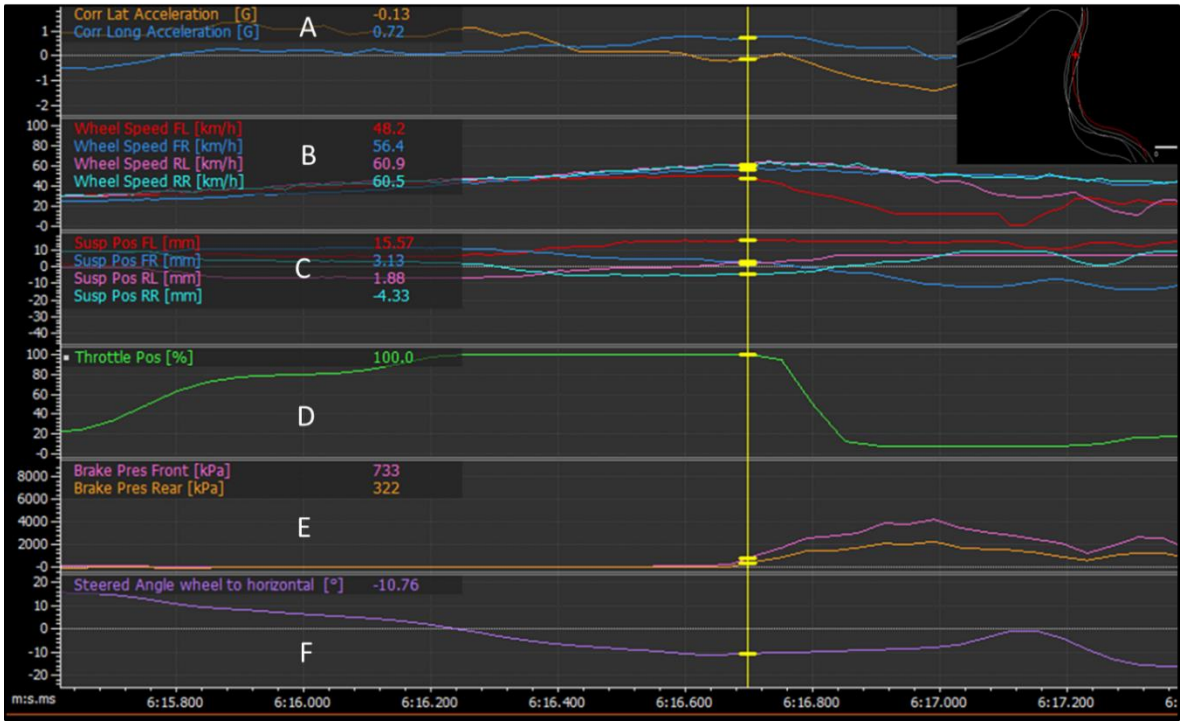

Figure 104 - Midpoint between right and left hand corner

It is interesting to know how much the car has rolled at this point, the suspension positions and trigonometry can be used to find the body roll angle of the car (Figure 105).

The rear of the car (in blue) has barely rolled compared to the front (in orange), indicating a stiffer rear setup. As the front ARB was not connected but the rear was set to the second softest setting, this was expected. However, it can be seen that the front rolls significantly with 11° per g of lateral acceleration. As this is a largely transient loading case, the large roll angle per lateral acceleration can be due to damper settings not letting the shock return to its original position quickly enough.

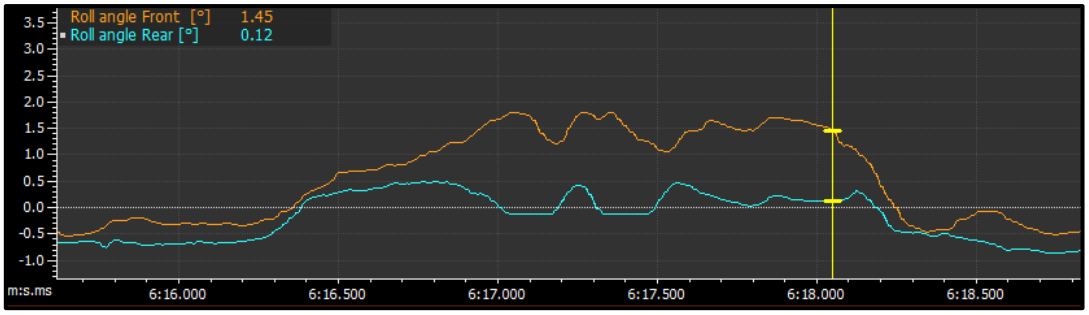

Figure 105 - Roll angle in between corners

As the driver continues through the corner, the rear left wheel (pink line) is starting to lift as well (graph B) (Figure 106). At this point the driver is off the throttle completely and fully applying the brakes (graphs D and E). As the rear wheel comes up (pink line in graph B), the car begins to understeer as seen by the steered angle going to zero and then turning back in within the span of milliseconds (graph F). The shock travel for the left wheel becomes constant at 7.03 mm indicating that the shock is fully extended and the wheel is being pulled off the ground (pink line in graph C).

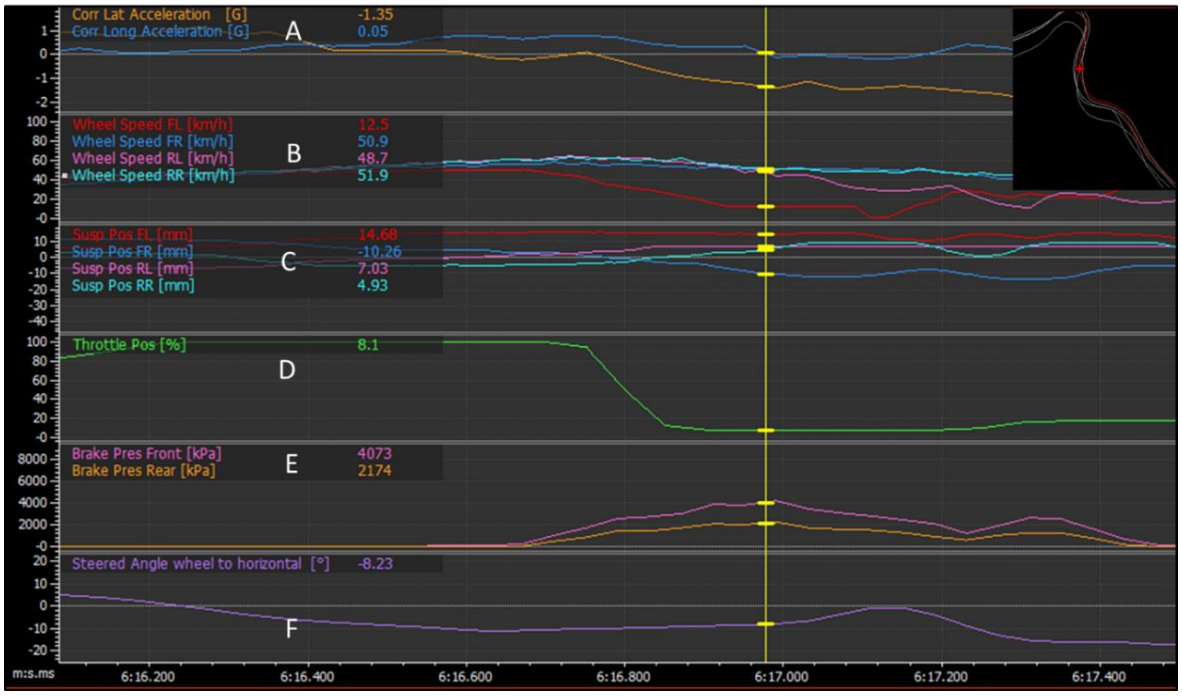

Figure 106 - Left hand corner

As the lateral acceleration is starting to decrease at the corner exit, the wheels are gaining traction again as the car rolls back towards a neutral position (Figure 107) and the driver accelerates out of the corner. After the corner (time: 6:18:300), the roll angles for the front and rear settle at similar magnitudes, indicating that the large discrepancy between the rolling behaviour of front and rear is due to damper speeds, not allowing the shock to return quick enough. Due to the large roll angle, the front inner wheel is levered off the ground losing traction. This can be solved by adjusting damper speeds to allow the spring to return to its original position quicker as well as stiffening the front to reduce the roll angle by connecting the ARB. Furthermore, if the driver was to apply the brakes earlier there would be more weight on the front tyres through the apex of the corner, reducing the risk of loss of traction. Even though braking earlier might cost the driver a bit of time it can prevent the understeer through the corner decreasing the overall time.

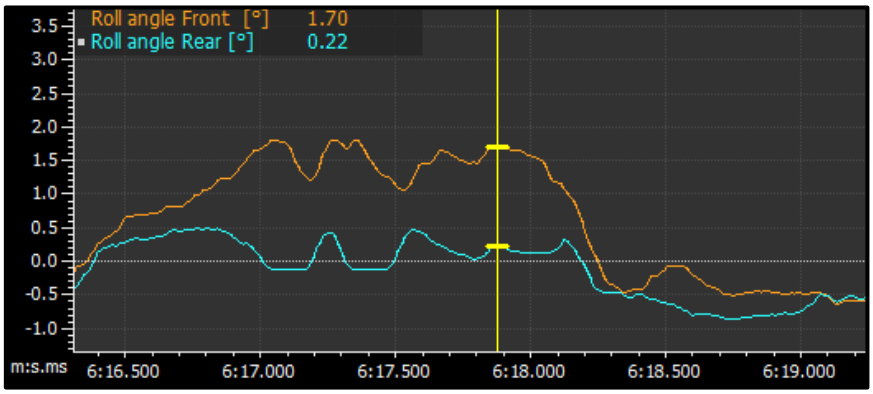

Figure 107 - Roll angle through a corner

4.3.2 Evaluation of grip levels

As discussed in section 3.6, grip factors can be helpful when evaluating grip levels and loss of traction. The larger the area under the curve for the combined acceleration (lateral and longitudinal) vs distance travelled, the better the grip during the loading scenario (Figure 108). The grip factors were filtered by lateral and longitudinal accelerations, i.e. cornering grip factor only applies when the lateral acceleration was greater than 0.5 g (refer to section 3.6.2 for boundary values).

In this scenario the car initially has good cornering grip (graph B). Acceleration and braking grip levels (graphs C and D) are not applicable as the car is in a state of pure cornering (low longitudinal acceleration). However, towards the end of the corner (~190 m) the cornering grip factor drops below the average, indicating a problem with continuous grip (graph B).

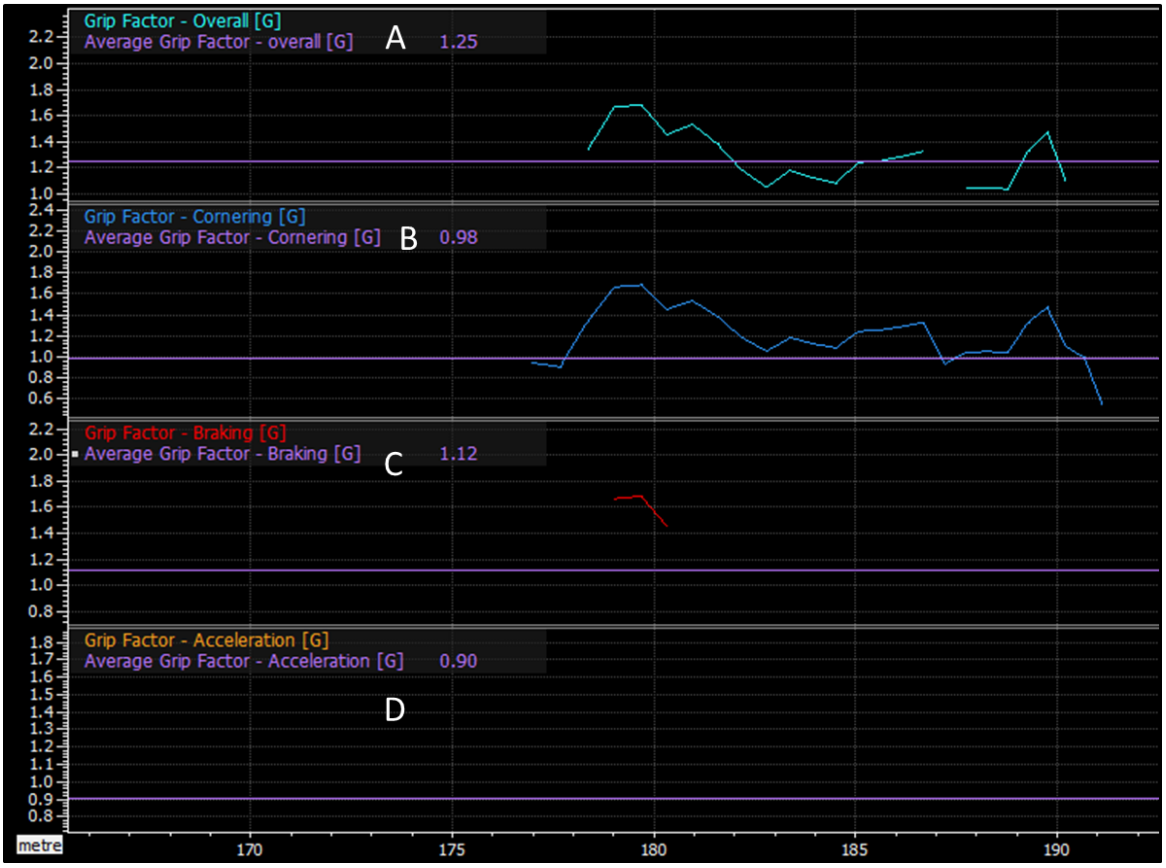

Figure 108 - Grip factors example

When looking at the wheel speeds for this scenario, it can indeed be seen that the car is continuously losing traction (front right – blue trace) from 190 m onwards (Figure 109).

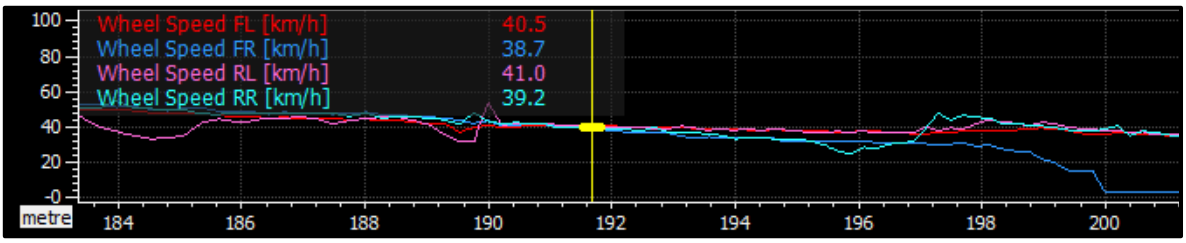

Figure 109 - Wheel speeds for loss of traction

Average grip factors for different runs can be helpful when looking at setup changes to quickly quantify improvements in grip. However, a consistent driver is needed to obtain comparable results.

From data from the 2018 competition, it could be seen that the car rolled too much at the front with no ARB connected. Some of the testing in 2019 focused on adjusting the ARB stiffness to reduce the roll. Therefore, various ARB combinations were tested during which the damper settings were kept constant. A comparison between grip factors was used to evaluate any improvements in the setup (Table 13).

Braking, acceleration and cornering factors are affected by the setup change. With none of the ARBs connected the average grip factors are much lower compared to when both are connected. Furthermore, grip levels are further improved when the front is stiffened to the middle. However, once the car becomes too stiff (both ARBs to stiffest setting), the grip levels drop again. From visual analysis as well as looking at wheel speeds, it was found that the car was increasingly lifting wheels for this setting. This is due to the suspension being too stiff and not allowing for enough travel and "pulling" the inner wheels off the ground with minimal lateral accelerations. Furthermore, from driver feedback it was found that the car was understeering mid corner.

Table 13 - Average grip factor comparison between ARB setups

Grip Factor	ARB Front: Stiffest ARB Rear: Stiffest	ARB Front: Middle ARB Rear: Softest	ARB Front: Softest ARB Rear: Softest	ARB Front: None ARB Rear: None
Overall	1.05	1.10	1.10	1.08
Braking	0.90	1.07	0.96	0.93
Acceleration	0.85	0.99	0.87	0.85
Cornering	0.64	0.73	0.70	0.61

4.3.3 Diagnosing under- and oversteer

There are a number of ways to diagnose under- and oversteer from logged data. Steering wheel angle can be a good first indicator as when the car oversteers, the driver tends to jerk the steering wheel the other way resulting in a sudden change in wheel angle (Figure 110). As can be seen, the driver quickly turned the steering wheel completely the other way mid corner, with no apparent reason, indicating oversteer. It is however important to note the track setup as sometimes a slalom course can mimic oversteer behaviour in regards to steering wheel angle. Understeer can be a bit harder to diagnose this way. The driver will hold the steering wheel at a constant position, once the car understeers they will quickly try and turn the wheel further (Figure 111).

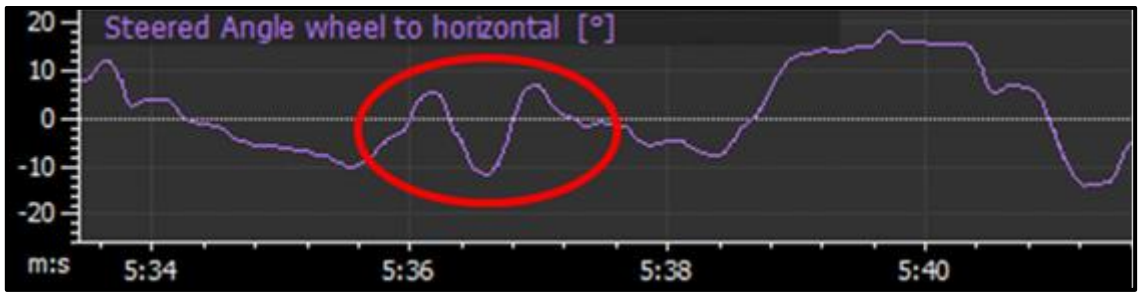

Figure 110 - Oversteer mid corner

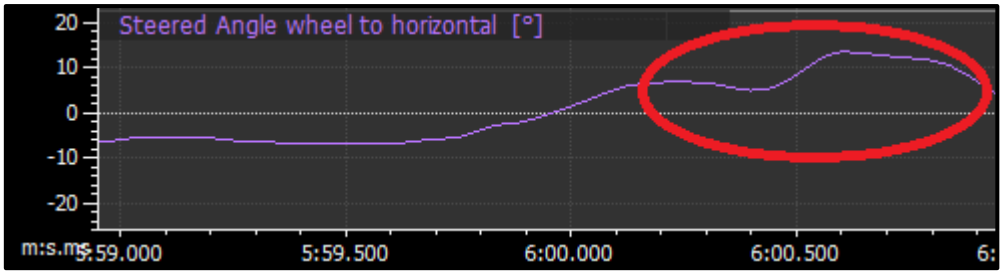

Figure 111 - Understeer mid corner

The above method involves looking through the data and identifying these specific points which can be tedious when there is lots of data, therefore a more mathematical way to diagnose under -and oversteer faster is needed. The easiest way to diagnose under- and oversteer is a yaw sensor, however the MoTeC in W-FS18 does not include such a sensor. The other way to find the amount of under- and oversteer is to find the difference between the theoretical minimum steering angle to navigate the corner (termed Ackermann angle) and the actual measured steering angle. However, this method relies on calculating the corner radius from the centrifugal force and the lateral acceleration (Figure 112) or knowing the corner radius of each corner on the track (proper racing tracks only, i.e. no slalom course). For this corner the understeer angle is large. Once the rest of the data was analysed, it was found that there always seemed to be a large understeer angle, even often larger than the Ackermann angle itself. This indicated a problem with this initially chosen method to diagnose steering problems. As this entire calculation was based on a correct radius derivation, a known radius corner was compared to the calculated radius. The skidpad setup from the 2018 competition was chosen to verify the radius calculations, as it consists of two circles of the same constant radius (Figure 113).

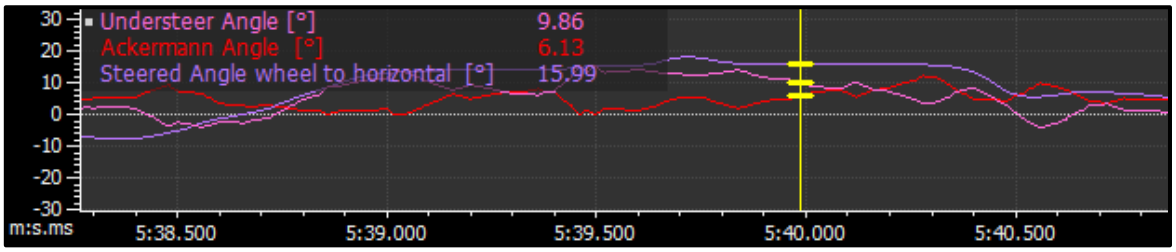

Figure 112 - Understeer angle based on Ackermann angle

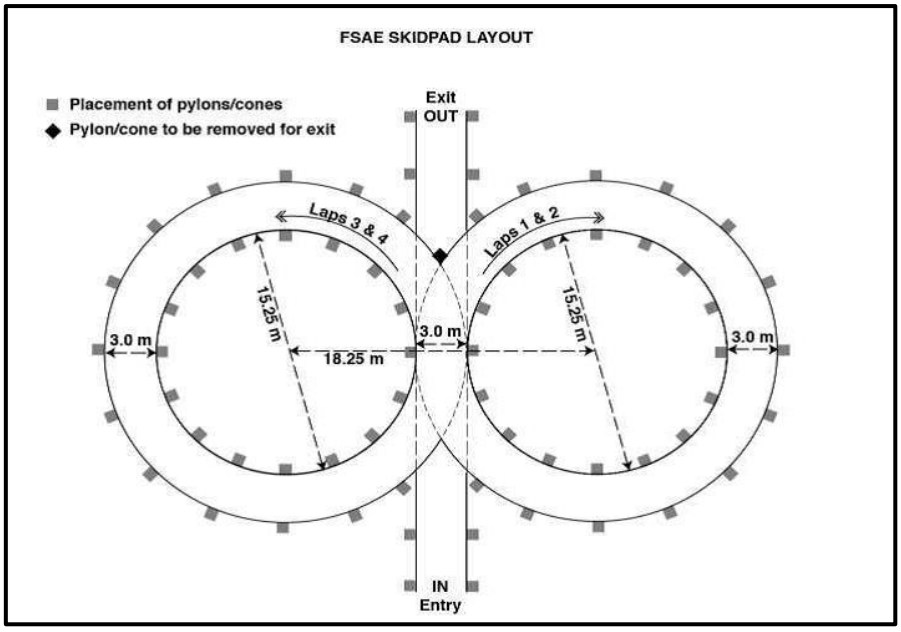

Figure 113 - Skidpad layout [39 p. 158]

If the distance travelled is known, the acceleration based radius can be compared to the distance based radius (Figure 114). The lateral acceleration varies a significantely, making it hard to calculate a consistent radius even in a constant radius corner. Therefore this method of calculating under- and oversteer angle is too inaccurate to draw meaningful conclusions from it.

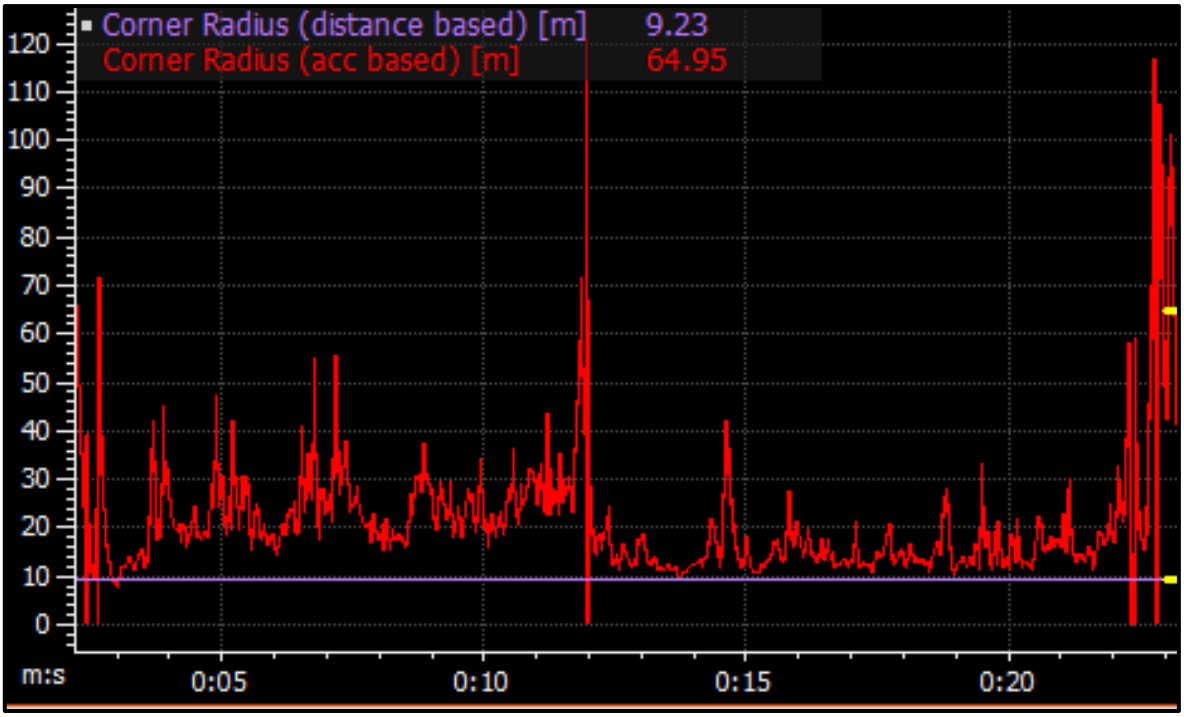

Figure 114 - Radius comparison

The last method mentioned in the Methodology section (3.6.2), relied on calculating the difference in slip angle between front and rear. Slip angle in turn is based on wheel loads, lateral acceleration and

cornering stiffness all of which can be calculated from the Tire Test Consortium data and logged vehicle data. Figure 115 shows this difference for a section of the track. The angle is much lower and only has spikes at certain positions, indicating understeer at these points.

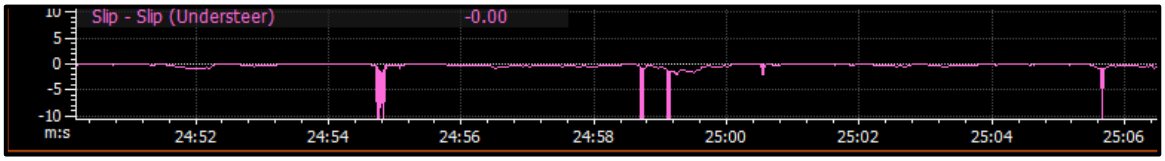

Figure 115 - Slip angle understeer angle

Further investigation into the understeer angle showed that the car understeered at the corner entrance and oversteered during mid corner (Figure 116). As the car enters the corner the understeer angle has large negative peaks indicating a tendency of the car to understeer. This is due to load transfer away from the inner wheel during initial cornering. As the car reaches the steady state cornering phase (middle) the difference in slip angles becomes noticeably larger and positive. This indicates an oversteer behaviour, that the driver tries to correct by turning the steering wheel less causing the spikes of understeer. The car shows relatively neutral steering behaviour on the corner exit and does not display "power understeer". Power understeer occurs when the down force on the inner front wheel is still less than static weight and is further reduced by the longitudinal acceleration towards the rear due to the driver accelerating out of the corner.

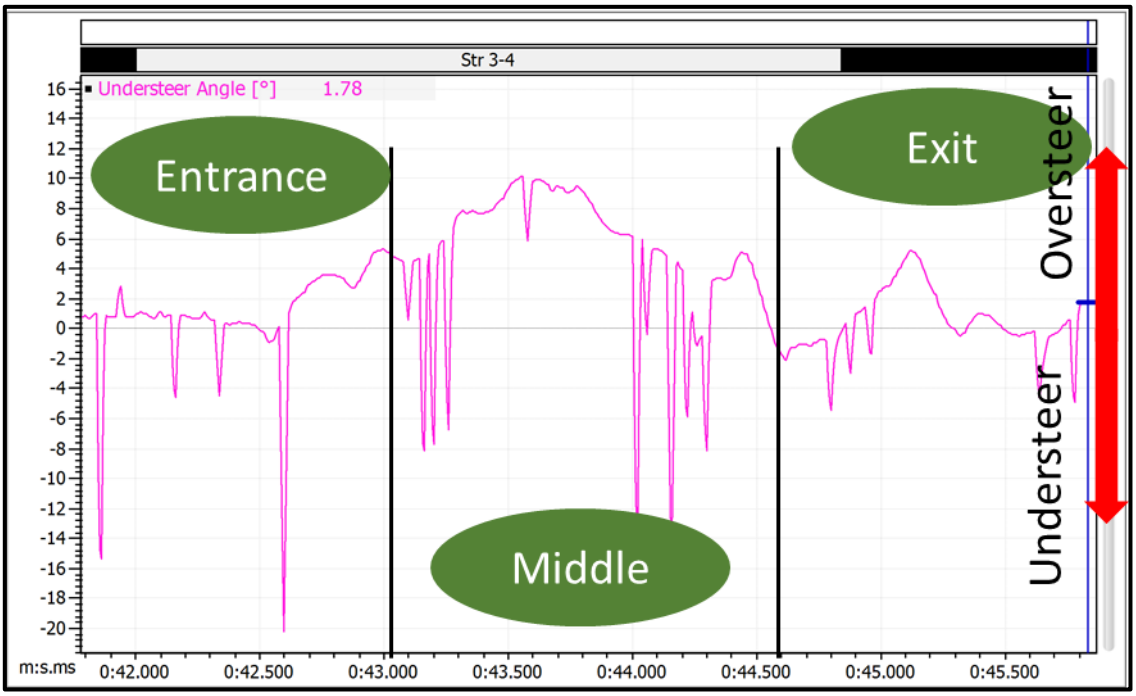

Figure 116 - Under- and Oversteer during a right hand corner

A variety of setup changes could be suggested in order to improve the corner handling of the car. One reason for the corner entrance understeer is too much load transfer causing the inner wheel to be lifted up. Added roll stiffness might aid with providing more contact between the tyre and the road. However, it is not always feasible to add stiffness through an antiroll bar or stiffer springs as this can cause the car to act as if it had a solid axle connecting the inside and outside wheels, levering the inner wheel off the ground with little deflection. Often the better way to increase contact is by adjusting damper settings to allow the wheel to return quicker and be loaded again.

4.3.4 Damper velocities

As mentioned before, track data was used to validate the Matlab four corner steady state model (refer to Appendix A 11 to A 13 for Matlab code), specifically damping models. Due to not being able to simulate a bump on the track consistently, a tight but fast slalom course was used as the instantaneous disturbance. Figure 117 shows the change in lateral acceleration from 0 to -1.3 g in 0.12 s through such a slalom. The longitudinal acceleration (0.2 g in braking at the maximum) is small enough to be neglected. To simulate this as accurately as possible and avoid transient loading scenarios, only the first slalom in each run was considered.

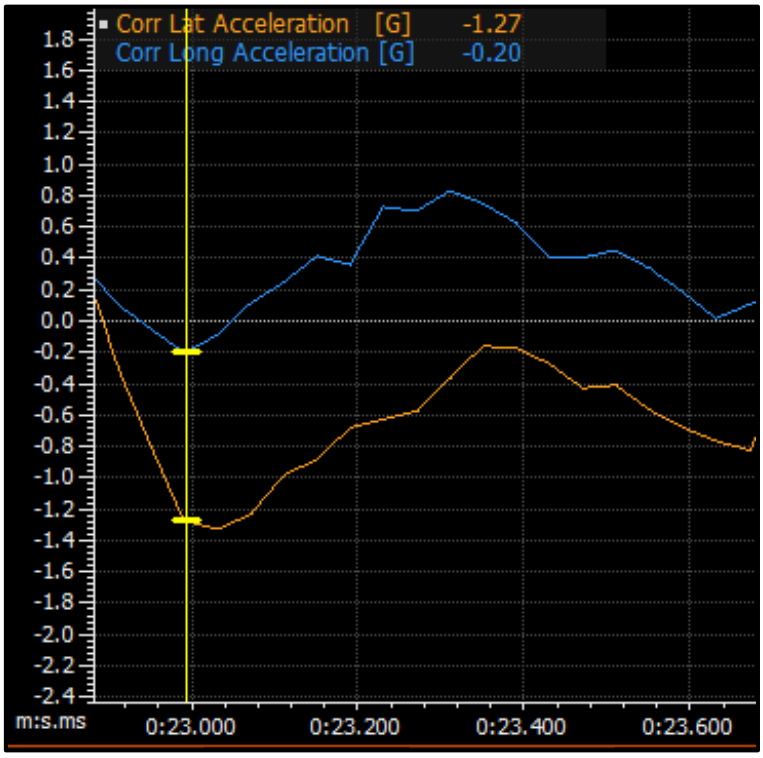

Figure 117 - Near instantaneous change in lateral acceleration

As previously mentioned in section 4.1, the damper histogram from the 2018 competition was asymmetrical between bump and rebound as well as showing varying stiffnesses between the four corners of the car. As the first step to create more mechanical grip, the car needed to be balanced.

Low speed bump and rebound were adjusted so the damper histogram followed a normal distribution and the difference between time spent in bump and rebound was minimized (Figure 118). Due to the scale the difference in height of the zero bin for the front looks large, however is only 5%, down by half from the original 10%.

Table 14 shows that the difference between time spent in bump and rebound has decreased significantly from 75% to 13% at the most.

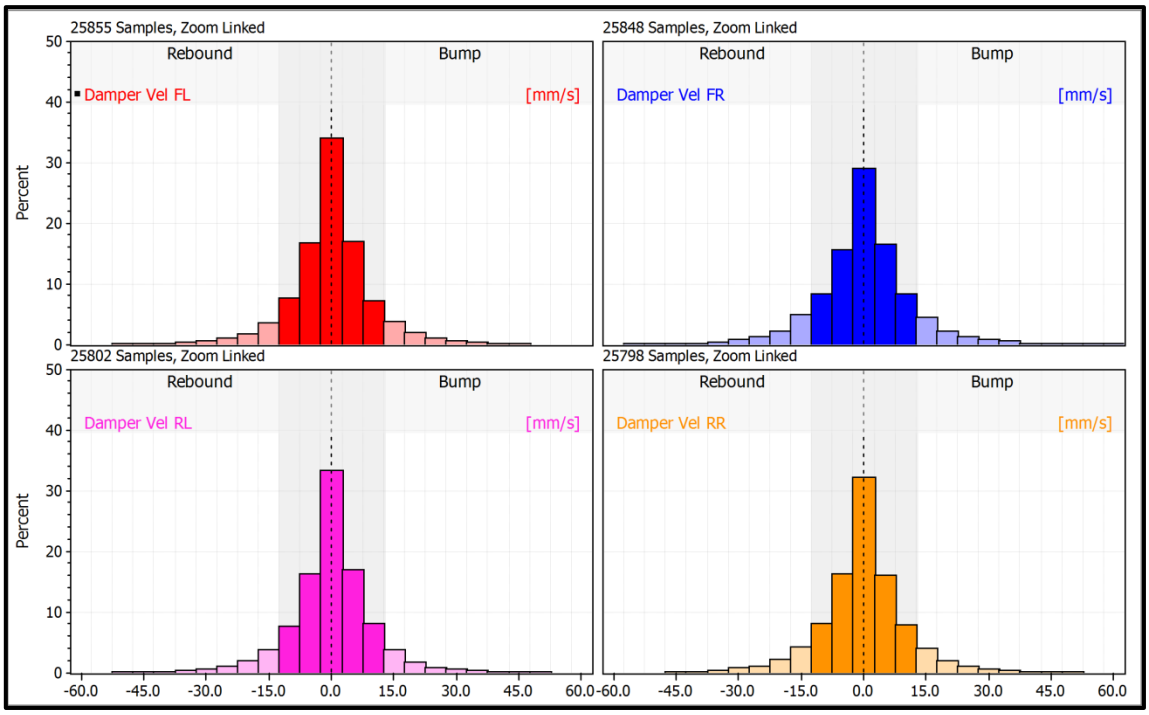

Figure 118 - Symmetrical damper histogram for W-FS18 for initial 2019 tuning

Table 14 - Damper speed analysis for initial 2019 tuning

		Bump	Rebound	% Difference	Average
Front – Left (FL)	Lo%	43.3	39.2	-10.5	41.3
	Hi%	8.8	8.6	-2.3	8.7
Front – Right (FR)	Lo%	40.2	37.7	-6.6	39.0
	Hi%	10.8	11.2	3.6	11.0
Rear – Left (RL)	Lo%	43.5	38.4	-13.3	41.0
	Hi%	8.5	9.4	9.6	9.0
Rear – Right (RR)	Lo%	40.6	39.8	-2.0	40.2
	Hi%	9.5	10.1	5.9	9.8

As previously mentioned, histograms are only useful to create balance between the four corners of the car and help with setting up asymmetrical damping rates to compensate for uneven damper settings. The height of the peaks and width of the base will depend on the track and other data needs

to be examined to adjust damping rates. It can be helpful to analyse damper speeds through a corner first.

Figure 119 shows the damper velocities measured on track. The velocities from the Matlab model can be found in Table 15. The slalom was a left hand corner meaning FL is the inside and FR is the outside of the corner. The difference between the theoretical and measured damper velocities is small for the front inside (FL), rear inside and outside (RL and RR). The small discrepancy is due to having to simulate a bump by using a very fast change in lateral acceleration (i.e. the slalom). The fast change in acceleration would cause an almost instantaneous change in suspension position, thereby "simulating" a bump. This was done as other methods of simulating a bump by driving over a piece of debris did not work and dragged the debris along on the underside of the diffuser. When the change in acceleration was slow and like a normal cornering situation, the difference became more noticeable. This was as expected as the low speed damping is more prevalent in a corner, whereas bumps (i.e. fast changes) are dampened by the high speeds. However the front outer (FR) damper velocity is fairly consistently at 130 mm/s. Looking at data for this particular damper, it was noticed that throughout testing sessions this corner appeared to get "stuck" at particularly high/low speeds for up to 2 seconds. This indicates a problem with the damper itself and it needs rebuilding. As no replacements were available testing was continued with the defective damper but data for this corner in regards to damping was examined critically. After investigating why this damper could be faulty after having been rebuilt in 2017, it was found that this damper was used on the 2017 car which used spring rates of up to 550 lbs/in (twice as much as the 2018 car), exposing the damper to very large forces. This is likely the cause for earlier than anticipated maintenance.

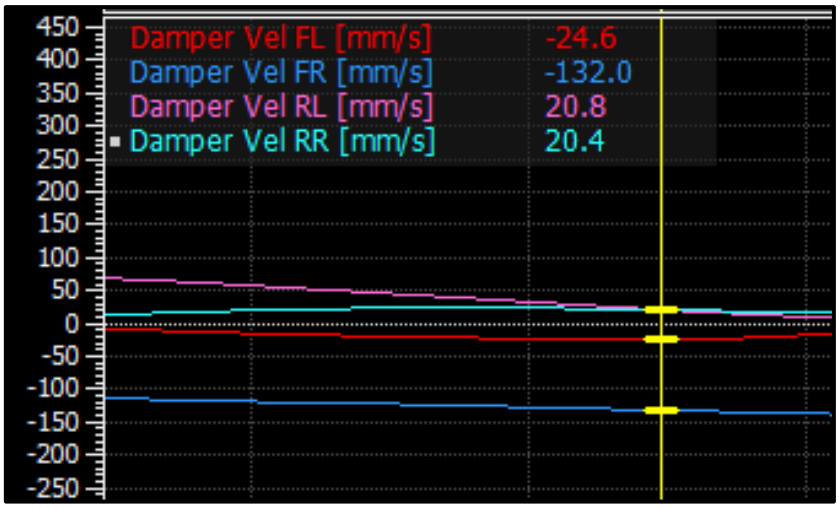

Figure 119 - On track damper velocities

Table 15 - Comparison between initial Matlab damper velocities and velocities measured on track

	Initial damper speed (mm/s)	Discrepancy to track data (mm/s)
Front Inner	20.1	4.5
Front Outer	23.0	108.9
Rear Inner	17.4	3.4
Rear Outer	19.9	0.6

When diagnosing understeer by the difference in slip angle in section 4.3.3, it was noticed that the car tended to understeer on corner entry and oversteer mid corner. Understeer occurs when the front wheels have not enough contact with the road and are not loaded to their full potential. In this case adding stiffness via the antiroll bar was not feasible as when the stiffness was increased the front became too stiff, not allowing enough suspension movement and the inner wheel was levered off the ground. The dampers were adjusted to increase the compliance between tyre and road. Figure 120 can be split into four distinct sections [30]:

Section 1: Straight line braking

In graph A, the brake pressure increases whereas the driver is off the throttle (graph B). The driver changes position on the track to optimise their driveline through the corner. This is indicated by the negative lateral acceleration (graph C). The load transfer is forward, causing the front shocks to go into bump, shown by the negative slope of the graphs D and E. The rear is in rebound, indicated by the positive slope (graphs F and G).

Section 2: Initial cornering and braking

After the driver has changed to the outer side of the corner, the driver turns the steering wheel into the direction of the corner, producing the increase in lateral acceleration with a positive slope (graph C). The front inner wheel (front right, graph E) shows the shock in rebound as expected as the weight is transferred to the outer left wheel. The front left (graph D) appears to be fluctuating about a fairly consistent shock position. The rear outer (left) wheel has a negative slope indicating compression (graph F). Whereas in graph G, the rear inner wheel is fluctuating around a constant position. In Figure 116 it was noticed that the car understeers during this phase.

Section 3: Steady state cornering

The lateral acceleration is reasonably constant at this stage (graph C), the driver has stopped braking and is starting to apply the throttle again (graphs A and B). Due to the squatting movement of the car

towards the back, the rear shocks start showing a slight negative slope (graphs F and G). The front is unloaded and the shocks start rebounding (graphs D and E). It is interesting to note that even though the rear is compressing the rear right (inner) wheel is still in the extension part of the movement (graph G is still above 0 mm deflection).

Section 4: Corner exit and acceleration

The driver is accelerating out of the corner decreasing lateral acceleration and increasing throttle application (graphs C and B). The rear shocks compress further (graphs F and G) as the longitudinal acceleration increases. Graphs D and E indicate consistent rebound motion at the front shock until the driver starts braking for the next bend at the end of the graph.

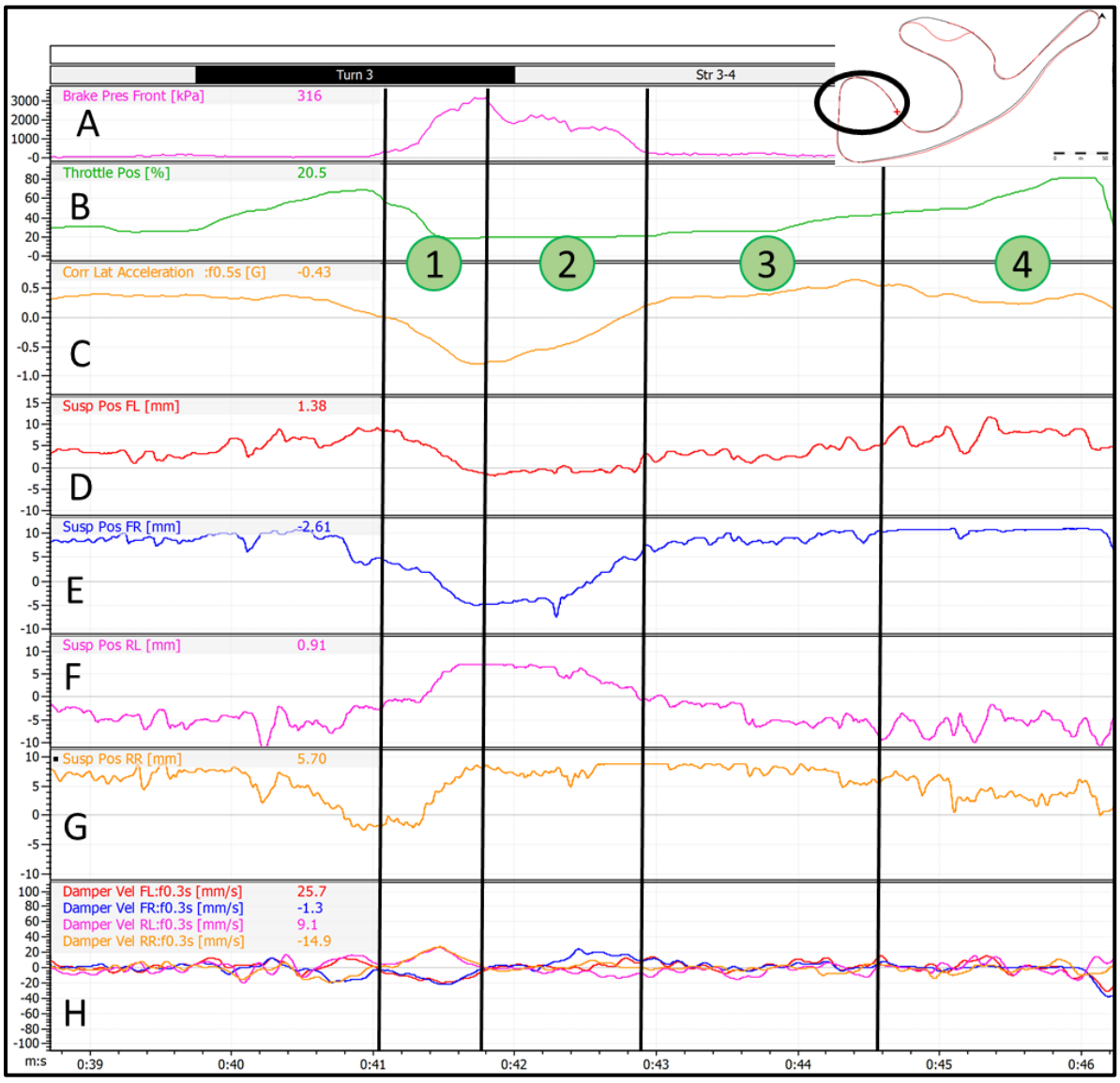

Figure 120 - Damper analysis

As mentioned previously the car understeers during section 2 of the corner. As the front inner wheel (graph E) shows the wheel in rebound, if rebound damping is decreased, it will allow the wheel to return to the ground faster, allowing it to be loaded quicker and thereby decreasing the chance of understeer. In section 3 (steady state cornering) the front inner and outer as well as the rear inner wheels (graphs D, E and G) show little movement. Looking at graph H, showing damper speeds, all damper speeds are below 20 mm/s. Little movement of the shocks as well as the low speed means that changes in low speed damping would have little effect on the car's behaviour. Furthermore, there are no noticeable regions of high damper speed, indicating that high speed damping is at a good level. The only noticeable region of higher speeds is during section 1, straight line braking, although speeds only reach 25mm/s which is right at the verge of the low and high speed region.

Driver feedback as well as the data from the MoTeC showed that the car oversteers during the steady state cornering phase (section 3), this is actually due to the earlier understeer. The shock position starts to stabilize but the driver is still anticipating understeer, thereby oversteering the car. It is interesting to note that the front outer (left) shock is only in compression (graph D) during the initial corner entry section. After that the shock shows rebound motion, which is odd as the outer wheel during a corner should be in compression. After investigating this, it was found that it occurred consistently when the driver started to accelerate through a corner. This indicates that the spring is too easily extended into the rebound region and stiffer springs or more preload can help prevent this. As the rebound motion is not excessive enough to max the shock out, it does not cause problems.

If the high speed damping is too low the damping speeds will look like the trace for the rear right (RR – orange) and the rear left (RL – pink) in Figure 121. The rear right reached a speed of more than 70 mm/s during rebound, whereas the rear left shows the same behaviour during compression (large negative damper speed). In this case both dampers should be adjusted in their high speed range.

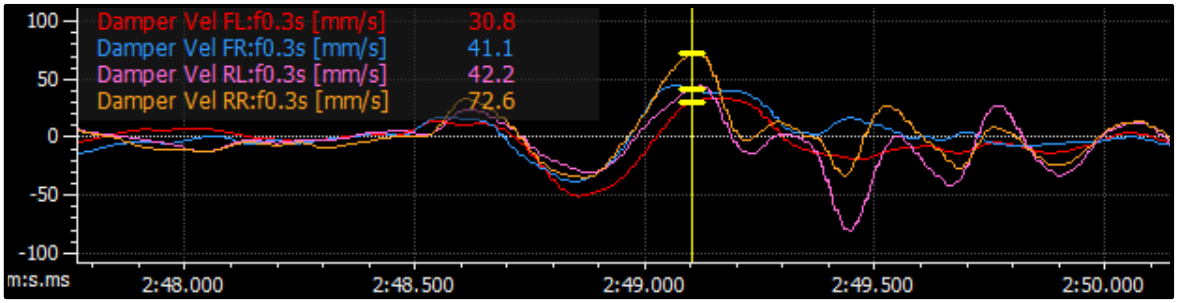

Figure 121 - Low high speed rebound and compression damper setting

4.4 HyperWorks

HyperWorks being a multibody dynamic simulation software can be used to model the dynamic behaviour of the car quickly and under many different scenarios. The main advantage to the previous models is the complexity of it, considering 360° of freedom. This means that the model considers changes in tyre temperature, camber gain and change in toe when running the iterations, more closely resembling the real car.

4.4.1 Validation with Track Data

This research was focused around W-FS18 and a HyperWorks model of it already existed from the 2018 WESMO team. As part of earlier research project the model was verified with track data and deemed to be accurate and reliable ([40] and [41]). Initially HyperWorks was intended to be used to simulate events like skidpad and an endurance course. However, this would require extensive work to simulate the engine correctly. This would include power and torque curves as well as fuel injection mapping. As this research was focused around the vehicle dynamics of suspension HyperWorks was used as a means to justify assumptions as well as visualize the effect of ARB stiffness on the rolling behaviour.

4.4.2 Verification of Assumptions

As previously mentioned the camber gain through suspension travel was small and its effect on the maximum lateral acceleration was neglected. However, camber gain through steering had not been considered. W-FS18 was designed to have a maximum steering lock of 120° at the steering wheel, however, examining numerical as well as visual data (mounted camera) it was found that the driver rarely utilised full lock. The driver negotiated majority of corners with about 90° of steering (Figure 122).

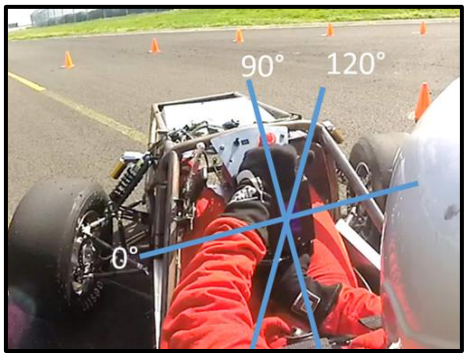

Figure 122 - W-FS18 steering wheel lock

HyperWorks was used to plot the camber gain for a steering wheel lock of up to 120° (Figure 123). Even at the maximum steering lock, the camber gain is only about 1.2° justifying the assumption of neglecting its effect on change in traction.

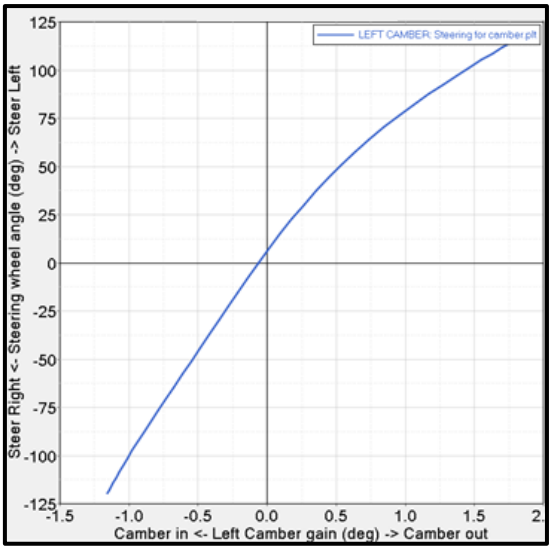

Figure 123 - Camber gain for up to 120° steering lock

4.4.3 Roll Analysis

HyperWorks was used to visualize the difference between ARB setting and their effect on the rolling behaviour of the car. Figure 124 shows the different roll angles and the various wheel displacements caused by a 1.8 g lateral acceleration at the front of the car. The lines are virtually the same (same gradient, x- and y-intercept) but have different lengths, i.e. for the same lateral acceleration the soft ARB allows for more roll angle.

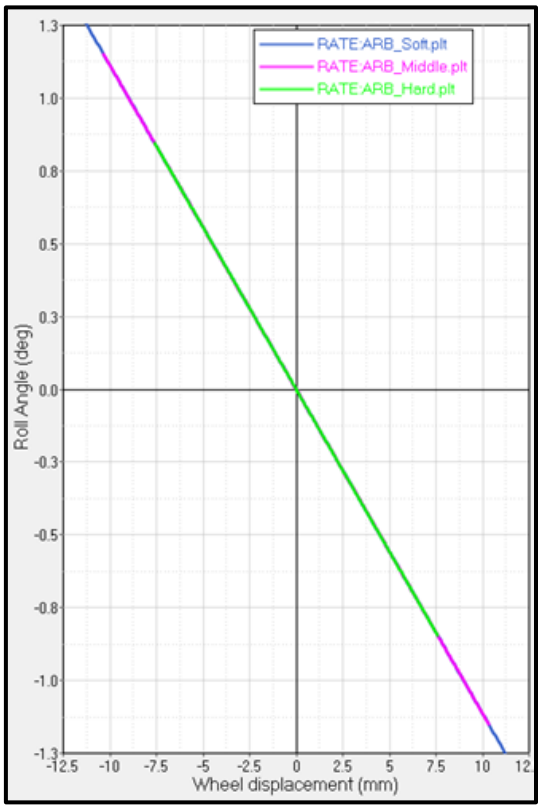

Figure 124 - Roll angle vs wheel displacement for different ARB settings

Knowing the lateral acceleration and the roll angle, the roll gradient (degrees of roll per lateral g were calculated and compared to those calculated using Excel (Table 16). There is a varying percentage error between the different settings. This is due to the assumption of the fixture of the lever not moving longitudinally as the tube is twisted (i.e. X_{Soft} and X_{Hard} are zero in Figure 125). The distance the fixture moves at the hard setting is smaller than at the soft setting, hence the lower error in the roll gradient for the hard setting.

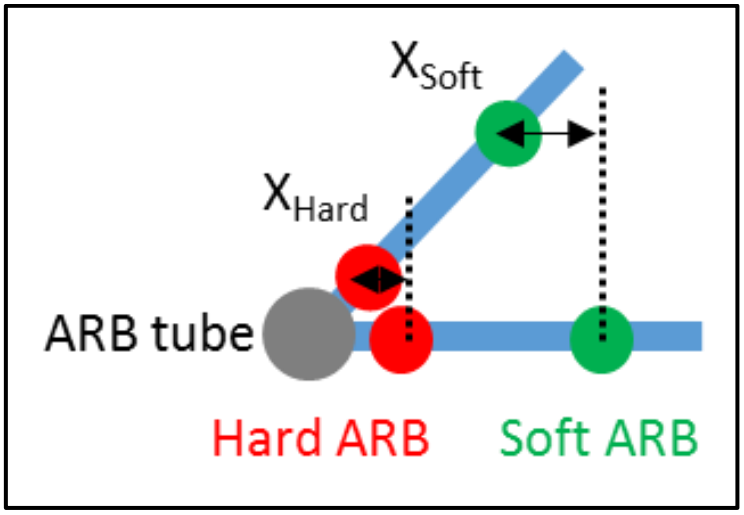

Figure 125 - ARB lever fixture moving longitudinally

Table 16 - Roll gradient comparison between HyperWorks and Excel

Roll Gradient (°/lat g)	ARB - Soft	ARB - Middle	ARB - Hard
HyperWorks	0.72	0.63	0.50
Excel	0.91	0.76	0.57
% Error	26.36 %	20.63 %	14.00 %

4.5 Testing for Improvements

After the testing was done and the room for handling improvement was clearly identified, the suggested changes in setup were tested. To identify the impact of the changes, a traction circle was plotted for the same course as with the previous settings (Figure 99). Furthermore, the corner steering behaviour was analysed again and checked for over- and understeer.

The antiroll bars at the front and rear were both set to their softest settings as this would reduce the roll angle of the car during cornering without being too stiff to lever the inner wheels off the ground. High speed damping for both compression and rebound was not changed and left at the middle setting as this provided good damper characteristics for track unevenness at the front. The driver tended to hit the curb during corner entry and this lifted the wheel off the ground. To help with this the rear

high speed rebound was slightly decreased. Low speed rebound damping was decreased at the front to allow the wheel to return to the ground faster and help with understeer. Similarly, the rear was also decreased as the inner wheel still lifted off the ground when not adjusted.

The last setup change was to be the swap in spring stiffness at the front from 225 lbs/in to the stiffer 300 lbs/in. However, due to a failure of the front right wheel bearing, this could not be tested.

Theory suggests that this change in setup would increase the possible lateral acceleration from 1.8 g to 2 g before the car loses traction. A comparison between logged data for the old setup (blue trace) and the improved one (yellow trace) shows that the improved settings fall well within the new boundary of traction (green ellipse). Even though the maximum lateral acceleration for this run was not as high, the car was not lifting wheels and the driver was more comfortable pushing the car to its boundaries. Unfortunately, due to the failed wheel bearing, this setup could only be tested once and the driver could not be given another chance to test the new setting. However, it is believed that the decrease in lateral acceleration is due to a decrease in understeer and is explored in more detail later on.

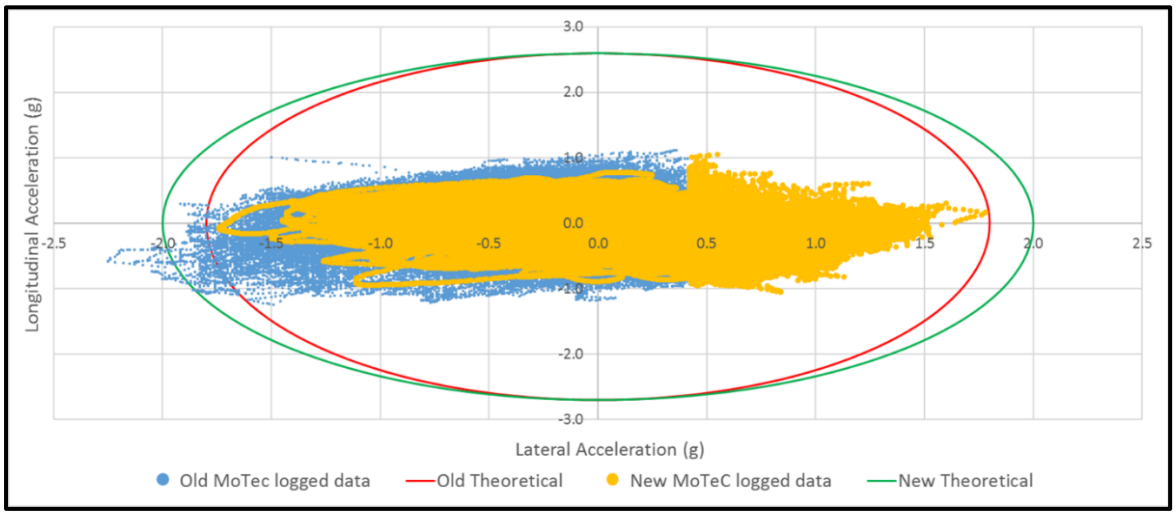

Figure 126 - Traction circle comparison between old and improves settings

From the traction circle it is visible that there was an improvement in traction but under- and oversteer behaviour cannot be determined from this. Comparing average understeer angles for the old setting (no ARB at front and softest at rear, all dampers set to their middle settings) to the improved setting shows a great decrease in understeer behaviour. The average understeer angle at the 2018 competition for the endurance was 3.98° (black trace in Figure 127), compared to 2.12° with the improved settings (pink trace in Figure 127), almost halving the angle. Looking at the same right hand corner that was analysed previously for understeer, the understeer during corner entry was visibly reduced. Furthermore, the mid corner oversteer was also decreased by the initial understeer being

eliminated. A small amount of understeer can still be detected at the corner entrance, however small compared to the large spikes of understeer that were previously detected. The mid corner understeer is almost completely gone and no visible spikes are visible. Overall the sudden under- and oversteer spikes have been eliminated due to improved damper settings allowing more contact between the tyre and the road, making the car saver for the driver to push to its limits.

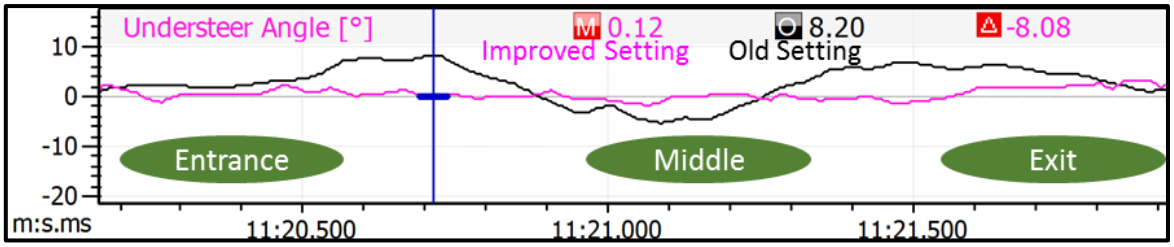

Figure 127 - Understeer with improved settings

It could be argued that with the maximum lateral acceleration being lower, the driver just was not pushing the car as hard and driving slower. Looking at the lap times (Table 17) for the old and the improved suspension settings, the lap times are noticeably shorter (roughly 2 seconds). This is in large due to the reduced understeer. As the car under- or oversteers through a corner the driver tries to correct, usually locking the steering wheel the other way. This motion can create sudden, large spikes in lateral acceleration. To verify this theory, the average lateral acceleration for both suspension settings were looked at. The average lateral acceleration was larger for the new setup even though the maximum was lower, meaning that the car was cornering at higher lateral accelerations and the spikes in acceleration were indeed caused by change in steering lock during understeer. Overall a large decrease in lap time and an increase in vehicle handling behaviour was possible by adjusting suspension parameters. The importance of a well-tuned suspension system can clearly be seen.

Table 17 - Improved lap times

	Old settings	**Improved settings**
Fastest lap time (s)	30.25	28.99
Slowest lap time (s)	34.63	31.65
Average lap time (s)	32.24	30.01
Maximum lateral gs (absolute)	2.25	1.78
Average lateral gs (absolute)	0.35	0.48

Chapter 5 - Conclusions and Recommendations

5.1 General Findings

The effect of suspension setup changes on a car's handling behaviour and track times was investigated based on the 2018 University of Waikato SAE car. This was done using theoretical models in Excel, Matlab and HyperWorks. The models were verified by comparison to track data gathered from the W-FS18 car. Even though the theoretical models assumed that camber gain and change in tyre temperature were negligible, a good correlation between track and theoretical data was found.

Starting the investigation at the point of contact, the tyre, the camber angle barely affected traction, hence the good correlation between theory and practise. However, a tyre with a low pressure (8 PSI in this case) was easily deformed, could not be loaded to its full potential and therefore showed low traction coefficients. Similarly, a high tyre pressure reduced deformation and resulted in lower traction due to a reduced contact patch size. The ideal tyre pressure was between 10 and 12 PSI.

To control traction and minimise wheel lift, different antiroll bar settings were investigated. During the 2018 competition the car did not have an ARB at the front and was on the softest setting at the rear. However, from track data it was found that the roll angle at the front was too large, reducing traction. Investigation showed that although the stiffest setting reduced the overall amount of roll that it was too stiff thereby levering the wheel off the ground. The softest setting at the front and rear produced the best traction characteristics by minimizing roll yet allowing enough for driver feedback and compliance between road and tyre.

A car often has a different weight distribution between the front and rear and hence uses different spring rates. A stiffer front compared to the rear of the car produced greater traction capabilities. This is due to a stiffer axle producing a faster transient response which is desirable in a front steered car, whereas a softer axle allowed for more compliance and more grip.

Diagnosing under- and oversteer based on steering wheel position is possible, however can be cumbersome when looking through large data sets that include slalom courses. Calculating understeer based on Ackermann angle was found to be fast but not reliable due to relying on accurate corner radius measurements. The best way to diagnose understeer was by considering the difference in front and rear slip angle. Provided that extensive and reliable tyre data is available and slip angles present are not excessively large (> 12°), this method provides an accurate indication of the cars under- and oversteer behaviour.

The dampers on the W-FS18 car were hard to model, due to being four way adjustable resulting in a large number of possible setting combinations. The best way to specifically tune dampers was found

to start at a rough damping ratio of 0.6 and then investigate the gathered data further. With the suspension setup from the 2018 competition the car lifted wheels repeatedly during cornering when lateral acceleration should not have been large enough to force the wheel off the ground. Furthermore, looking at the spring displacement the travel was not maxed out and hence not levered off the ground by being too stiff. Investigating damper speeds, it could be seen that the rebound damping was too large, not allowing the wheel to return to the ground fast enough after a disturbance. Furthermore, it was seen that the car tended to understeer during corner entry and then oversteer mid corner as a result of driver response. Decreasing low speed rebound damping at the front allowed for more compliance between the road and the tyre reducing understeer and allowing the driver to take the corner faster. Furthermore, one corner in particular (a chicane) in the 2018 competition endurance course was problematic as the car continuously lifted the front and often the rear wheels, creating an enormous amount of understeer. If the driver braked later, he would have increased the weight on the front wheels while the lateral acceleration was at its maximum, thereby decreasing the likelihood of understeer and wheel lift occurring. This shows that it would be advantageous to implement a live data acquisition system as well as live driver communication.

Putting the front ARB back into the car as well as changing damper settings on all four corners to allow for more compliance, particularly in the low speed region, a two second lap time improvement on a 365 m track was achieved and the corner entry understeer was nearly completely eliminated. It is hypothesized that the car would have perfromed better at the 2018 competition with the improved settings. The autocross track at the 2018 competition was 1.2 km long, possibly resulting in a seven second decrease in lap time with the improved setup (extrapolated from testing times), meaning that WESMO could have potentially placed third instead of eighth.

The effect of suspension tuning can be seen to be large and one of the most effective ways to improve lap times immensely, especially in a competition as strictly regulated as SAE. It is advisable that WESMO takes more time testing and developing settings for specific events, making the car more competitive with high class teams like the Monash University SAE team, Monash Motorsport, who continuously rank highly at competition.

5.2 Recommendations for future work for WESMO

Throughout this research different areas of further investigation were discovered.

- Due to a wheel bearing issue preventing testing, the W-FS18 should be tested with stiffer springs at the front, specifically 250 lbs/in or even 300 lbs/in at the front and 225 lbs/in at the rear.
- Implementation of a yaw sensor to accurately verify the understeer calculations based on slip angle.
- Implementation of live data transfer to the pits as well as live communication with the driver. This would help with noticing driver mistakes early during the race and give the driver an opportunity to remedy them.
- Investment into a damper rebuild kit to ensure even settings for all four corners.
- Design and implementation of a shock dyno to verify damper settings and curves as well as early fault detection for shocks.
- Redesign the rear suspension to have a higher roll centre as this would help with decreasing the amount of roll that needed to be controlled at the rear.

References

1. Britannica, T.E.o.E. *Encyclopædia Britannica - Automobile racing*. 2019 [cited 2019; Available from: https://www.britannica.com/sports/automobile-racing.
2. Vousden, M. *What is body roll or lean?* . 2015 [cited 2019; Available from: https://www.carwow.co.uk/guides/glossary/what-is-car-body-roll-0184.
3. Milliken, D.L., *Race Car Vehicle Dynamics*. 1994: SAE International.
4. Gillespie, T.D., *Fundamentals of Vehicle Dynamics*. 1992, Warrendale, PA: Society of Automotive Engineers.
5. Schramm, D., M. Hiller, and R. Bardini, *Modeling of the Road-Tire-Contact*, in *Vehicle Dynamics: Modeling and Simulation*, D. Schramm, M. Hiller, and R. Bardini, Editors. 2018, Springer Berlin Heidelberg: Berlin, Heidelberg. p. 145-186.
6. Trzesniowski, M., *Fahrwerk*. 2017, Graz: Springer Vieweg.
7. Balkwill, J., *Performance Vehicle Dynamics - Engineering and Applications*. 2018, Oxford: Butterworth-Heinemann.
8. Dixon, J.C., *Tires, Suspension and Handling*. 1996, Warrendale, PA: Society of Automotive Engineers.
9. Liftarn. *Solid Axle Diagram*. 2007 [cited 2019; Available from: https://en.wikipedia.org/wiki/Beam_axle.
10. Alamy. *Craven Carriage Coach Messrs Hooper & Co wheeled vehicle horse-drawn private passenger elegance transport suspension leaf spring*. 2015 [cited 2019; Available from: https://www.alamy.com/stock-photo-craven-carriage-coach-messrs-hooper-co-wheeled-vehicle-horse-drawn-77584230.html.
11. Franco Nugnes, G.P., Jake Boxall-Legge, Jonathan Noble. *Piola: Mercedes F1 W10 rear suspension innovation explained*. 2019; Available from: https://www.autosport.com/f1/news/143927/piola-mercedes-suspension-innovation-explained.
12. Jazar, R.N., *Vehicle Dynamics. Theory and Application*. 1st ed. 2008. Corr. 3rd printing ed. 2008: Springer. 1022.
13. Staniforth, A., *Competition Car Suspension - Design, Construction, Tuning*. 1999, Newbury Park: Haynes Publishing
14. Reze, M. and M. Osajda, *2 - MEMS sensors for automotive vehicle stability control applications*, in *MEMS for Automotive and Aerospace Applications*, M. Kraft and N.M. White, Editors. 2013, Woodhead Publishing. p. 29-53.
15. Smith, C., *Tune to Win: The art and science of race car development and tuning*. 1978, Fallbrook: Aero Publishers.
16. Pütz, R. and T. Serné, *Rennwagentechnik-Praxislehrgang Fahrdynamik - Eine praktische Anleitung für Amateure und Profis*. 2017, Graz: Springer Vieweg.
17. Calspan, *FSAE TTC: Formula SAE Tire Test Consortium*. 2005.
18. Evans, R.D., *Traction (Definition and Measurement)*, in *Encyclopedia of Tribology*, Q.J. Wang and Y.-W. Chung, Editors. 2013, Springer US: Boston, MA. p. 3713-3718.
19. International, S., *Surface Vehicle Recommended Practice.* Vehicle Dynamics Terminology, 1976.
20. Happian-Smith, J., *Introduction to Modern Vehicle Design*. 2001.
21. Harbin, W. *Vehicle load transfer part i ii_dec17*. 2017 [cited 2020; Available from: https://www.slideshare.net/billharbin/vehicle-load-transfer-part-i-iidec17.
22. Secrets, S. *LATERAL AND LONGITUDINAL LOAD TRANSFER*. 2019; Available from: https://suspensionsecrets.co.uk/lateral-and-longitudinal-load-transfer/.
23. Niklass, K. *Lateral Weight Transfer*. 2010 27/10/2010 [cited 2019 16/12]; Available from: http://white-smoke.wikifoundry.com/page/Lateral+Weight+Transfer.
24. Parczewski, K. and H. Wnek. *The influence of vehicle body roll angle on the motion stability and maneuverability of the vehicle*. 2017.

25. Widner, A. and G. Bári, *Investigating the effects of roll center height in simulation, for safety-margin research.* IOP Conference Series: Materials Science and Engineering, 2018. **393**: p. 012034.
26. ÖHLINS. *TTX25 MKII*. Available from: https://www.ohlinsusa.com/suspension-products/ttx25-mkii.
27. Kimberley, M. *Monotube Vs Twin-Tube Dampers: How Do They Work?* 2018 [cited 2020; Available from: https://www.carthrottle.com/post/monotube-vs-twin-tube-dampers-how-do-they-work/.
28. Motorsport, B. *Damper Dyno Testing* Available from: https://www.blinkmotorsport.com/blink-motorsport/damper-dyno-testing/.
29. Giaraffa, M., *Tech Tip: Springs & Dampers*. OptimumG.
30. Segers, J., *Analysis Techniques for Racecar Data Acquisition* 2014: SAE International.
31. K.Manoj, M., G. Prasanna, and D. Anindya, *Mathematical Models for Designing Vehicles for Ride Comfort.* 2009.
32. Rajeev, N. and PratheekSudi, *Natural Frequency, Ride Frequency and their Influence in Suspension System Design.* Journal of Engineering Research and Application 2019. **9**(3): p. 60-64.
33. Lamers, W., *Development and analysis of a multi-link suspension for racing applications*, in *Department Mechanical Engineering, Dynamics and Control Group*. 2008, Technische Universiteit Eindhoven: Eindhoven.
34. Chepkasov, S., G. Markin, and A. Akulova, *Suspension Kinematics Study of the "Formula SAE" Sports Car.* 2nd International Conference on Industrial Engineering (Icie-2016), 2016. **150**: p. 1280-1286.
35. Rijk, S.v., *Optimization of the damper settings of the URE05e*, in *Department of Mechanical Engineering; Dynamics and Control Group*. 2010, Eindhoven University of Technology: Eindhoven
36. WESMO, *WESMO - 2018 Design report - Various Sections*. 2018.
37. Elders, W., *Wheel Alignment* W. Team, Editor. 2018.
38. Clement, F. and L. Kopf, *WESMO - 2018 Design report - Suspension* 2018.
39. Engineers, S.o.A., *2017-18 Formula SAE Rules*. 2018.
40. Clement, F. *WESMO: Validation of Multibody Dynamics Model of Formula SAE Suspension*. in *Oji Fibre Solution Engineering Design Show 2018 - ENGEN492 Research Presentations*. 2018. Hamilton, New Zealand University of Waikato.
41. Kopf, L. *WESMO: Validation of Formula SAE Suspension Forces, Using Multibody Dynamics Simulation*. in *Oji Fibre Solution Engineering Design Show 2018 - ENGEN492 Research Presentations*. 2018. Hamilton, New Zealand: University of Waikato

Appendix

A 1 *Centre of Gravity Calculations*

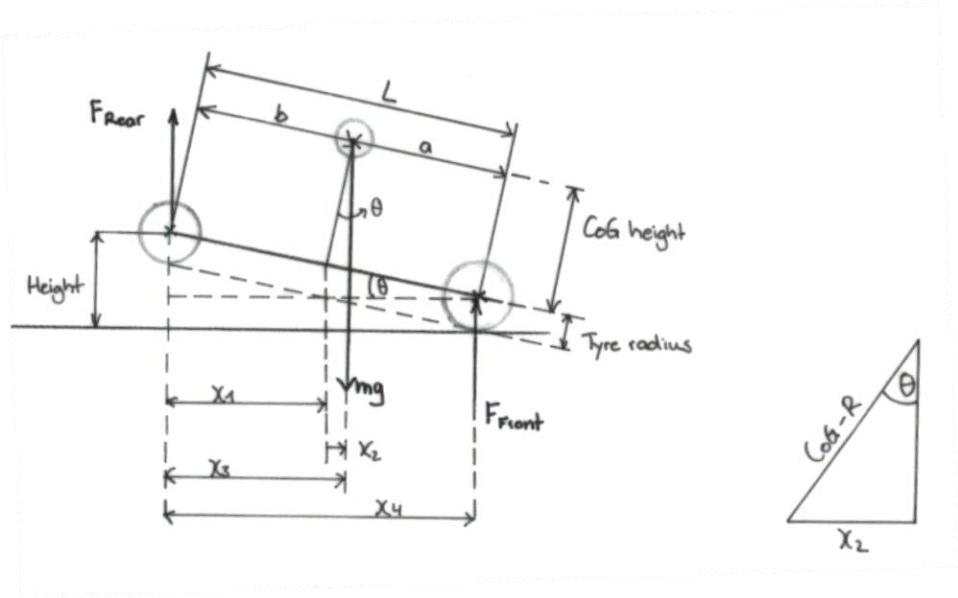

Figure A 1 - Centre of Gravity free body diagram

$$x_3 = x_1 + x_2$$
$$x_1 = b\cos\theta$$
$$x_2 = (CoG - R)\sin\theta$$
$$x_4 = L\cos\theta$$

$$\sin\theta = \frac{height}{L}$$

$$\sum M_{Rear} = 0$$

$$Wx_3 - F_F x_4 = 0 \quad \text{With } W = mg$$
$$Wx_3 = F_F x_4$$
$$W[b\cos\theta + \sin\theta\,(CoG - R)] = F_F L\cos\theta$$
$$b\cos\theta + \sin\theta\,(CoG - R) = \frac{F_F L\cos\theta}{W}$$
$$\sin\theta\,(CoG - R) = \frac{F_F L\cos\theta}{W} - b\cos\theta$$
$$CoG = \frac{F_F L\cos\theta - wb\cos\theta}{W\sin\theta} + R$$

$$\boxed{CoG = \frac{F_F L - wb}{W\tan\theta}}$$

A 2 *Centre of Gravity Measurements for W-FS18*

Table A 1 - Measured centre of gravity heights

Front Lift	0	0	0	0	0	mm
Rear Lift	0	45	100	145	190	mm
FL	60.3	60.6	62.5	63.4	63.1	kg
FR	69.2	68.7	67.9	67.4	68.3	kg
RR	59.3	60.2	62.3	62.8	63.5	kg
RL	73.1	74.4	74.4	74.8	73.9	kg
Favg	129.5	129.3	130.4	130.8	131.4	kg
Ravg	132.4	134.6	136.7	137.6	137.4	kg
Total Weight	261.9	263.9	267.1	268.4	268.8	kg
Average Weight			266.02			kg
a	0.78	0.80	0.81	0.81	0.81	m
Average a			0.80			m
b	0.79	0.78	0.77	0.76	0.76	m
Average b			0.77			m
Thita	0	0.03	0.06	0.09	0.12	rad
Thita	0	1.64	3.63	5.26	6.88	deg
CoG Height		9.323163672	223.5899481	245.8412243	267.3681662	mm

A 3 *W-FS18 Specification Sheet (submitted for the 2018 competition)*

Table A 2 - Full list of specifications for the W-FS18

FSAE Design Spec Sheet							2018
Competitors: **Please read the Instructions**-Tips (tab below) prior to the completion and submission of this sheet.							
Car No.	25						
School	University of Waikato						
Dimensions	**Units**						
Overall Dimensions	mm	Length:	2865	Width:	1228	Height:	1209
Wheelbase & Track	mm	Wheelbase:	1575	Front Track:	1100	Rear Track:	1050
Center of Gravity Design Height	mm	CG Height:	0.3	Confirmed Via:	Corner balance test		
Mass without driver	kg	Front:	78.9	Rear:	108.2	Total:	187.1
Weight Distribution with 68kg driver		% Front:	47.0	% Left:	48.0		
Suspension Parameters	**Units**	**Front**			**Rear**		
Tire Size, Compound and Make		Hoozier 18.0x6.0-10 Road Racing C2000 R25B			Hoozier 18.0x6.0-10 Road Racing C2000 R25B		
Wheels (width, construction)		10x6.0" -18.7, 3-piece aluminium, billet			10x6.0" -18.7, 3-piece aluminium, billet		
Suspension Type		Double A-Arm, Pushrod			Double A-arm, Pushrod		
Suspension design travel	mm	Jounce (col D): Rebound (col E):	36	36	Jounce (col G): Rebound (col H):	36	36
Wheel rate (chassis to wheel center)	N/mm	56			63		
Roll rate (chassis to wheel center)	Nm/deg	592			607		
Sprung mass natural frequency	Hz	3.07			3.24		
Jounce Damping	% critical	70	at __ mm/sec:	25	70	at __ mm/sec:	25
Rebound Damping	% critical	65	at __ mm/sec:	50	65	at __ mm/sec:	50
Motion ratio	_.__:1	0.79	Type:	Linear	0.79	Type:	Linear
Ride Camber (Rate of Camber Change)	deg/m	-52.7			-36.2		
Roll Camber	deg/deg	-0.34			-0.95		
Static Toe (- out, + in)	deg	-2.40			+1.20		
Static camber	deg	-1.00			-1.00		
Static camber adjustment method		Shims at upper control arm upright bracket			Shims at upper control arm upright bracket		
Anti dive / Anti Squat	%	0			0		
Roll center height above ground, static	mm	94.1			50.1		
Roll center position at 1g lateral acc	mm	Height (col D): Lateral (col E):	84.09	15.5	Height (col G): Lateral (col H):	40.7	8.2
Front Caster, Trail, and Scrub Radius		Caster (deg):	4.1	Kin Trail (mm):	16.6	Scrub Rad (mm)	52.9
Front Kingpin Axis		Inclination (deg):	3.8	Offset (mm):	68.2		
Static Ackermann	%	100	Adjustable?	no			
Suspension Adjustment Methods		Rod ends on the end of tie rods. Fine pitch thread					
Steer Ratio, C-Factor, Steer Arm Length		Steer Ratio (x:1)	5:1	c-factor (mm)	85.7	Steer Arm Length	240.0

Brake System / Hub & Axle	Units	Front				Rear			
Rotors		200 mm Diameter, stainless steel				200 mm Diameter, stainless steel			
Master Cylinder		Kawasaki Ninja ZX-6R, 14mm bore				Kawasaki Ninja ZX-6R, 14mm bore			
Calipers		AP Racing CP4226-2S0				AP Racing CP4226-2S0			
Brake Pad/Lining Material		Steel pad with brake compound				Steel pad with brake compound			
Force and Pressures @ 1g Deceleration		Front Pres. (bar):	38.0	Rear Pres. (bar):		24.3	Pedal Force (kN)		0.2
Upright Assembly		CNC machined 6061-T6 Aluminium				CNC machined 6061-T6 Aluminium			
Hub Bearings		SKF Deep GrooveBB 61815-2RZ, low friction NBR seals, rotating inner ring.				SKF Deep GrooveBB 61815-2RZ, low friction NBR seals, rotating inner ring.			
Axle type, size, and material									

Ergonomics	Units				
Driver Size Adjustments		2 Pedal positions for adjustment for driver comfortability			
Seat (materials, padding/damping)		Carbon Fibre seat with 3D printed seat blocks			
Steering Wheel (dia, construction)		Diamter (mm)	235.0	Construction	Laser cut aluminium with PLA 3D printed grips
Shift Actuator (type, location)		Electronic actuation, electric solenoid assisted, fixed paddle system, behind steering wheel			
Clutch Actuator (type, location)		Pull cable actuation, Spring assisted, fixed paddle system, behind steering wheel			
Instrumentation		Arduino controlled steering wheel mounted display, with shift lights and warning lights			
Optional: Driver Safety Systems?		6-point harness, radio controlled warning lights for immediate notification of hazards			

Electrical	Units	
Power Management / Control		ECU Link G4+ Monsoon
Wiring / Loom / ECM mounting		DT, DTM and OEM connectors. Integrated Link loom, accessible ECU mounting and fuse box.
Battery / Charging System		Shorai Lithium Battery 12V. OEM KTM Charging system (stator)
Grounding		Chassis Ground, Engine ground, and ground blocks situated the front and rear of the car
Driver Assist Systems		Launch control, traction control
Logging / Telemetry		Motec SDL3 in built data logger. Logging suspension travel, steering travel, engine vitals, brake pressure.
Special Sensing Technology		GPS Logging, with lateral and longititudinal Gforce outputs.

Frame	Units						
Frame Construction		Mild Steel Spaceframe					
Material		AISI 1020 Mild Steel					
Joining method and material		TIG welded with ER70S-6 rod					
Bare frame mass with brackets & paint	kg	Target:	34.0	Physical Test:	34.8		
Torsional stiffness	N-m/deg	Target:	2250	Simulated:	2399	Physical Test:	2104
Torsional stiffness validation method		ANSYS FEA simulation and physical torsional test					
Impact Attenuator configuration		Dow Impaxx 700 Foam, 4mm Aluminium Anti-Intrusion plate, 25.4 x 1.2mm Cross Bracing					
Impact Attenuator dimensions	mm	Width:	356	Height:	305	Depth:	254
Impact Attenuator energy capacity	kJ	Energy:	N/A	Method:	Standard Purchased Impact Attenuater		

Powertrain	Units						
Manufacturer / Model		KTM 690 Duke R					
Cylinders & Fuel		Cylinders:		1	Fuel Type:	RON 98	
Displacement & Compression		Displacement (cc):		693	Compression (_:1):		12.7:1
Bore & Stroke	mm	Bore:		105.0	Stroke:		80.0
Engine Output		Peak Power (kW)	45	PeakTorque (Nm)	59		
Design Speeds	rpm	Max Power:	7000	Max Torque:	5200	80% Torque:	4500
Induction (natural or forced, intercooled)		Natural					
Throttle Body / Mechanism		Butterfly valve, 24mm in diameter. Pulley on throttle mechanism and directly actuated cable on pedal					
Fuel Injection System (manf'r, and type)		Bosch injector, sequential Fuel injection, 300kpa					
Fuel System Sensors (for fuel mapping)		Fuel Pressure sensor (150 PSI Honeywell)					
Fuel Pressure	bar	3					
Injector location		100 mm before valves and directed 30 degrees from perpendicular to the port entry					
Intake Plenum		Volume (cc):	3450	Runner length (mm):	500.0		
Exhaust Header Configuration		1	Effective Runner Length (mm):		983.0	Variation (mm):	N/A
Exhaust Header Diameters		Primary (mm):	38.8	Collector (mm):	N/A		
Ignition System		Link Coil Packs. Denso Ignition coils, Link Controlled sequential firing					
Ignition Timing		24-2 teeth OEM crank signal					
Oiling System (wet/dry sump, mods)		Standard KTM					
Engine Lubricants / Friction Treatment		15W-40 Wet Clutch Motorcycle oil					
Coolant System and Radiator location		Left side mounted, 308 x 205 x 40 mm core aluminium radiator, 2x 360 cfm fan mounted on rear of radiator					
Fuel Tank Location, Type		Under seat on left side of car. Baffled aluminum				Capacity (L):	5.7 L
Muffler		Kawasaki ER-6n Muffler					
Other significant engine modifications							

Drivetrain	Units						
Drive Type		520ZVM-X x 106ZB X'Ring DID chain					
Differential System		Drexler LSD FS 2010 V2					
Final Drive Ratio	_:1	3:1					
Vehicle Speed @ max power (design) rpm	kph	1st gear:	47.1	2nd gear:	67.3	3rd gear:	88.4
Vehicle Speed @ max power (design) rpm	kph	4th gear:	107.6	5th gear:	123.2	6th gear:	135.5
Half shaft size and material		Size: 20.5 mm OD, 10 mm ID, Material: High tensile steel DIN 1.2767, Hardness: 44 HRC					
Axle Joint type and grease used		Inside: Drexler LSD output shaft and tripod, Outside: Custom hub to fit Taylor Race FORMULA SAE tripod, Grease: LMM					

Aerodynamics (if applicable)	Units						
Type / Configuration		Carbon fibre with foam core and carbon/kevlar undertray and diffuser					
Forces (at 80 kph, ρ= 1.162 kg/m^3)		Downforce (N):	301	% Front:	7.8	Drag (N):	231
Coefficients & Reference Area		Cl:	-0.55	Ref. Area (m^2):	0.68	Cd:	0.60
Noteable Features (active, etc)							

Other Information	Units	
Body Work (material, process)		Fibreglass mould constructed from MDF plug. Carbon fibre part produced using resin infusion method.
Optional Information		

A 4 *MoTeC Accelerometer Correction*

$$Acceleration_{Lateral} = Longitudinal_{Logged} * \sin 61.35 + Vertical_{Logged} * \sin 14 + Lateral_{Logged} * \sin 14 + Longitudinal_{Logged} * \sin 14$$

$$Acceleration_{Longitudinal} = Lateral_{Logged} * \sin 14 - Longitudinal_{Logged} * \sin 14$$

$$Acceleration_{Vertical} = Vertical_{Logged} * \sin 61.35 - Longitudinal_{Logged} * \sin 61.35$$

A 5 *Tire Test Consortium Measurements*

Table A 3 - Tyre Data Measurements

Symbols	Parameters	Dimensions	
		English	S. I.
	Forces and Moments		
AVL	ANALOG VERTICAL LOAD	Lb	N
BFT	BEARING FRICTION TORQUE	ft-lb	n-m
FR	ROLLING RESISTANCE OF STRAIGHT FREE-ROLLING TIRE (DEF. 1)	Lb	N
FX	LONGITUDINAL FORCE *	Lb	N
FY	LATERAL FORCE *	Lb	N
FZ	NORMAL FORCE *	Lb	N
HT	DRIVE OUTPUT TORQUE (DEF. 3)	ft-lb	N-m
MX	OVERTURNING MOMENT *	ft-lb	N-m
MY	ROLLING RESISTANCE MOMENT *	ft-lb	N-m
MZ	ALIGNING TORQUE *	ft-lb	N-m
FY	NEGATIVE LATERAL FORCE (-FY)	Lb	N
FY_NEW	CORRECTED LATERAL FORCE (-FY), Near SA = 0	Lb	N
T	WHEEL TORQUE *	ft-lb	N-m
	Energy Loss		
ER	ENERGY LOSS OF STRAIGHT ROLLING BRAKED OR DRIVEN TIRE (DEF. 2)	ft-lb/ft	N-m/m
	Pressure		
P	INFLATION PRESSURE	psi	kPa
	Speeds		
N	WHEEL ROTATIONS PER MINUTE	rpm	rpm
R	WHEEL ROTATIONS PER MILE (or km.) (DEF. 4)	rev/mi	rev/km
V	ROAD SPEED	mph	kph
	Longitudinal Slip		
SL	SLIP-LONGITUDINAL * (DEF. 6)	-	-
SR	SLIP RATIO (DEF. 5)	-	-

Symbols	Parameters	Dimensions	
		English	S. I.
Angles			
IA	INCLINATION ANGLE *	deg	deg
SA	SLIP ANGLE *	deg	deg
SAD	SLIP ANGLE (Processed)	Deg	Deg
Tire Radii			
RL	LOADED RADIUS-*	in	cm
RE	EFFECTIVE ROLLING RADIUS* (DEF. 7)	in	cm
Time			
ET	TIME ELAPSED	sec	sec
Temperature			
CAT	CONTAINED AIR TEMPERATURE	F	C
TSTI	TREAD SURFACE TEMPERATURE INBOARD	F	C
TSTC	TREAD SURFACE TEMPERATURE CENTER	F	C
TSTO	TREAD SURFACE TEMPERATURE OUTBOARD	F	C
RST	ROAD SURFACE TEMPERATURE	F	C
Tire Coefficients			
NFX	FX ÷FZ	-	-
NFY	FY ÷ FZ	-	-
NFR	FR ÷ FZ	-	-
CS	CORNERING STIFFNESS	lbs/deg	kg/deg
CSC	CORNERING STIFFNESS COEFFICIENT	-	-
F	GM f-function	-	-
G	GM g-function	-	-
H	GM h-function	-	-
ATC	GM ALIGNING TORQUE COEFFICIENT	ft	cm

A 6 *Suspension Setups for W-FS18 in 2019*

Table A 4 - Suspension setups tested on W-FS18 for this thesis

Run	ARB Position		Damping		Spring rate	
	Front	Rear	Front	Rear	Front	Rear
1	None	None	All middle	All middle	225 lbs/in	225 lbs/in
2	None	None	LSR Max	All middle	225 lbs/in	225 lbs/in
3	None	None	LSR Min	All middle	225 lbs/in	225 lbs/in
4	None	None	LSC Max	All middle	225 lbs/in	225 lbs/in
5	None	None	LSC Min	All middle	225 lbs/in	225 lbs/in
6	None	None	All middle	LSR Max	225 lbs/in	225 lbs/in
7	None	None	All middle	LSR Min	225 lbs/in	225 lbs/in
8	None	None	All middle	LSC Max	225 lbs/in	225 lbs/in
9	None	None	All middle	LSC Min	225 lbs/in	225 lbs/in
10	None	None	LSR 5 clicks decreased	LSR 5 clicks decreased	225 lbs/in	225 lbs/in
11	None	Soft	LSR 5 clicks decreased	LSR 5 clicks decreased	225 lbs/in	225 lbs/in
12	Soft	Soft	LSR 5 clicks decreased	LSR 5 clicks decreased	225 lbs/in	225 lbs/in
13	Soft	Middle	LSR 5 clicks decreased	LSR 5 clicks decreased	225 lbs/in	225 lbs/in
14	Middle	Middle	LSR 5 clicks decreased	LSR 5 clicks decreased	225 lbs/in	225 lbs/in
15	Middle	Soft	LSR 5 clicks decreased	LSR 5 clicks decreased	225 lbs/in	225 lbs/in
16	Stiff	Stiff	LSR 5 clicks decreased	LSR 5 clicks decreased	225 lbs/in	225 lbs/in
17	Soft	Stiff	LSR 5 clicks decreased	LSR 5 clicks decreased	225 lbs/in	225 lbs/in
18	Stiff	Soft	LSR 5 clicks decreased	LSR 5 clicks decreased	225 lbs/in	225 lbs/in
19	Soft	Middle	LSR 5 clicks decreased	LSR 5 clicks decreased	250 lbs/in	225 lbs/in
20	Soft	Middle	LSR 5 clicks decreased	LSR 5 clicks decreased	300 lbs/in	225 lbs/in

Note: Red highlighted not tested due to failed wheel bearing

A 7 *Slip Angle*

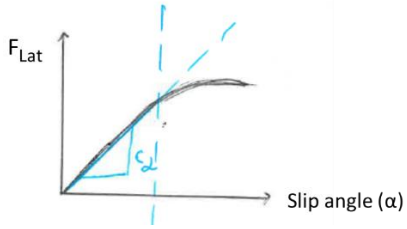

c_α = *cornering stiffness* → *tyre property*

$$F_{Lat} = c_\alpha * \alpha \quad I$$

$$F_{CG} = \frac{mv^2}{R} \quad II$$

Top View *Side View*

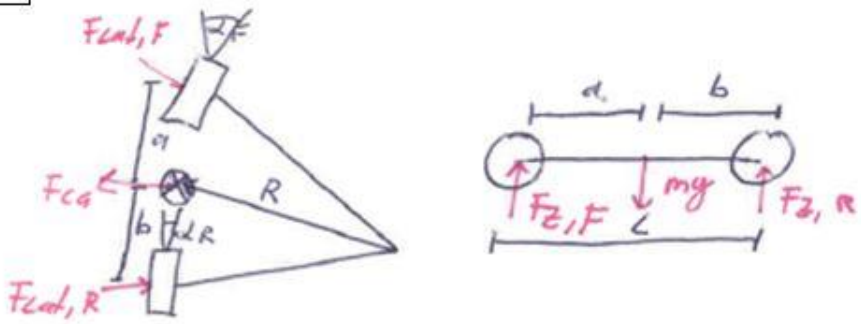

For small slip angles at front and rear

$F_{CG} = F_{Lat,F} + F_{Lat,R}$

$$\Rightarrow \frac{mv^2}{R} = F_{Lat,F} + F_{Lat,R} \quad III$$

$\sum M_{CG} = 0$

$F_{Lat,F} * a - F_{Lat,R} * b = 0$

$$F_{Lat,F} = \frac{F_{Lat,R} * b}{a} \quad IV$$

$$\frac{mv^2}{R} = \frac{F_{Lat,R} * b}{a} + F_{Lat,R}$$

$$\frac{mv^2}{R} = F_{Lat,R}\left(\frac{b}{a} + 1\right)$$

$a+b = wheelbase(L)$

$$\Rightarrow F_{Lat,R} = \frac{ma}{L} * \frac{v^2}{R} \quad V$$

$\sum M_F = 0; a + b = L$

$mg * a - F_{Z,R} * (a + b) = 0$

$$\frac{ma}{L} = \frac{F_{Z,R}}{g} \quad VI$$

$$\Rightarrow F_{Lat,R} = \frac{F_{Z,R}}{g} * \frac{v^2}{R} \quad VII$$

Sub VII into I

$$\frac{F_{Z,R}}{g} * \frac{v^2}{R} = c_\alpha * \alpha_R$$

$$\Rightarrow \alpha_R = \frac{F_{Z,R}}{c_{\alpha,R}} * \frac{v^2}{gR} \qquad \frac{v^2}{R} = a_{Lat}$$

$$\alpha_F = \frac{F_{Z,F}}{c_{\alpha,F}} * \frac{v^2}{gR} \qquad \frac{v^2}{R} = a_{Lat}$$

A 8 *Longitudinal Traction Coefficients*

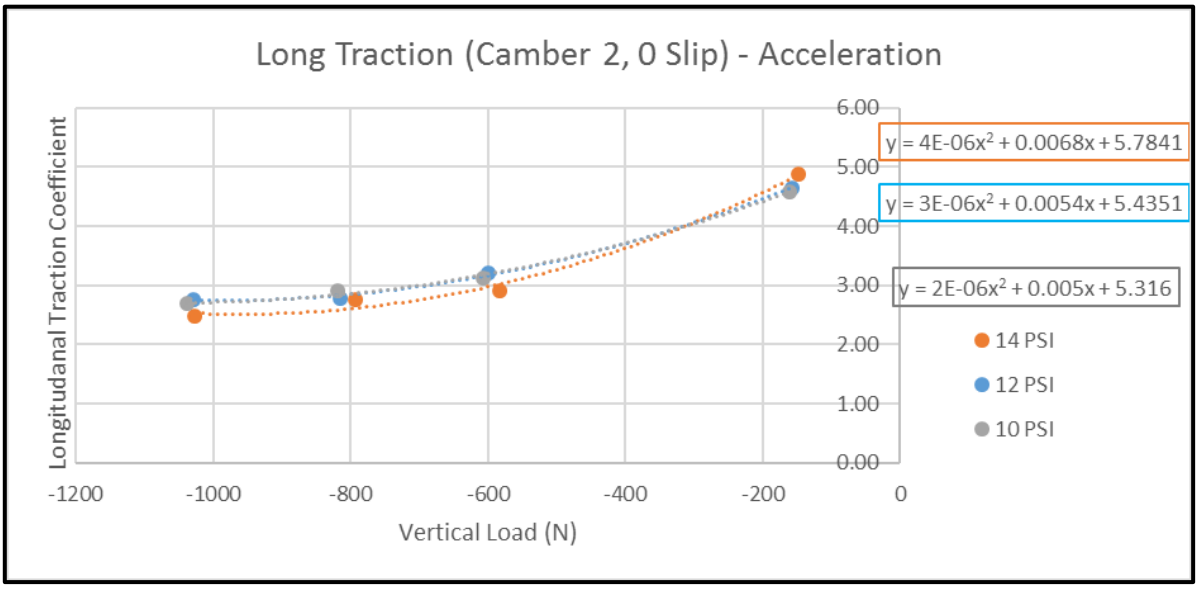

Figure A 2 - Acceleration traction coefficient with different pressures

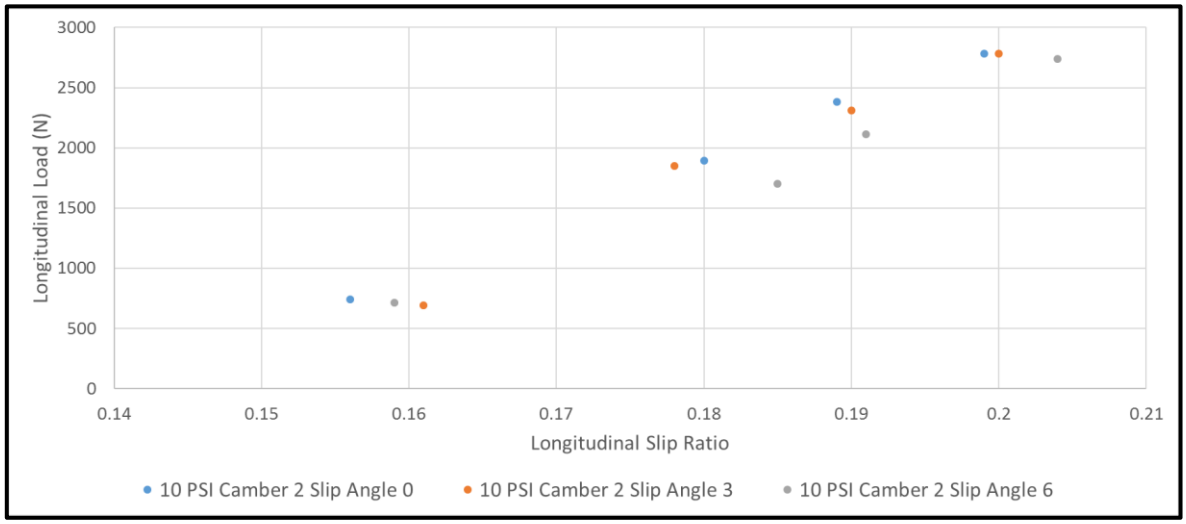

Figure A 3 - Longitudinal force versus slip ratio for different slip angles

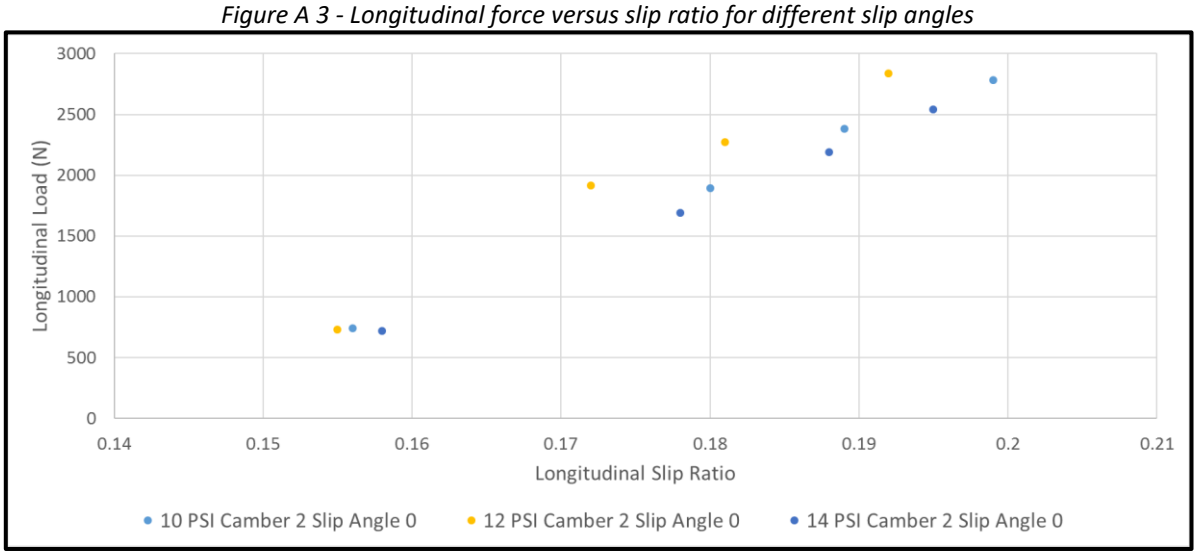

Figure A 4 - Longitudinal force versus slip ratio for different tyre pressures

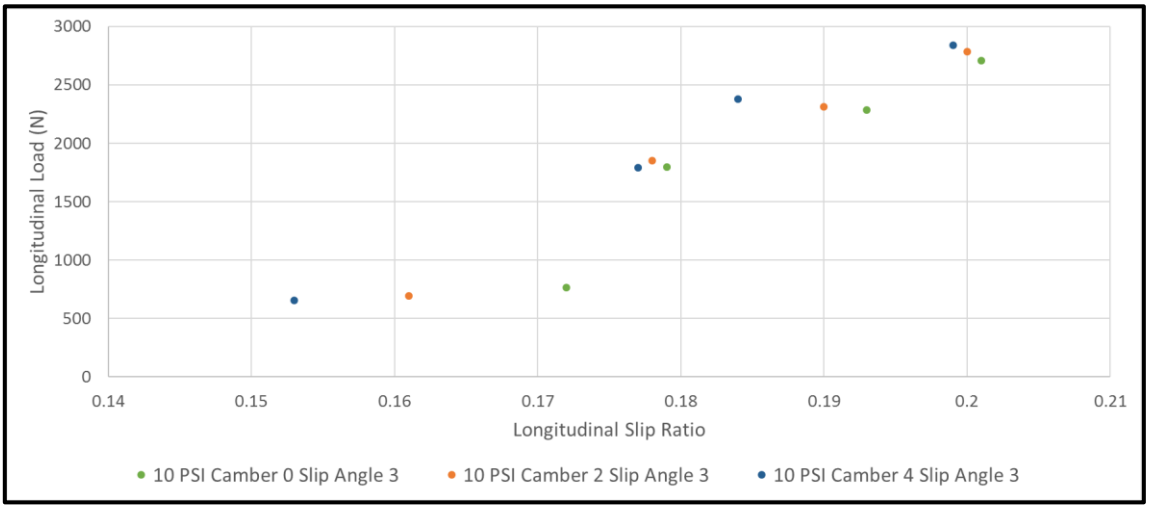

Figure A 5 - Longitudinal force versus slip ratio for different camber angles

A 9 *Average Wheel Travel for W-FS18*

Table A 5 - Average and maximum suspension travel during 2018 endurance

	Out Lap	Lap 1	Lap 2	Lap 3	Lap 4	Lap 5	Lap 6	Lap 7	Lap 8	Lap 9	In Lap	Overall Avg
	02:21.5	01:33.7	01:30.8	01:29.1	01:29.3	01:30.4	01:32.4	01:30.8	01:30.2	01:31.8	00:35.0	
Abs Susp FL [mm]	2.39	5.9	6.27	6.49	6.22	6.29	6.01	5.98	6.34	5.96	3.04	5.54
Abs Susp FR [mm]	1.44	5.55	5.96	6.25	5.96	5.94	5.84	5.85	5.83	5.73	2.25	5.15
Abs Susp RL [mm]	1.5	3.68	3.79	4.09	3.85	3.92	3.98	3.9	3.97	3.98	4.13	3.71
Abs Susp RR [mm]	0.9	4.89	5.07	5.16	5.24	5.34	5.26	5.3	5.01	5.16	3.94	4.66
Absolute Avg [mm]												4.76
												Overall Max
Abs Susp FL [mm]	13.32	15.61	15.71	15.73	15.73	15.75	15.79	15.83	15.73	15.73	10.91	15.83
Abs Susp FR [mm]	6.65	13.14	12.64	13.97	15.8	15.22	14.93	13.5	16.75	14.82	5.9	16.75
Abs Susp RL [mm]	8.37	7.66	8.65	9.27	9.12	10.14	8.13	7.37	9.38	9.46	7.03	10.14
Abs Susp RR [mm]	8	8.79	15.45	16.01	8.02	10.5	7.9	7.9	9.8	9.2	6.55	16.01
Absolute Max [mm]												16.75

A 10 *Vertical Tyre Loads for W-FS18*

Table A 6 - Vertical loads for braking, acceleration and cornering

	Down Force per wheel (N)	
	Front	**Rear**
Braking (-1.6 g)	820	577
Acceleration (1.1 g)	468	930
Cornering (1.8 g)	Inner: 20 Outer: 1376	Inner: 15 Outer: 1382

A 11 *Matlab: Front corner inside*

```
% Larissa Kopf
% Date: 11/05/2019
% Models damper behaviour of front inside corner of W-FS18
% Prompted to input damming ratios

clear all

% Defining variables
mt = 285; % total mass of the car
mfc = 62.25; % sprung corner weight front (kg)
mun = 9; % unsprung weight per corner (kg)
ksf = 39.4; % spring stiffness front (N/mm)
kTire = 103.32; % tire spring rate from tyre data 590 lb/in value (N/mm)
g = 9.81; % gravitational constant (m/s^2)
MRf = 0.79; % motion ratio front (spring/wheel travel)
dratiof = 0.7; % damping ratio front
xc = 0; % displacement of sprung mass
dxc = 0;% 1st differential of displacement of sprung mass
ddxc = 0; % 2nd differential of displacement of sprung mass


% Calculating
kwf = ksf/MRf^2; % wheel rate of front wheel (N/mm)
kRide = ((kwf*kTire)/(kwf+kTire))*1000; % caculating ride rate (N/m)
dfcr = 2*sqrt(kwf*1000*mfc*2); % critical damping front (Ns/mm)
Fdf = dfcr*dratiof; % damping force front (N)
cfront = dratiof*dfcr; % calculating actual damping (Ns/mm)
ktot = (ksf*kTire)/(ksf+kTire); % totl spring rate for simplified system
(N/mm)

%undamped natural frequencies
%wnSprungF= (1/(2*pi))*sqrt(ksF*1000/mfc);
wSprung = 1/(2*pi)*sqrt(kRide/mfc); %sprung undamped natural frequency (Hz)
wUnsp = 1/(2*pi)*sqrt(((ksf+kTire)*1000)/mun); %sprung undamped natural
frequency (Hz)
%From simplified differential equation and lplace we can solve the system
fre = (1/MRf)*sqrt(ktot/mfc);

%plotting chassis displacement for different damping ratios
dratio = [ 0 0.5 0.7 0.8 0.9 1.000001 1.5 3];
for i = 1:length(dratio)
```

```
    zita = dratio(i);
    time = (0:0.01:2);
    for j=1:length(time)

      Part1= exp(-zita*wSprung*time(j));
      Part2= cos(wSprung*sqrt(1-zita^2)*time(j));
      Part3= zita/(sqrt(1-zita^2));
      Part4=sin(wSprung*sqrt(1-zita^2)*time(j));
      Output_in(j,i) = 1-(Part1*(Part2+(Part3*Part4)));

%with 1 chosen damping ratio and certain disturbance find chassis movement
        if zita==0.7
            Xbump = 8; %disturbance (mm)
            Xchassis(j) = (Output_in(j,i)*Xbump); %absolute chassis
displacement
        end
    end
end

%plot different zita
figure(1);
clf;
hold on;
for a=1:length(dratio)
plot(time,Output_in(:,a));
end
line([0 time(end)], [1 1],'Color', 'red', 'LineStyle','--');
legendCell = cellstr(num2str(dratio','Zita=%1.1f'));
legend(legendCell)
xlabel('Time (sec)');
ylabel('Chassis displacement / Disturbance');
title ('General damping ratios');

% % %plot chassis displacement
% % figure(2);
% % clf;
% % hold on;
% % plot(time,Xchassis);
% % line([0 time(end)], [Xbump Xbump],'Color', 'red', 'LineStyle','--');
% % xlabel('Time (sec)');
% % ylabel('Chassis displacement (mm)');


% Choosing damping ratios

prompt = {'Enter chosen Low Speed Compression'};
        dlgtitle = 'LSC';
        answ = inputdlg(prompt,dlgtitle,[1 20]);
        LSC = str2num(cell2mat(answ));

prompt = {'Enter chosen Low Speed Rebound'};
        dlgtitle = 'LSR';
        answ = inputdlg(prompt,dlgtitle,[1 20]);
        LSR = str2num(cell2mat(answ));

prompt = {'Enter chosen High Speed Compression'};
        dlgtitle = 'HSC';
        answ = inputdlg(prompt,dlgtitle,[1 20]);
        HSC = str2num(cell2mat(answ));
```

```
prompt = {'Enter chosen High Speed Rebound'};
        dlgtitle = 'HSR';
        answ = inputdlg(prompt,dlgtitle,[1 20]);
        HSR = str2num(cell2mat(answ));

ratioFront = [LSC LSR HSC HSR]; %damping ratios front LSC, LSR,HSC,HSR

% enter bump in mm (compression-> negative bump, rebound -> positive bump)

prompt = {'Bump (mm) (compression-> negative bump, rebound -> positive
bump)'};
        dlgtitle = 'Bump';
        answ = inputdlg(prompt,dlgtitle,[1 20]);
        Bump = str2num(cell2mat(answ));

 for i=1:length(ratioFront)
    zita = ratioFront(i);
    time = (0:0.01:2);
    for j=1:length(time)
        Part1= exp(-zita*wSprung*time(j));
        Part2= cos(wSprung*sqrt(1-zita^2)*time(j));
        Part3= zita/(sqrt(1-zita^2));
        Part4=sin(wSprung*sqrt(1-zita^2)*time(j));
        Output_in(j,i) = 1-(Part1*(Part2+(Part3*Part4)));
        Xchassis2(j,i) = (Output_in(j,i)*Bump)-Bump;
    end
 end

%plot absolute chassis displacement for chosen dratios
figure(3);
clf;
hold on;
for a=1:length(ratioFront)
plot(time,Xchassis2(:,a));
end
line([0 time(end)], [0 0],'Color', 'red', 'LineStyle','--');
legendCell2 = cellstr(num2str(ratioFront','Zita=%1.1f'));
dim = [.6 .6 .3 .3];
annotation('textbox',dim,'String',legendCell2,'FitBoxToText','on');
legend('LSC', 'LSR','HSC','HSR','Location', 'northeast');
xlabel('Time (sec)');
ylabel('Absolute chassis displacement (mm)');
title ('Chassis displacement for chosen damping ratios');

%Damper curves
KneeS = 6/1000; %rebound knee speed from mm/s to m/s
LowS = 2/1000; %Low speed from mm/s to m/s
HighS = 30/1000; %High speed from mm/s to m/s

% critical damping
CcrUn = 2*sqrt((ksf*1000+kTire*1000)*mun); % Critical damping for unsprug
mass (Ns/m)
CcrSp = 2*sqrt(kRide*mfc); % Critical damping for sprug mass (Ns/m)

% Damping rates
for i=1:length(ratioFront)+2 %+2 for knee speeds
    if i<=2
    DR(i)= CcrUn*ratioFront(i);
```

```
    DF(i) = DR(i)*LowS;
    elseif i==3 %knee speeds compression
    DF(i) = DR(1)*KneeS;
    elseif i==4 %knee speeds rebound
    DF(i) = DR(2)*KneeS;
    else
    DR(i-2) = CcrSp*ratioFront(i-2);
    DF(i) = DR(i-2)*HighS;
    end
end
DR=[0;DR(:)];
DF=[0;DF(:)];
%DR(0) = {'Damping Rate (Ns/m'}
```

A 12 *Matlab: Full car rolling – Wheel lift*

```
% Larissa Kopf
% Date: 20/06/2019
% Models all corners on steady state loading for W-FS18
% Shows wheel lift for particular scenario (1.8 g lateral acceleration)

clear all
%Front ARB definition
ARBf="YES";
Hf=3; % measured from closest to tube
%Rear ARB definition
ARBr="YES";
Hr=3; % measured from closest to tube

% lateral acceleration
ay=1.8; %in g

%damper input front
LSCf = 0.36;
LSRf = 0.24;
HSCf = 0.1;
HSRf = 0.1;

ratioFront = [LSCf LSRf HSCf HSRf]; %damping ratios front LSC, LSR,HSC,HSR

VkneeF = 12.5; %knee speed front in mm/sec
%damper input rear
LSCr = 0.36;
LSRr = 0.24;
HSCr = 0.1;
HSRr = 0.1;

ratioRear = [LSCr LSRr HSCr HSRr]; %damping ratios front LSC, LSR,HSC,HSR
VkneeR = 12.5; %knee speed rear in mm/sec

%%%%%%%%%%%%%%%%%%%%%%%%%%%%%%%%%%%%%%%%%%%%%%%%%%%%%%%%%%%%%%%%%%%%%%%%%%%%%%%
%creating front and rear damper lookup table look at excel dyno stuff
FrontDamper = [672.22 450.71 187.01 166.23]; % LSC LSR HSC HSR
RearDamper = [672.22 450.71 187.01 166.23]; % LSC LSR HSC HSR
%%%%%%%%%%%%%%%%%%%%%%%%%%%%%%%%%%%%%%%%%%%%%%%%%%%%%%%%%%%%%%%%%%%%%%%%%%%%%%%
% Defining geometry
% total car
mt = 285; % total mass of the car
kTire = 103.32; % tire spring rate from tyre data 590 lb/in value (N/mm)
```

```
g = 9.81; % gravitational constant (m/s^2)
CoGh = 0.3; %CoG height (m)
wheelL= 1.575; %wheel base (m)
rollRate = 0.7; % roll rate (deg/lat g)

%front
ksF = 39.4; % spring stiffness front (N/mm)
munF = 4; % unsprung weight per corner front(kg)
mfc = 66.75; % sprung corner weight front (kg)
MRf = 0.79; % motion ratio front (spring/wheel travel)
dratiof = 0.7; % damping ratio front
rollHf = 0.09; %roll centre heigh front (m)
trackF = 1.1; %track width front (m)
CoGUnF = 0.23; % CoG height front (m)

% % %rear
ksR = 39.4; % spring stiffness rear (N/mm)
munR = 5; % unsprung weight per corner rear (kg)
mrc = 66.75; % sprung corner weight rear (kg)
MRr = 0.79; % motion ratio rear (spring/wheel travel)
dratior = 0.7; % damping ratio front
rollHr = 0.06; %roll centre heigh Rear (m)
trackR = 1.05; %track width rear (m)
CoGUnR = 0.23; % CoG height rear (m)



trackAvg = (trackF+trackR)/2;
rollAvg = (rollHf+rollHr)/2;
rollCogAvg = CoGh-rollAvg;
%%%%%%%%%%%%%%%%%%%%%%%%%%%%%%%%%%%%%%%%%%%%%%%%%%%%%%%%%%%%%%%%%%%%%%%%%%%%%%%

%ARB front
if ARBf == "Yes"
    G = 80e9; %shear modolus (Pa)
    afront = [0.02; 0.03; 0.04; 0.05; 0.06]; %lever arm for ARB front (m)
depending on hole
    aF = afront(Hf); %lever arm for ARB front (m)
    Lf = 0.72362; %front ARB length (m)
    DouterF = 0.0191; % Inner diameter of tube front (m)
    DinnerF = 0.0151; % Outer diameter of tube front (m)
    MRarbF = 2.13; %Motion Ratio ARb front (wheel/arb mounting point)
DEPENDANT ON lever arm!!!
    If = pi()*(DouterF^4-DinnerF^4)/32; %second moment of area for front
ARB (m4)
    kARBf = G* If/(aF^2*Lf); % torsional stiffness of front ARB (N/meter
the lever arm point moves)
    kRollARBf = (kARBf*trackF^2)*pi()/(MRarbF*180); %torsional stiffness of
front ARB (Nm/DEG)
else
    kRollARBf = 0;

end

%ARB rear
if ARBr == "Yes"
    G = 80e9; %shear modolus (Pa)
    arear = [0.02; 0.03; 0.04; 0.05; 0.06]; %lever arm for ARB rear (m)
depending on hole
    aR = arear(Hr); %lever arm for ARB rear (m)
```

```
    Lr = 0.53932; %rear ARB length (m)
    DouterR = 0.0191; % Inner diameter of tube rear (m)
    DinnerR = 0.0151; % Outer diameter of tube rear (m)
    MRarbR = 2.13; %Motion Ratio ARb rear (wheel/arb mounting point)
DEPENDANT ON lever arm!!!
    Ir = pi()*(DouterR^4-DinnerR^4)/32; %second moment of area for rear ARB
(m4)
    kARBr = G* Ir/(aR^2*Lr); % torsional stiffness of rear ARB (N/meter the
lever arm point moves)
    kRollARBr = (kARBr*trackR^2)*pi()/(MRarbR*180); %torsional stiffness of
front ARB (Nm/DEG)
else
    kRollARBr = 0;

end

%%%%%%%%%%%%%%%%%%%%%%%%%%%%%%%%%%%%%%%%%%%%%%%%%%%%%%%%%%%%%%%%%%%%%%%%%%%%

% springs front
kwF = ksF/MRf^2; % wheel rate of front wheel (N/mm)
kRideF = ((kwF*kTire)/(kwF+kTire))*1000; % caculating ride rate (N/m)
ktotF = (ksF*kTire)/(ksF+kTire); % totl spring rate for simplified system
(N/mm)
krollSf = (ksF*1000*trackF^2*pi())/(2*(1/MRf)^2*180); %roll stiffness of
body due to springs (Nm/deg)
krollTotF = krollSf+kRollARBf; %total roll stiffness of front (Nm/rad)
wnSprungF= (1/(2*pi))*sqrt(ksF*1000/mfc);

% springs rear
kwR = ksR/MRr^2; % wheel rate of front wheel (N/mm)
kRideR = ((kwR*kTire)/(kwR+kTire))*1000; % caculating ride rate (N/m)
ktotR = (ksR*kTire)/(ksR+kTire); % totl spring rate for simplified system
(N/mm)
krollSr = (ksR*1000*trackR^2*pi())/(2*(1/MRr)^2*180); %roll stiffness of
body due to springs (Nm/deg)
krollTotR = krollSr+kRollARBr; %total roll stiffness of front (Nm/rad)
rollRatioF = krollTotF/(krollTotR+krollTotF);
rollRatioR=1-rollRatioF;
wnSprungR= (1/(2*pi))*sqrt(ksR*1000/mrc);

%%%%%%%%%%%%%%%%%%%%%%%%%%%%%%%%%%%%%%%%%%%%%%%%%%%%%%%%%%%%%%%%%%%%%%%%%%%%
RollStifness = ["-" "Front" "Rear";
                "Roll Stiffness Spring 4(Nm/deg)" krollSf krollSr;
                "Roll Stiffness ARB (Nm/deg)" kRollARBf kRollARBr
                "Roll Stiffness total (Nm/deg)" krollTotF krollTotR;
                "Roll stiffness ratio" rollRatioF rollRatioR] ;
%%%%%%%%%%%%%%%%%%%%%%%%%%%%%%%%%%%%%%%%%%%%%%%%%%%%%%%%%%%%%%%%%%%%%%%%%%%%
% Static Loads per corner
ZLoadUnspF = munF*9.81;
ZLoadSpF = mfc*9.81;

ZLoadUnspR = munR*9.81;
ZLoadSpR = mrc*9.81;

%%%%%%%%%%%%%%%%%%%%%%%%%%%%%%%%%%%%%%%%%%%%%%%%%%%%%%%%%%%%%%%%%%%%%%%%%%%%

%Lateral load transfer NO DAMP
dLoadUnspF = munF*ay*9.81*CoGUnF/trackF;
dLoadSpF = 2*mfc*ay*9.81*rollHf/trackF;
```

```
dLoadRoll = (2*mfc+2*mrc)*ay*9.81*rollCogAvg/trackAvg;

dLoadUnspR = munR*ay*9.81*CoGUnR/trackR;
dLoadSpR = 2*mrc*ay*9.81*rollHr/trackR;

dLoadLatF = (dLoadRoll*rollRatioF)+dLoadUnspF+dLoadSpF;
dLoadLatR = (dLoadRoll*rollRatioR)+dLoadUnspR+dLoadSpR;

ZloadInnerF = ZLoadSpF-dLoadLatF;
ZloadOuterF = ZLoadSpF+dLoadLatF;

ZloadInnerR = ZLoadSpR-dLoadLatR;
ZloadOuterR = ZLoadSpR+dLoadLatR;
%%%%%%%%%%%%%%%%%%%%%%%%%%%%%%%%%%%%%%%%%%%%%%%%%%%%%%%%%%%%%%%%%%%%%%%%%%%%
%Calculating wheel displacement  STATIC
xFrontStatic = mfc*9.81/kwF;
xRearStatic = mrc*9.81/kwR;
%%%%%%%%%%%%%%%%%%%%%%%%%%%%%%%%%%%%%%%%%%%%%%%%%%%%%%%%%%%%%%%%%%%%%%%%%%%%
%Calculating wheel displacement  Dynamic (NO damper or spring force in lat
load transfer)
%Outer wheels
xOuterF = xFrontStatic-(ZloadOuterF/kwF);
xOuterR = xRearStatic-(ZloadOuterR/kwR);
%Inner wheels
xInnerF = xFrontStatic-(ZloadInnerF/kwF);
xInnerR = xRearStatic-(ZloadInnerR/kwR);

xFront = [xOuterF xInnerF];
xRear = [xOuterR xInnerR];
%%%%%%%%%%%%%%%%%%%%%%%%%%%%%%%%%%%%%%%%%%%%%%%%%%%%%%%%%%%%%%%%%%%%%%%%%%%%
%Calculating effect of dampers on wheel displacement

LowSpeedRatioF = [LSCf LSRf];
LowSpeedRatioR = [LSCr LSRr];
HighSpeedRatioF = [HSCf HSRf];
HighSpeedRatioR = [HSCr HSRr];

%Front chassis displacement
for i=1:length(LowSpeedRatioF)
% outer wheel - compression damping, inner - rebound
    zita = LowSpeedRatioF(i);
    time = (0:0.01:4);
    for j=1:length(time)
        syms t
   % General formula in terms of t
        % Sprung weight displacement (xsprung)
        XofTf = 1-((exp(-zita*wnSprungF*t))*((cos(wnSprungF*sqrt(1-
zita^2)*t))+((zita/(sqrt(1-zita^2)))*(sin(wnSprungF*sqrt(1-zita^2)*t)))));
        % differentiate to get velocity of sprung weight
        XdotofTf = diff(XofTf);

   % Calculating actual values
        % Calculate xsprung and velocity at each time
        Output_in(j,i) = vpa(subs(XofTf,t,time(j)));
        XsprungFront(j,i) = (Output_in(j,i)*xFront(i))-xFront(i);
        diffOutputF(j,i) = vpa(subs(XdotofTf,t,time(j)));
        VsprungF= diffOutputF*xFront(i);
```

```
        if VsprungF > VkneeF
                        zita = HighSpeedRatioF(i);
                time = (0:0.01:4);
                for j=1:length(time)
                    syms t
                % General formula in terms of t
                    % Sprung weight displacement (xsprung)
                    XofTf = 1-((exp(-
zita*wnSprungF*t))*((cos(wnSprungF*sqrt(1-zita^2)*t))+((zita/(sqrt(1-
zita^2)))*(sin(wnSprungF*sqrt(1-zita^2)*t)))));
                    % differentiate to get velocity of sprung weight
                    XdotofTf = diff(XofTf);

                % Calculating actual values
                    % Calculate xsprung and velocity at each time
                    Output_in(j,i) = vpa(subs(XofTf,t,time(j)));
                    XsprungFront(j,i) = (Output_in(j,i)*xFront(i))-
xFront(i);
                    diffOutputF(j,i) = vpa(subs(XdotofTf,t,time(j)));
                    VsprungF= diffOutputF*xFront(i);
                end
        end
end
end
%Rear chassis displacement
for i=1:length(LowSpeedRatioR)
% outer wheel - compression damping, inner - rebound
    zita = LowSpeedRatioR(i);
    time = (0:0.01:4);
    for j=1:length(time)
        syms t
   % General formula in terms of t
        % Sprung weight displacement (xsprung)
        XofTr = 1-((exp(-zita*wnSprungR*t))*((cos(wnSprungR*sqrt(1-
zita^2)*t))+((zita/(sqrt(1-zita^2)))*(sin(wnSprungR*sqrt(1-zita^2)*t)))));
        % differentiate to get velocity of sprung weight
        XdotofTr = diff(XofTr);

   % Calculating actual values
        % Calculate xsprung and velocity at each time
        Output_inR(j,i) = vpa(subs(XofTr,t,time(j)));
        XsprungRear(j,i) = (Output_inR(j,i)*xRear(i))-xRear(i);
        diffOutputR(j,i) = vpa(subs(XdotofTr,t,time(j)));
        VsprungR= diffOutputR*xRear(i);

        if VsprungR > VkneeR
                    zita = HighSpeedRatioR(i);
            time = (0:0.01:4);
            for j=1:length(time)
                syms t
           % General formula in terms of t
                % Sprung weight displacement (xsprung)
                XofTr = 1-((exp(-zita*wnSprungR*t))*((cos(wnSprungR*sqrt(1-
zita^2)*t))+((zita/(sqrt(1-zita^2)))*(sin(wnSprungR*sqrt(1-zita^2)*t)))));
                % differentiate to get velocity of sprung weight
                XdotofTr = diff(XofTr);

            % Calculating actual values
                % Calculate xsprung and velocity at each time
                Output_inR(j,i) = vpa(subs(XofTr,t,time(j)));
```

```
                XsprungRear(j,i) = (Output_inR(j,i)*xRear(i))-xRear(i);
                diffOutputR(j,i) = vpa(subs(XdotofTr,t,time(j)));
                VsprungR= diffOutputR*xRear(i);
        end

    end
    end
end


% repeat for different damper rates
%%%%%%%%%%%%%%%%%%%%%%%%%%%%%%%%%%%%%%%%%%%%%%%%%%%%%%%%%%%%%%%%%%%%%%%%%%%%%%%

%damper input front
LSCf = 0.1;
LSRf = 0.1;
HSCf = 0.1;
HSRf = 0.1;

ratioFront = [LSCf LSRf HSCf HSRf]; %damping ratios front LSC, LSR,HSC,HSR

VkneeF = 12.5; %knee speed front in mm/sec
%damper input rear
LSCr = 0.01;
LSRr = 0.01;
HSCr = 0.01;
HSRr = 0.01;

ratioRear = [LSCr LSRr HSCr HSRr]; %damping ratios front LSC, LSR,HSC,HSR
VkneeR = 12.5; %knee speed rear in mm/sec

%Calculating effect of dampers on wheel displacement

LowSpeedRatioF = [LSCf LSRf];
LowSpeedRatioR = [LSCr LSRr];
HighSpeedRatioF = [HSCf HSRf];
HighSpeedRatioR = [HSCr HSRr];

%Front chassis displacement
for i=1:length(LowSpeedRatioF)
% outer wheel - compression damping, inner - rebound
    zita = LowSpeedRatioF(i);
    time = (0:0.01:4);
    for j=1:length(time)
        syms t
   % General formula in terms of t
        % Sprung weight displacement (xsprung)
        XofTf = 1-((exp(-zita*wnSprungF*t))*((cos(wnSprungF*sqrt(1-
zita^2)*t))+((zita/(sqrt(1-zita^2)))*(sin(wnSprungF*sqrt(1-zita^2)*t)))));
        % differentiate to get velocity of sprung weight
        XdotofTf = diff(XofTf);

   % Calculating actual values
        % Calculate xsprung and velocity at each time
        Output_in(j,i) = vpa(subs(XofTf,t,time(j)));
        XsprungFront2(j,i) = (Output_in(j,i)*xFront(i))-xFront(i);
        diffOutputF(j,i) = vpa(subs(XdotofTf,t,time(j)));
        VsprungF= diffOutputF*xFront(i);
```

```
        if VsprungF > VkneeF
                        zita = HighSpeedRatioF(i);
                time = (0:0.01:4);
                for j=1:length(time)
                    syms t
                % General formula in terms of t
                    % Sprung weight displacement (xsprung)
                    XofTf = 1-((exp(-
zita*wnSprungF*t))*((cos(wnSprungF*sqrt(1-zita^2)*t))+((zita/(sqrt(1-
zita^2)))*(sin(wnSprungF*sqrt(1-zita^2)*t)))));
                    % differentiate to get velocity of sprung weight
                    XdotofTf = diff(XofTf);

                % Calculating actual values
                    % Calculate xsprung and velocity at each time
                    Output_in(j,i) = vpa(subs(XofTf,t,time(j)));
                    XsprungFront2(j,i) = (Output_in(j,i)*xFront(i))-
xFront(i);
                    diffOutputF(j,i) = vpa(subs(XdotofTf,t,time(j)));
                    VsprungF= diffOutputF*xFront(i);
                end
        end
end
end
%Rear chassis displacement
for i=1:length(LowSpeedRatioR)
% outer wheel - compression damping, inner - rebound
    zita = LowSpeedRatioR(i);
    time = (0:0.01:4);
    for j=1:length(time)
        syms t
   % General formula in terms of t
        % Sprung weight displacement (xsprung)
        XofTr = 1-((exp(-zita*wnSprungR*t))*((cos(wnSprungR*sqrt(1-
zita^2)*t))+((zita/(sqrt(1-zita^2)))*(sin(wnSprungR*sqrt(1-zita^2)*t)))));
        % differentiate to get velocity of sprung weight
        XdotofTr = diff(XofTr);

   % Calculating actual values
        % Calculate xsprung and velocity at each time
        Output_inR(j,i) = vpa(subs(XofTr,t,time(j)));
        XsprungRear2(j,i) = (Output_inR(j,i)*xRear(i))-xRear(i);
        diffOutputR(j,i) = vpa(subs(XdotofTr,t,time(j)));
        VsprungR= diffOutputR*xRear(i);

        if VsprungR > VkneeR
                    zita = HighSpeedRatioR(i);
            time = (0:0.01:4);
            for j=1:length(time)
                syms t
           % General formula in terms of t
                % Sprung weight displacement (xsprung)
                XofTr = 1-((exp(-zita*wnSprungR*t))*((cos(wnSprungR*sqrt(1-
zita^2)*t))+((zita/(sqrt(1-zita^2)))*(sin(wnSprungR*sqrt(1-zita^2)*t)))));
                % differentiate to get velocity of sprung weight
                XdotofTr = diff(XofTr);

            % Calculating actual values
                % Calculate xsprung and velocity at each time
                Output_inR(j,i) = vpa(subs(XofTr,t,time(j)));
```

```
                XsprungRear2(j,i) = (Output_inR(j,i)*xRear(i))-xRear(i);
                diffOutputR(j,i) = vpa(subs(XdotofTr,t,time(j)));
                VsprungR= diffOutputR*xRear(i);
        end

    end
    end
end

%%%%%%%%%%%%%%%%%%%%%%%%%%%%%%%%%%%%%%%%%%%%%%%%%%%%%%%%%%%%%%%%%%%%%%%%%%%%%%%
%plot rolling wheel displacement with dampers plotting ONLY INNER WHEELS
figure(1);
clf;
hold on;

plot(time,XsprungFront(:,1));
plot(time,XsprungRear(:,1));
plot(time,XsprungFront2(:,1));
plot(time,XsprungRear2(:,1));
legend('Front inner high damp', 'Rear inner high damp','Front inner low
damp', 'Rear inner low damp');
xlabel('Time (sec)');
ylabel('Sprung weight displacement (mm)');
% title ('Chassis displacement during rolling with dampers');
annotation('textbox', [0.5, 0.2, 0.1, 0.1], 'String', "High damp = 0.24 and
Low damp = 0.1 ")
line([0 time(end)], [0 0],'Color', 'black', 'LineStyle','--'); % zero line
line([0 time(end)], [11 11],'Color', 'red', 'LineStyle','--'); % when we
lift wheels
```

A 13 *Matlab: Damper Velocities*

```
% Larissa Kopf
% Date: 18/10/2019
% Models all corners on steady state loading for W-FS18
% Differentiates shock position for damper speed - checks if low or high
speed and adjusts displacements accordingly

%Front ARB definition
ARBf="YES";
Hf=3; % measured from closest to tube
%Rear ARB definition
ARBr="YES";
Hr=3; % measured from closest to tube

% lateral acceleration
ay=1.3; %in g

%damper input front
LSCf = 0.36;
LSRf = 0.24;
HSCf = 0.1;
HSRf = 0.1;

ratioFront = [LSCf LSRf HSCf HSRf]; %damping ratios front LSC, LSR,HSC,HSR

VkneeF = 12.5; %knee speed front in mm/sec
%damper input front
LSCr = 0.36;
```

```
LSRr = 0.24;
HSCr = 0.1;
HSRr = 0.1;

ratioRear = [LSCr LSRr HSCr HSRr]; %damping ratios front LSC, LSR,HSC,HSR
VkneeR = 12.5; %knee speed rear in mm/sec

%%%%%%%%%%%%%%%%%%%%%%%%%%%%%%%%%%%%%%%%%%%%%%%%%%%%%%%%%%%%%%%%%%%%%%%%%%%%%%%
%creating front and rear damper lookup table look at excel dyno stuff
FrontDamper = [672.22 450.71 187.01 166.23]; % LSC LSR HSC HSR
RearDamper = [672.22 450.71 187.01 166.23]; % LSC LSR HSC HSR
%%%%%%%%%%%%%%%%%%%%%%%%%%%%%%%%%%%%%%%%%%%%%%%%%%%%%%%%%%%%%%%%%%%%%%%%%%%%%%%
% Defining geometry
% total car
mt = 285; % total mass of the car
kTire = 103.32; % tire spring rate from tyre data 590 lb/in value (N/mm)
g = 9.81; % gravitational constant (m/s^2)
CoGh = 0.296; %CoG height (m)
wheelL= 1.575; %wheel base (m)
rollRate = 0.6; % roll rate (deg/lat g)

%front
ksF = 39.4; % spring stiffness front (N/mm)
munF = 4; % unsprung weight per corner front(kg)
mfc = 66.75; % sprung corner weight front (kg)
MRf = 0.79; % motion ratio front (spring/wheel travel)
dratiof = 0.7; % damping ratio front
rollHf = 0.09; %roll centre heigh front (m)
trackF = 1.1; %track width front (m)
CoGUnF = 0.23; % CoG height front (m)

% % %rear
ksR = 39.4; % spring stiffness rear (N/mm)
munR = 5; % unsprung weight per corner rear (kg)
mrc = 66.75; % sprung corner weight rear (kg)
MRr = 0.79; % motion ratio rear (spring/wheel travel)
dratior = 0.7; % damping ratio front
rollHr = 0.05; %roll centre heigh Rear (m)
trackR = 1.05; %track width rear (m)
CoGUnR = 0.23; % CoG height rear (m)



trackAvg = (trackF+trackR)/2;
rollAvg = (rollHf+rollHr)/2;
rollCogAvg = CoGh-rollAvg;
%%%%%%%%%%%%%%%%%%%%%%%%%%%%%%%%%%%%%%%%%%%%%%%%%%%%%%%%%%%%%%%%%%%%%%%%%%%%%%%

%ARB front
if ARBf == "Yes"
    G = 80e9; %shear modolus (Pa)
    afront = [0.02; 0.03; 0.04; 0.05; 0.06]; %lever arm for ARB front (m)
depending on hole
    aF = afront(Hf); %lever arm for ARB front (m)
    Lf = 0.72362; %front ARB length (m)
    DouterF = 0.0191; % Inner diameter of tube front (m)
    DinnerF = 0.0151; % Outer diameter of tube front (m)
    MRarbF = 2.13; %Motion Ratio ARb front (wheel/arb mounting point)
DEPENDANT ON lever arm!!!
```

```
    If = pi()*(DouterF^4-DinnerF^4)/32; %second moment of area for front
ARB (m4)
    kARBf = G* If/(aF^2*Lf); % torsional stiffness of front ARB (N/meter
the lever arm point moves)
    kRollARBf = (kARBf*trackF^2)*pi()/(MRarbF*180); %torsional stiffness of
front ARB (Nm/DEG)
else
    kRollARBf = 0;

end

%ARB rear
if ARBr == "Yes"
    G = 80e9; %shear modolus (Pa)
    arear = [0.02; 0.03; 0.04; 0.05; 0.06]; %lever arm for ARB rear (m)
depending on hole
    aR = arear(Hr); %lever arm for ARB rear (m)
    Lr = 0.53932; %rear ARB length (m)
    DouterR = 0.0191; % Inner diameter of tube rear (m)
    DinnerR = 0.0151; % Outer diameter of tube rear (m)
    MRarbR = 2.13; %Motion Ratio ARb rear (wheel/arb mounting point)
DEPENDANT ON lever arm!!!
    Ir = pi()*(DouterR^4-DinnerR^4)/32; %second moment of area for rear ARB
(m4)
    kARBr = G* Ir/(aR^2*Lr); % torsional stiffness of rear ARB (N/meter the
lever arm point moves)
    kRollARBr = (kARBr*trackR^2)*pi()/(MRarbR*180); %torsional stiffness of
front ARB (Nm/DEG)
else
    kRollARBr = 0;

end

%%%%%%%%%%%%%%%%%%%%%%%%%%%%%%%%%%%%%%%%%%%%%%%%%%%%%%%%%%%%%%%%%%%%%%%%%%%%

% springs front
kwF = ksF/MRf^2; % wheel rate of front wheel (N/mm)
kRideF = ((kwF*kTire)/(kwF+kTire))*1000; % caculating ride rate (N/m)
ktotF = (ksF*kTire)/(ksF+kTire); % totl spring rate for simplified system
(N/mm)
krollSf = (ksF*1000*trackF^2*pi())/(2*(1/MRf)^2*180); %roll stiffness of
body due to springs (Nm/deg)
krollTotF = krollSf+kRollARBf; %total roll stiffness of front (Nm/rad)
wnSprungF= (1/(2*pi))*sqrt(ksF*1000/mfc);

% springs rear
kwR = ksR/MRr^2; % wheel rate of front wheel (N/mm)
kRideR = ((kwR*kTire)/(kwR+kTire))*1000; % caculating ride rate (N/m)
ktotR = (ksR*kTire)/(ksR+kTire); % totl spring rate for simplified system
(N/mm)
krollSr = (ksR*1000*trackR^2*pi())/(2*(1/MRr)^2*180); %roll stiffness of
body due to springs (Nm/deg)
krollTotR = krollSr+kRollARBr; %total roll stiffness of front (Nm/rad)
rollRatioF = krollTotF/(krollTotR+krollTotF);
rollRatioR=1-rollRatioF;
wnSprungR= (1/(2*pi))*sqrt(ksR*1000/mrc);

%%%%%%%%%%%%%%%%%%%%%%%%%%%%%%%%%%%%%%%%%%%%%%%%%%%%%%%%%%%%%%%%%%%%%%%%%%%%
RollStifness = ["-" "Front" "Rear";
                "Roll Stiffness Spring 4(Nm/deg)" krollSf krollSr;
```

```
                "Roll Stiffness ARB (Nm/deg)" kRollARBf kRollARBr
                "Roll Stiffness total (Nm/deg)" krollTotF krollTotR;
                "Roll stiffness ratio" rollRatioF rollRatioR] ;
%%%%%%%%%%%%%%%%%%%%%%%%%%%%%%%%%%%%%%%%%%%%%%%%%%%%%%%%%%%%%%%%%%%%%%%%%%%%%%%
% Static Loads per corner
ZLoadUnspF = munF*9.81;
ZLoadSpF = mfc*9.81;

ZLoadUnspR = munR*9.81;
ZLoadSpR = mrc*9.81;

%%%%%%%%%%%%%%%%%%%%%%%%%%%%%%%%%%%%%%%%%%%%%%%%%%%%%%%%%%%%%%%%%%%%%%%%%%%%%%%

%Lateral load transfer NO DAMP
dLoadUnspF = munF*ay*9.81*CoGUnF/trackF;
dLoadSpF = 2*mfc*ay*9.81*rollHf/trackF;

dLoadRoll = (2*mfc+2*mrc)*ay*9.81*rollCogAvg/trackAvg;

dLoadUnspR = munR*ay*9.81*CoGUnR/trackR;
dLoadSpR = 2*mrc*ay*9.81*rollHr/trackR;

dLoadLatF = (dLoadRoll*rollRatioF)+dLoadUnspF+dLoadSpF;
dLoadLatR = (dLoadRoll*rollRatioR)+dLoadUnspR+dLoadSpR;

ZloadInnerF = ZLoadSpF-dLoadLatF;
ZloadOuterF = ZLoadSpF+dLoadLatF;

ZloadInnerR = ZLoadSpR-dLoadLatR;
ZloadOuterR = ZLoadSpR+dLoadLatR;
%%%%%%%%%%%%%%%%%%%%%%%%%%%%%%%%%%%%%%%%%%%%%%%%%%%%%%%%%%%%%%%%%%%%%%%%%%%%%%%
%Calculating wheel displacement  STATIC
xFrontStatic = mfc*9.81/kwF;
xRearStatic = mrc*9.81/kwR;
%%%%%%%%%%%%%%%%%%%%%%%%%%%%%%%%%%%%%%%%%%%%%%%%%%%%%%%%%%%%%%%%%%%%%%%%%%%%%%%
%Calculating wheel displacement  Dynamic (NO damper or spring force in lat
load transfer)
%Outer wheels
xOuterF = xFrontStatic-(ZloadOuterF/kwF);
xOuterR = xRearStatic-(ZloadOuterR/kwR);
%Inner wheels
xInnerF = xFrontStatic-(ZloadInnerF/kwF);
xInnerR = xRearStatic-(ZloadInnerR/kwR);

xFront = [xOuterF xInnerF];
xRear = [xOuterR xInnerR];
%%%%%%%%%%%%%%%%%%%%%%%%%%%%%%%%%%%%%%%%%%%%%%%%%%%%%%%%%%%%%%%%%%%%%%%%%%%%%%%
%Calculating effect of dampers on wheel displacement

LowSpeedRatioF = [LSCf LSRf];
LowSpeedRatioR = [LSCr LSRr];
HighSpeedRatioF = [HSCf HSRf];
HighSpeedRatioR = [HSCr HSRr];

%Front chassis displacement
for i=1:length(LowSpeedRatioF)
% outer wheel - compression damping, inner - rebound
    zita = LowSpeedRatioF(i);
    time = (0:0.01:4);
```

```
    for j=1:length(time)
        syms t
   % General formula in terms of t
        % Sprung weight displacement (xsprung)
        XofTf = 1-((exp(-zita*wnSprungF*t))*((cos(wnSprungF*sqrt(1-
zita^2)*t))+((zita/(sqrt(1-zita^2)))*(sin(wnSprungF*sqrt(1-zita^2)*t)))));
        % differentiate to get velocity of sprung weight
        XdotofTf = diff(XofTf);

   % Calculating actual values
        % Calculate xsprung and velocity at each time
        Output_in(j,i) = vpa(subs(XofTf,t,time(j)));
        XsprungFront(j,i) = (Output_in(j,i)*xFront(i))-xFront(i);
        diffOutputF(j,i) = vpa(subs(XdotofTf,t,time(j)));
        VsprungF= diffOutputF*xFront(i);

        if VsprungF > VkneeF
                        zita = HighSpeedRatioF(i);
                time = (0:0.01:4);
                for j=1:length(time)
                    syms t
               % General formula in terms of t
                    % Sprung weight displacement (xsprung)
                    XofTf = 1-((exp(-
zita*wnSprungF*t))*((cos(wnSprungF*sqrt(1-zita^2)*t))+((zita/(sqrt(1-
zita^2)))*(sin(wnSprungF*sqrt(1-zita^2)*t)))));
                    % differentiate to get velocity of sprung weight
                    XdotofTf = diff(XofTf);

               % Calculating actual values
                    % Calculate xsprung and velocity at each time
                    Output_in(j,i) = vpa(subs(XofTf,t,time(j)));
                    XsprungFront(j,i) = (Output_in(j,i)*xFront(i))-
xFront(i);
                    diffOutputF(j,i) = vpa(subs(XdotofTf,t,time(j)));
                    VsprungF= diffOutputF*xFront(i);
                end
        end
end
end
%Rear chassis displacement
for i=1:length(LowSpeedRatioR)
% outer wheel - compression damping, inner - rebound
    zita = LowSpeedRatioR(i);
    time = (0:0.01:4);
    for j=1:length(time)
        syms t
   % General formula in terms of t
        % Sprung weight displacement (xsprung)
        XofTr = 1-((exp(-zita*wnSprungR*t))*((cos(wnSprungR*sqrt(1-
zita^2)*t))+((zita/(sqrt(1-zita^2)))*(sin(wnSprungR*sqrt(1-zita^2)*t)))));
        % differentiate to get velocity of sprung weight
        XdotofTr = diff(XofTr);

   % Calculating actual values
        % Calculate xsprung and velocity at each time
        Output_inR(j,i) = vpa(subs(XofTr,t,time(j)));
        XsprungRear(j,i) = (Output_inR(j,i)*xRear(i))-xRear(i);
        diffOutputR(j,i) = vpa(subs(XdotofTr,t,time(j)));
        VsprungR= diffOutputR*xRear(i);
```

```
        if VsprungR > VkneeR
                    zita = HighSpeedRatioR(i);
             time = (0:0.01:4);
             for j=1:length(time)
                 syms t
            % General formula in terms of t
                 % Sprung weight displacement (xsprung)
                 XofTr = 1-((exp(-zita*wnSprungR*t))*((cos(wnSprungR*sqrt(1-
zita^2)*t))+((zita/(sqrt(1-zita^2)))*(sin(wnSprungR*sqrt(1-zita^2)*t)))));
                 % differentiate to get velocity of sprung weight
                 XdotofTr = diff(XofTr);

            % Calculating actual values
                 % Calculate xsprung and velocity at each time
                 Output_inR(j,i) = vpa(subs(XofTr,t,time(j)));
                 XsprungRear(j,i) = (Output_inR(j,i)*xRear(i))-xRear(i);
                 diffOutputR(j,i) = vpa(subs(XdotofTr,t,time(j)));
                 VsprungR= diffOutputR*xRear(i);
        end

    end
    end
end
%%%%%%%%%%%%%%%%%%%%%%%%%%%%%%%%%%%%%%%%%%%%%%%%%%%%%%%%%%%%%%%%%%%%%%%%%%%%%%%
%plot rolling wheel displacement with dampers
figure(1);
clf;
hold on;
plot(time,XsprungFront);
plot(time,XsprungRear);
line([0 time(end)], [0 0],'Color', 'black', 'LineStyle','--'); % zero line
line([0 time(end)], [11 11],'Color', 'red', 'LineStyle','--'); % when we
lift wheels
legend('Front Outer', 'Front Inner','Rear Outer', 'Rear Inner');
xlabel('Time (sec)');
ylabel('Sprung weight displacement (mm)');
title ('Chassis displacement during rolling with dampers');

figure(2);
clf;
hold on;
plot(time,VsprungF);
plot(time,VsprungR);
line([0 time(end)], [0 0],'Color', 'black', 'LineStyle','--');
legend('Damper Speed Front Inner','Damper Speed Front Outer', 'Damper Speed
Rear Inner','Damper Speed Rear Outer');
xlabel('Time (sec)');
ylabel('Damper Velocity (mm/sec)');
% title ('Velocity of dampers');
```